SPECTRAL EFFICIENCY OF CDMA BASED AD-HOC NETWORKS

A thesis submitted to the University of Manchester
for the degree of Doctor of Philosophy
in the Faculty of Engineering and Physical Sciences

2010

By
Junaid Ahmed
School of Electrical and Electronic Engineering

Contents

List of Figures

Abstract

Spectrum efficiency and energy efficiency are two important attributes driving innovation in wireless communication. Efficient spectrum utilization and sharing with multiple access techniques and using under-utilized spectra by cognitive radios is the current focus due to the scarcity and cost of the available radio spectrum. Energy efficiency to increase operating time of portable handheld devices like smartphones that handle simultaneous voice/video streaming and web browsing and battery powered nodes in a sensor network where battery capacity determines the lifetime of the network is another area attracting researchers. The focus of this thesis is the spectral efficiency of multicarrier code division multiple access (CDMA) in wireless ad-hoc networks. Furthermore, energy efficiency to maximize lifetime of a network are also studied.

In a multicarrier CDMA system inter-carrier interference (ICI) due to carrier frequency offset and multiple access interference (MAI) are two major factors that deteriorate the performance. Previous work in this area has been mostly focused on simulation results due to the complexity of the analysis due to the large number of random variables involved. Taking into account accurate statistical models for ICI and MAI that account for the correlation between adjacent subcarriers, this thesis presents new mathematical analysis for the spectral efficiency of multicarrier CDMA communication systems over a frequency selective Rayleigh fading environment. We analyze and compare three multicarrier CDMA schemes which are multicarrier CDMA, multicarrier direct-sequence CDMA and multitone CDMA. We also present simulation results to confirm the validity of our analysis. We also analyze the performance of three simple multiple access techniques or coexistence etiquettes in detail, which are simple to implement and do not require any central control. Accurate interference models are developed and are used to derive accurate expressions for packet error rates in the case

of direct sequence CDMA and slotted packet transmission schemes. These results are then used to study the performance of the coexistence etiquettes and compare them with each other. Finally we present a new joint node selection and power allocation strategy that increases lifetime of an ad-hoc network where nodes cooperate to enable diversity in transmission.

Declaration

No portion of the work referred to in this thesis has been submitted in support of an application for another degree or qualification of this or any other university or other institute of learning.

Copyright

Acknowledgements

Firstly, I would like to acknowledge the help and support provided by my supervisor Dr. Khairi Ashour Hamdi, Lecturer in the school of Electrical and Electronic Engineering at the University of Manchester. He has always guided me with affection and encouragement while ignoring my shortcomings. He was always ready and available to guided me with his deep knowledge and broad experience.

I also owe deep gratitude to my loving parents Mr. Bashir Ahmad and Mrs. Aqila Akhtar who always wanted to see me as a doctor. I would not be what I am without their love, guidance, support and encouragement. My gratitude also goes to my wife Mrs. Sania Ahmed who always supported me during the difficult times. I would also like to thank my brothers Mr. Asif Mahmood, Mr Naveed Ahmad and my sister Miss Fatima Ferheen for always encouraging me and helping me financially when I needed the most. My loving thanks are also due to my two little ones Ms. Zainab Ahmed and Ms. Hamnah Ahmed for always cheering me up and filling my heart with happiness.

I would also like to say thanks to all my colleagues who helped, encouraged and cheered me, namely, Mr Muhammad Nouman, Mr Sarmad Sohaib, Mr Inamulhasan Shaikh, Mr Asim Khan, Mr Abubakar Makarfi, Mr Muhammad Obaidullah, Mr Rashid Saleem and others.

Lastly, I would like to acknowledge the financial support from COMSATS Institute of Information Technology, Islamabad, Pakistan.

The Author

Mr. Junaid Ahmed received the Bachelor of Science degree in Electrical and Electronics Engineering from Middle East Technical University, Ankara, Turkey in 1997. He received the Masters of Science degree in Electrical Engineering from Oklahoma State University, Stillwater, Oklahoma, United States in 2000.

From 1998 to 1999 he worked as a software engineer at Crescent Software in Islamabad, Pakistan. From 2000 to 2002 he worked as an embedded systems engineer at General Bandwidth in Austin, Texas, United States. From 2003 to 2004 he worked as senior software engineer at Streaming Networks in Islamabad, Pakistan. In 2004 he changed his carrier path from industry to academia and joined COMSATS Institute of Information Technology (CIIT) as assistant professor and worked there until 2007. Currently, he is pursuing his PhD degree in Electrical Engineering with research focus on spread spectrum communication, multiple access techniques and ad-hoc networks.

List of Abbreviations

AWGN	additive white Gaussian noise
BER	bit error rate
B-CDMA	binary code division multiple access
CDF	cumulative distribution function
CDMA	code division multiple access
CTS	clear to send
DS-CDMA	direct sequence code division multiple access
DFT	discrete Fourier transform
ECG	electrocardiography
EGC	equal gain combining
FFT	fast Fourier transform
GA	Gaussian approximation
HSDPA	high-speed downlink packet access
HSUPA	high-speed uplink packet access
ICI	intercarrier interference
IEEE	institute of electrical and electronics engineers
IFFT	inverse fast Fourier transform
LTE	long term evolution
MACA	multiple access with collision avoidance

MACAW	multiple access with collision avoidance for wireless
MC-CDMA	multicarrier code division multiple access
MC DS-CDMA	multicarrier direct sequence code division multiple access
MAI	multiple access interference
MRC	maximal ratio combining
MT-CDMA	multitone code division multiple access
MGF	moment generating function
OFDM	orthogonal frequency-division multiplexing
PDF	probability density function
PER	packet error rate
Q-CDMA	quadriphase code division multiple access
RTS	request to send
SINR	signal to interference and noise ratio
SNR	signal to noise ratio
WCDMA	wideband code division multiple access

List of Mathematical Notations

$(\cdot)^*$	complex conjugate
$\det(\cdot)$	determinant of a matrix
$\mathbb{E}(\cdot)$	expectation operator of a random variable
$\mathrm{diag}(\cdot)$	a vector that contains all diagonal elements of a matrix
$\log_2(\cdot)$	base-2 logarithm
$\mathbf{I}_M$	$M \times M$ Identity matrix
$\lvert . \rvert$	magnitude of a complex number
$(\cdot)^H$	matrix Hermitian
$\exp(.)$	exponential function
$\mathrm{Var}\{.\}$	variance of a random variable
$\Gamma(.)$	Gamma function
$\frac{\partial}{\partial x}$	partial derivative with respect to x
$\mathrm{rect}(.)$	rectangular function
$\mathrm{Re}\{.\}$	real part of a complex number
$\Pr(.)$	probability of an event
${}_2\mathrm{F}_1(.)$	hypergeometric function
$\mathrm{W}(.)$	Lambert W function or omega function or product log
$\mathrm{E}_{(.)}(.)$	generalized exponential integral
$\mathrm{erf}(.), \mathrm{erfc}(.)$	error function, complementary error function

List of Variables

P_T	transmit power
P_R	receive power
β	path-loss exponent
r	distance between transmitter and receiver
g_l	complex amplitude of the lth propagation path
τ_l	propagation delay of the lth propagation path
$h(t)$	time domain channel impulse response
G_n	frequency domain channel impulse response
L	total number of resolvable propagation paths
$c(t)$	spreading signal
$b(t)$	information bearing signal
f_n	frequency of the nth subcarrier
$s(t)$	transmitted signal
T	symbol duration
T_g	length of the cyclic prefix
Z	receiver decision variable
$r(t)$	receive signal
N_p	length of the spreading code
N_c	number of subcarriers

T_c	chip duration
L_F	number of fingers in the rake receiver
C	spectral efficiency
$\mathrm{C_p}$	capacity
Γ	signal to noise ratio gap
E_s	signal energy
α	channel delay spread
$\eta\,(t)$	additive white Gaussian noise
N_0	two sided AWGN power spectral density
ϕ	phase difference between transmitter and receiver's oscillator
S	desired signal component
I	interference component
N	noise component
$\mathbf{\Lambda}$	complex covariance matrix
σ	delay spread normalized to the symbol time
SINR	signal to interference and noise ratio
Δf	carrier frequency offset
Δ	normalized carrier frequency offset
K	total number of transmitters
$v(t)$	signal of a packet
s_k	mean receive power of the kth signal
d_k	distance between the kth transmitter-receiver pair
λ	spatial density of the interferers
b	radius of circular area of interest around receiver
R	minimum distance between an interferer and the receiver of interest

a	spreading code sequence
$\psi(t)$	chip waveform
L_s	number of symbols per packet
W	multiple access interference component
δ_k	transmission permission from access protocol
ξ	differential chip delay
γ_{th}	SNR threshold
S	throughput
P_s	packet success probability
γ_i	instantaneous signal to noise ratio
P_i^{out}	probability of failed transmission
T_i^{inter}	inter-transmission time
L_i	lifetime of node i
$L^{network}$	lifetime of network
E_0	initial battery energy
n_i^{tx}	number of transmissions before a successful transmission is achieved

Chapter 1

Introduction

Wireless communication has seen remarkable growth in the last two decades. The first generation of cellular telephone system was deployed in 1979 by Nippon Telephone and Telegraph company in Japan [1]. This was followed by the second generation (2G) using digital technology in 1990 and third generation (3G) in 2001. The history of wireless ad-hoc networks is also as old, it dates back to 1970s when packet radio networks (PRNETs) was developed by Advanced Research Project Agency (ARPA) [2]. Ad-hoc networks do not require a central control and hence are suitable when none is possible like military conflicts or when the infrastructure is destroyed by a natural disaster. It also has applications in areas where deploying an infrastructure is not feasible like sensor networks distributed over large areas of a jungle to monitor environmental conditions. Due to the absence of a central control in ad-hoc networks it suffers from self interference generated by similar nodes in the same area transmitting in the same time and frequency. Due to this self interference code division multiple access (CDMA) is a good choice of communication technique due to its robustness to interference. CDMA was first developed by Qualcomm Inc. in USA in 1993 [1] and is in use in cellular as well as ad-hoc networks. Many communication techniques based on the basic CDMA principles have been proposed and developed including

wideband code division multiple access (WCDMA), high-speed downlink packet access (HSDPA), high-speed uplink packet access (HSUPA) etc.

Multicarrier CDMA is one of the derivatives of CDMA, it is a combination of orthogonal frequency-division multiplexing (OFDM) with CDMA and was first proposed in 1993 [3–5]. It combines the benefits of both OFDM and CDMA and offers high spectral efficiency, robustness to frequency selective fading, multiple access capability etc. It can be used in ad-hoc networks as well as cellular networks due to the inherent robustness to interference and high data rates. Numerous performance evaluation and design techniques have been proposed but nevertheless there are still interesting unresolved problems. In this dissertation we present several original performance analyses and results for CDMA and multicarrier CDMA in ad-hoc or cellular network environment.

1.1 Contributions

The major contributions of this dissertation can be given as follows.

- Derive accurate spectral efficiency expressions or a tight lower bound expression where exact expression was not possible, for multicarrier CDMA (MC-CDMA), multicarrier direct sequence CDMA (MC DS-CDMA) and multitone CDMA (MT-CDMA) in multipath Rayleigh fading and additive white Gaussian noise environment.

- Derive spectral efficiency expressions that account for carrier frequency offset and analyze the degradation in performance of the three multicarrier CDMA schemes in the presence of frequency offset.

- Derive spectral efficiency expressions and analyze the performance of the three multicarrier schemes in the presence of asynchronous interferers in

an ad-hoc network where each interferer has a separate random carrier frequency offset.

- Analyze three coexistance protocols in a large CDMA based ad-hoc network and derive accurate expressions for packet error rates and throughput for DS-CDMA. The expressions are used to study the performance of the coexistence etiquettes and compare them with each other.

- Analyze lifetime of an ad-hoc network and propose a new cooperative power allocation protocol that maximizes lifetime of the network.

1.2 Thesis Organization

The rest of the thesis is organized such that Chapter 2 gives background on some of the important concepts in wireless communication that the thesis relies on. It also contains the block diagrams of the CDMA and multicarrier CDMA transmitters and receivers that we use in the rest of the chapters and the signal representation for all the communication schemes. It does not contain any new contribution from the author and all information given is from the available literature. The novel contribution from the author starts from Chapter 3, where accurate expressions for the spectral efficiency of basic MC-CDMA, MC DS-CDMA and MT-CDMA communication systems in a multipath Rayleigh fading environment and additive white Gaussian noise but free from any other impairments, are derived. Using the derived expressions the performance of the three multicarrier schemes is analyzed and compared.

In Chapter 4 we extend our results to include the effect of carrier frequency offset, which degrades the signal power as well as adds a new source of interference reducing the received signal to interference and noise ratio. In an uncoordinated ad-hoc network there are always other interferers in the neighborhood that are

another source of interference and we further extend our results from Chapter 4 to include this source of interference in Chapter 5. The interferers are considered to be asynchronous to the transmitter and receiver of interest and have random frequency offset.

In Chapter 6 we analyze coexistance protocols in an ad-hoc network of uncoordinated asynchronous transmitters in an interference limited Rayleigh fading channel. New accurate expressions of performance of such a system are derived for three coexistance protocols and compared with each other. The derived expressions cater for bit-to-bit error dependence and can be used to find network design parameters like packet size, length of error correcting code, choice of binary or quadriphase CDMA etc.

In Chapter 7 we analyze lifetime of a cooperative ad-hoc network consisting of limited battery powered transmitters. We also propose a power allocation protocol that increases the average lifetime of such a network. Finally we conclude the thesis in Chapter 8 and propose future work.

1.3 List of Publications

1. J. Ahmed, and K. A. Hamdi, "On the Coexistence of Uncoordinated Ad-hoc Networks," *in Proc. IEEE GLOBECOM,* pp. 1-5, 6-10 Dec. 2010.

2. J. Ahmed, and K. A. Hamdi, "Spectral Efficiency Degradation of Multicarrier CDMA due to Carrier Frequency Offset," *to appear in IEEE ICC*, June 2011.

3. J. Ahmed, and K. A. Hamdi, "Spectral Efficiency of Asynchronous MC-CDMA in Correlated Rayleigh Fading and Frequency Offset," *submitted to IEEE Trans. Wireless Commun.*

4. J. Ahmed, and K. A. Hamdi, "On the Coexistence of Uncoordinated Ad-hoc Networks," *in preparation, to be submitted to IEEE Trans. Wireless Commun.*

5. J. Ahmed, and K. A. Hamdi, "Performance of Asynchronous MC-CDMA, MC DS-CDMA and MT-CDMA in Correlated Rayleigh Fading and Frequency Offset," *in preparation, to be submitted to IEEE Trans. Wireless Commun.*

6. J. Ahmed, and K. A. Hamdi, "Lifetime Analysis of Cooperative Ad-hoc Sensor Networks," *presented at PGR conference, University of Manchester*, Nov. 2009.

Chapter 2

Background

2.1 Characterization of Mobile Radio Channel

The mobile radio channel plays a vital role in determining the performance of a wireless communication system. There are multiple factors that influence the electromagnetic wave propagation including but not limited to reflection, diffraction and scattering [1] from various objects around the transmitter-receiver pair. At the receiver, multiple wavefronts are received after traveling along different paths of different lengths and subjected to multiple reflections and diffractions . The combined effect of these waves rapidly varies with time, frequency and spatial locations of transmitter and receiver. Numerous models have been proposed to model these variations and they can be broadly categorized into two groups, large scale path loss and short scale multipath fading. These are briefly described below.

2.1.1 Large Scale Path Loss

The average signal strength of a transmitted signal reduces with distance from transmitter. In free space this reduction is solely due to the reduction of average

power per area of a spherical wavefront due to its expansion as it moves away from the source. In other environments, like rural or urban environment, the combined effect of multiple impairments result in a faster reduction in the average signal strength as the distance from the transmitter increases. The most widely used model to capture this effect is the log-distance path loss model. According to the model the received power (P_R) as a function of transmitted power (P_T) is given as

$$P_R = P_T r^{-\beta}$$

where r is the distance between transmitter and receiver and β is called the path loss exponent. The value β varies from 2 in free space to greater than 4 in dense urban areas [6]. We have used this model to capture large scale path loss in this dissertation.

2.1.2 Short Scale Multipath Fading

The constructive and destructive addition of multiple wavefronts that have traversed multiple paths and gone through varied reflections and diffractions before arriving at the receiver result in rapid fluctuations in the received signal power. To capture this effect consider a transmitter-receiver pair, there are multiple propagation paths between them, each having separate attenuation factor and delay. The channel impulse response can be given as [7]:

$$h(t) = \sum_{l=0}^{L-1} g_l(t)\,\delta(t - \tau_l) \tag{2.1}$$

where $\delta(.)$ is the Dirac delta function, L is the total number of resolvable propagation paths, $g_l(t)$ and τ_l are the complex amplitude and propagation delay of the lth path and $\tau_0 \leq \tau_1 \leq \ldots \leq \tau_{L-1}$. The complex amplitude $g_l(t)$ is time varying in general, however, we assume it to be slowly varying in time and constant over

the duration of a symbol, hence in the rest of the thesis we represent $g_l(t)$ as g_l. The frequency domain channel response can be calculated from (2.1) as

$$G_n = \sum_{l=0}^{L-1} g_l \mathrm{e}^{-j2\pi f_n \tau_l}$$

where G_n is the frequency-selective multipath fading channel at frequency f_n. When L is large, central limit theorem can be applied and G_n can be modeled as a complex valued Gaussian random process. When there is no direct line-of-sight path or fixed signal reflectors G_n can be modeled as a zero mean complex Gaussian random process and the envelop $|G_n|$ becomes Rayleigh distributed [7]. The channel in this case is called Rayleigh fading channel, this is the most common channel used in literature and we have also used it in this dissertation.

In the presence of line-of-sight path and/or fixed reflectors/scatterers G_n can not be modeled as zero mean and in this case the envelope has a Rice distribution and the channel is called a Ricean fading channel. Nakagami-m distribution and Weibull distribution are other probability density functions that have been used to model the channel and are called Nakagami fading channel and Weibull fading channel respectively.

2.2 Multiple Access Techniques

Multiple access techniques allow sharing of a limited radio spectrum among different users. Efficient sharing of radio spectrum is necessary due to its high cost and scarcity. However, when more than one user communicate over the same frequency range at the same time; they cause interference to each other, degrading each others performance. The purpose of the multiple access techniques is to find efficient ways of sharing the spectrum with minimum or no interference so that simultaneous high quality transmissions can take place and no part of the

spectrum gets wasted.

Code division multiple access (CDMA) and orthogonal frequency division multiple access (OFDM) are the two multiple access techniques that have recently seen wide implementation. CDMA is the basic multiplexing technique used in the third generation (3G) cellular mobile networks and OFDM in the fourth generation (4G) cellular mobile networks as well as in digital audio broadcast and digital video broadcast. We describe these techniques in the following sections.

2.2.1 Code Division Multiple Access

In code division multiple access (CDMA) the narrow band signal of each user is spread over a large bandwidth by multiplying it with a spreading signal. A spreading signal or spreading code is a pseudo random noise signal having a much larger bandwidth than the data signal of the user. At the receiver the received signal is correlated with the same spreading signal to recover the original narrow band signal. Multiple access is achieved by assigning different orthogonal spreading signals to each user resulting in the appearance of signal from other users as merely white noise at the correlator output at the receiver. Hence in this scheme signal from every user occupies all of the available frequencies for all time and orthogonality is achieved by the spreading code as shown in Fig. 2.1.

This scheme has many advantages such as having a soft capacity limit meaning there is no hard limit to the number of users that can use the available frequency range at the same time. Whenever a new user starts to communicate it increases the noise floor for all users, hence incrementally effecting the capacity of other users.

The origins of spread spectrum techniques can be traced back to Second World War where it was used in radars [8]. In 1978 a spread spectrum technique was first proposed for cellular communication [9, 10] but it was not until 1993 when the

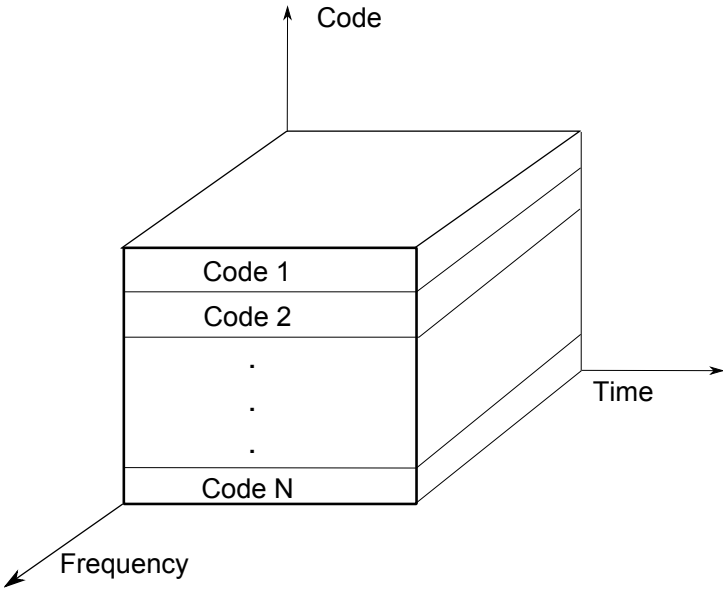

Figure 2.1: Code division multiple access where spreading code for all users occupy all frequencies at all times

first CDMA based standard (IS-95) was developed by Qualcomm Inc [1]. CDMA has since seen much wide usage and many standards have since been developed including WCDMA, HSDPA, HSUPA etc.

A block diagram of basic CDMA transmitter and receiver are shown in Fig. 2.2. The transmitted CDMA signal can be represented during an arbitrary signaling interval as

$$s(t) = b\,(t)\,c\,(t)\,\mathrm{e}^{j2\pi f_n t}, \quad t \in [0, T]$$

where $b\,(t)$ is the information bearing signal, $c\,(t)$ is the spreading signal, f_n is the frequency of the nth subcarrier, T is the symbol duration.

The received signal is decoded by the conventional correlation receiver with maximal-ratio combining. Let Z represent the receiver decision variable then

$$Z = \frac{1}{T}\int_0^T G^* c\,(t)\,\mathrm{e}^{-j2\pi f t}\,r\,(t)\,\mathrm{d}t$$

where $r\,(t)$ is the receive signal and G^* is the complex conjugate of the channel

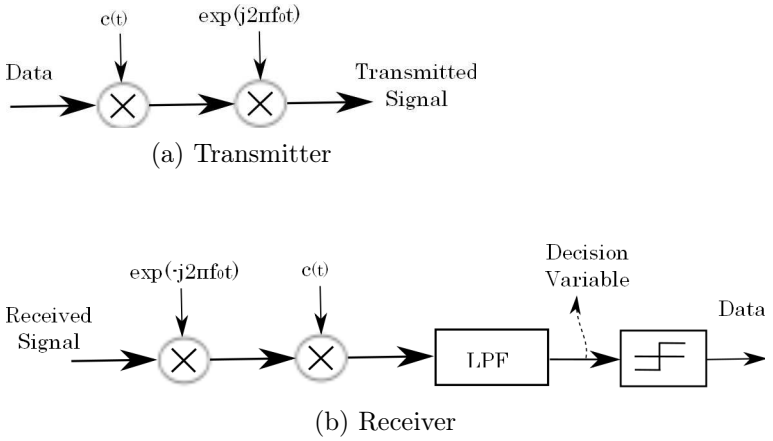

Figure 2.2: CDMA transmitter and receiver block diagrams

transfer function.

The basic description of CDMA given above is one type of CDMA which is known as direct sequence CDMA (DS-CDMA). Other types of CDMA include frequency-hopped CDMA (FH-CDMA) and time-hopping CDMA (TH-CDMA) [7]. In FH-CDMA the available spectrum is divided into a number of frequency slots and during any signaling interval one or more of these slots, which are randomly selected, are used. Similarly, in TH-CDMA a large time interval is divided into a number of smaller time slots, which are randomly picked for transmission. In this thesis we only use DS-CDMA and hence forth any reference to CDMA would imply DS-CDMA.

2.2.2 Orthogonal Frequency Division Multiple Access

In orthogonal frequency division multiplexing (OFDM) the input data stream is first serial to parallel converted and then each data stream is modulated onto a separate subcarrier. Mutually orthogonal subcarriers are selected so that there is no intercarrier interference in the ideal case and hence guard bands are not required. OFDM is suitable for high data rate transmission as it offers high spectral efficiency. It was first proposed in 1966 [11] and in 1971 transmitter-receiver

design using discrete Fourier transform (DFT) was presented [12]. However, due to the recent advancements in the digital signal processing hardware that can efficiently implement fast Fourier transform (FFT) that this scheme has becomes realistic [13].

OFDM is currently being used in digital audio broadcasting, digital video broadcasting, wireless local area networks (IEEE 802.11a, IEEE 802.11g) and the 4G mobile network technology, namely long term evolution (LTE).

A block diagram of basic OFDM transmitter and receiver are shown in Fig. 2.3. Fig. 2.4 shows an alternate implementation of OFDM transmitter and receiver using FFT and IFFT blocks. The transmitted OFDM signal can be represented during an arbitrary signaling interval as

$$s(t) = \sum_{l=1}^{N_c} b_l\,(t)\ \mathrm{e}^{j2\pi f_l t}, \quad t \in [0, N_c T]$$

where $b_l\,(t)$ is the information bearing signal, f_l is the frequency of the lth subcarrier, N_c is the number of subcarriers and T is the symbol duration.

The received signal is decoded by the conventional correlation receiver with maximal-ratio combining. Let Z_1 represent the receiver decision variable for the first subcarrier stream then

$$Z_1 = \frac{1}{N_c T} \int_0^{N_c T} G_1^* \mathrm{e}^{-j2\pi f_1 t}\, r\,(t)\, \mathrm{d}t$$

where $r\,(t)$ is the received signal and G_1^* is the complex conjugate of the channel transfer function.

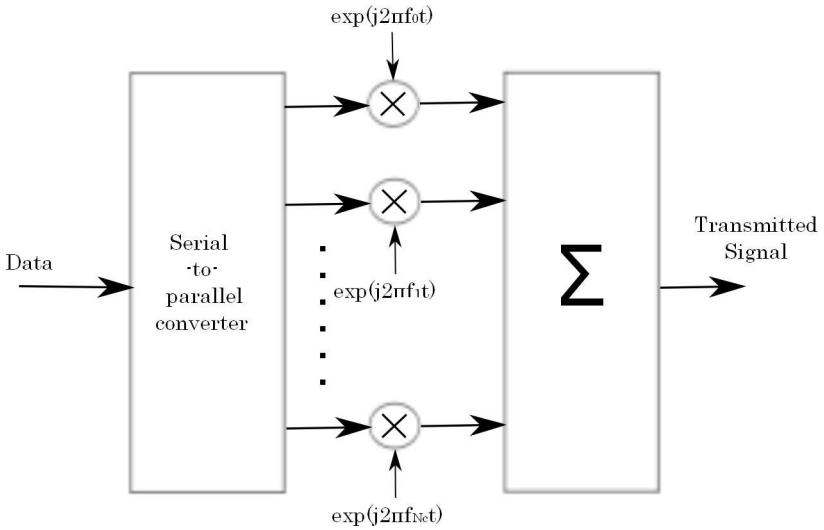

(a) Transmitter

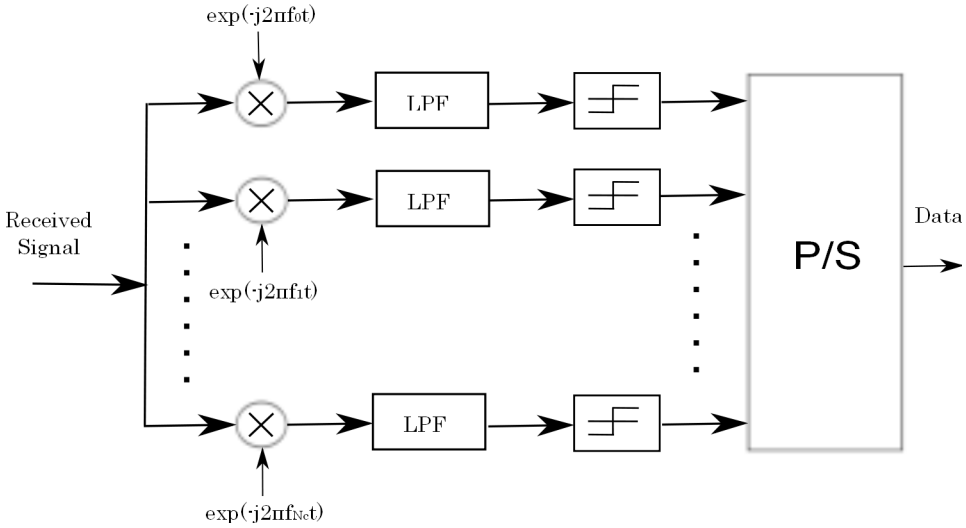

(b) Receiver

Figure 2.3: OFDM transmitter and receiver block diagrams

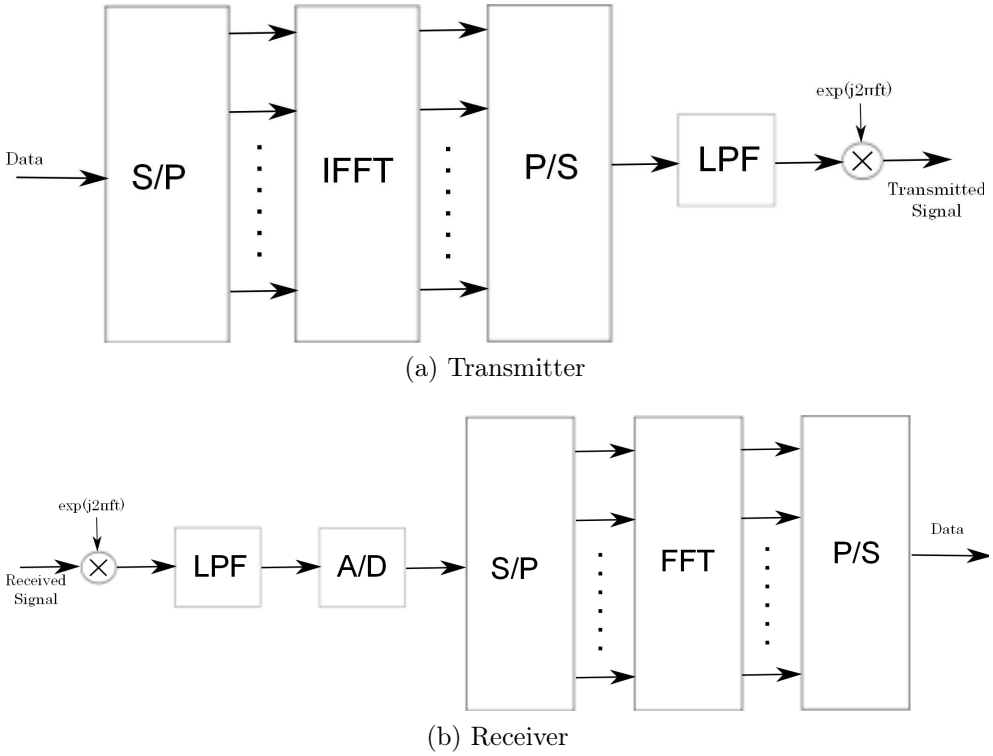

(a) Transmitter

(b) Receiver

Figure 2.4: Alternate transmitter and receiver block diagrams of OFDM.

In the future we may see a combination of OFDM and CDMA in high data rate communication systems. This combination can give high spectral efficiency and data rates of OFDM as well as diversity gain of CDMA systems. This makes OFDM-CDMA or multicarrier CDMA an important area of research. We introduce this new and important multiple access technique in the next section.

2.3 Multicarrier CDMA

Multicarrier CDMA is a multiple access technique that combines OFDM with CDMA, it spreads the signal in frequency domain and modulates over multiple subcarriers. It was first proposed in 1993 [3–5], two other variants namely multicarrier DS-CDMA and multitone CDMA (MT-CDMA) were also proposed the same year by [14] and [15] respectively. Multicarrier CDMA signals can be easily generated and received using fast Fourier transform (FFT) and efficient FFT

algorithms and devices are widely available. They offer other attractive features such as high spectral efficiency, robustness to frequency selective fading, multiple access capability and narrow band interference rejection among others.

2.3.1 MC CDMA

In MC-CDMA each symbol is spread using the wireless device's unique spreading code and then modulated over different frequency subcarriers. Hence each symbol is spread over all subcarriers and each subcarrier carries a single chip. Fig. 2.5 shows the block diagram of an implementation of MC-CDMA transmitter and receiver [16]. At the receiver the received signal is demodulated by all subcarriers separately and then corresponding chips are multiplies before taking a low pass filter. The outputs of the filters are then combined to give the decision variable, any combining method can be used here, however, we only analyze maximal ratio combining (MRC) as that is the optimum combining method. Data is recovered from the decision variable using a simple step function. Fig. 2.6 shows an alternate implementation of MC-CDMA transmitter and receiver using FFT and IFFT blocks [9].

The benefits of this scheme include robustness to frequency selective fading, this is achieved by keeping small the bandwidth occupied by a single subcarrier and hence fading experienced by a single subcarrier is can be considered to be flat. When the data rate is too high or frequency selectivity too narrow to have flat fading over the bandwidth of subcarrier then data must be first serial to parallel converted first before further processing and every parallel stream modulated over a separate set of subcarriers. Another benefit is that the symbol synchronization is easier as the chip duration is increased to the symbol duration and even bigger if serial to parallel conversion is used. The limitation of using this scheme is that the chip rate or the length of the spreading code has to be equal or lesser than the

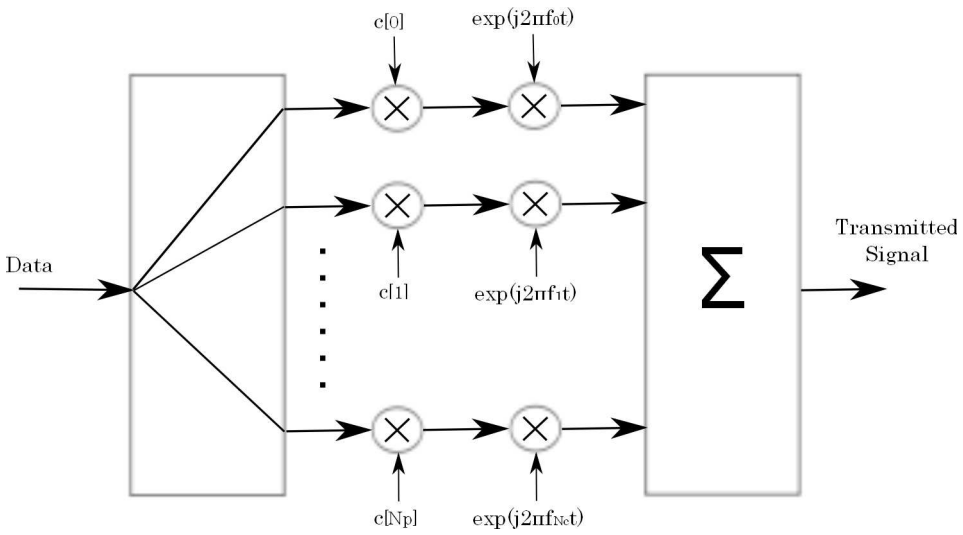

(a) Transmitter

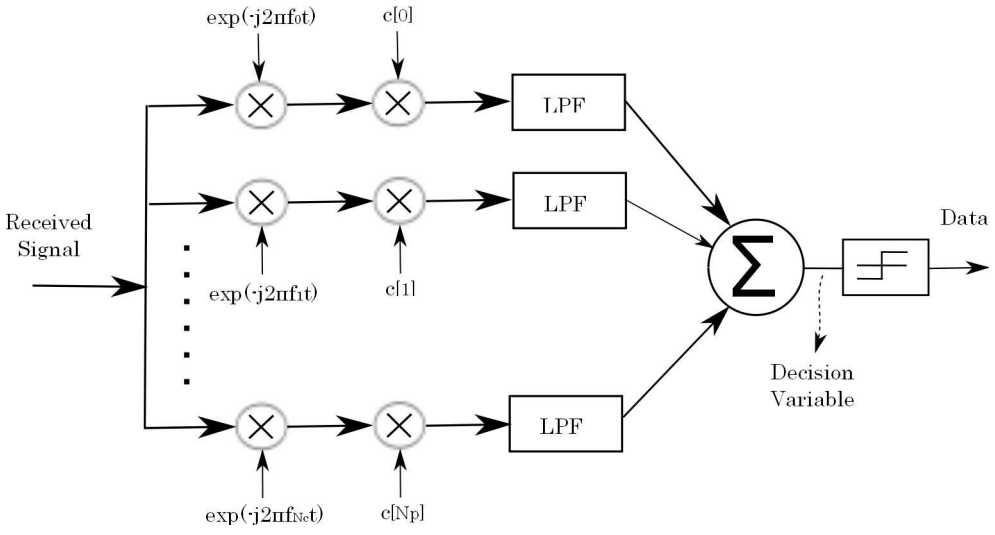

(b) Receiver

Figure 2.5: MC-CDMA transmitter and receiver block diagrams.

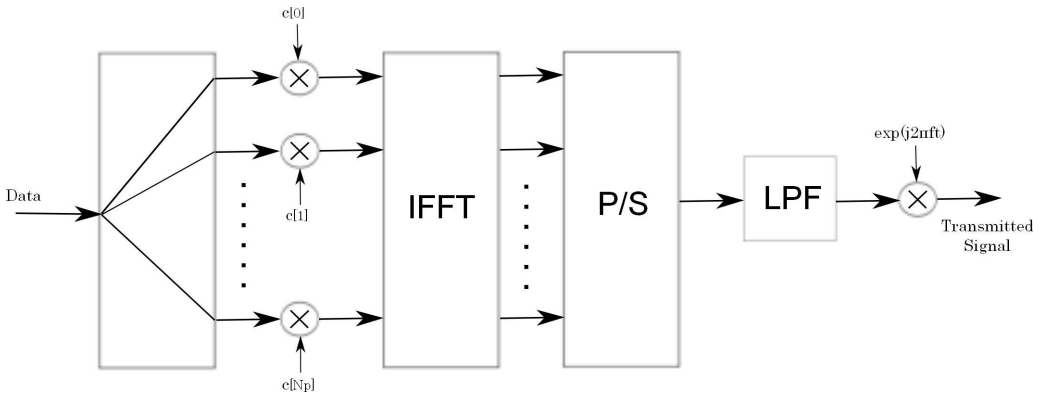

(a) Transmitter

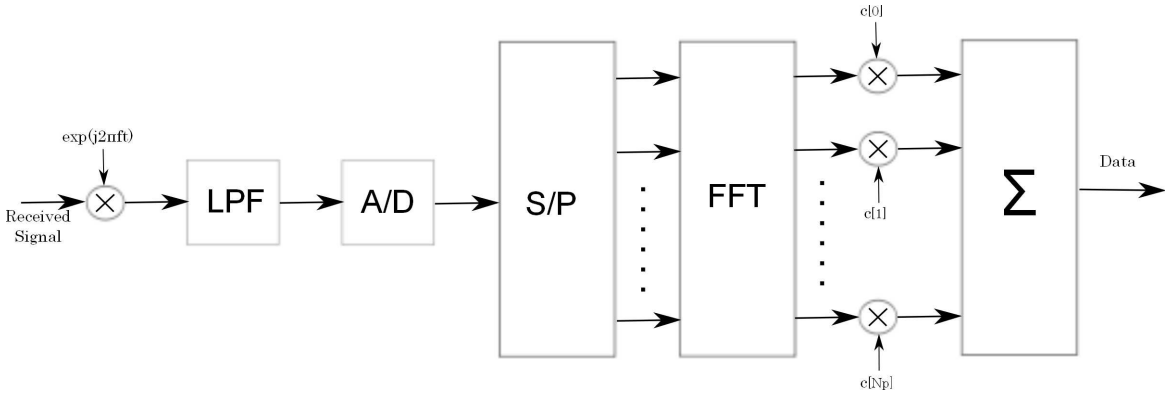

(b) Receiver

Figure 2.6: Alternate transmitter and receiver block diagrams of MC-CDMA.

number of subcarriers used in transmission and since the number of users that can be supported simultaneously depends on the length of the spreading code, the total number of subcarriers also limits the number of simultaneous users.

The transmitted multicarrier CDMA signal can be represented during an arbitrary signaling interval as

$$s(t) = \frac{1}{\sqrt{N_p}} \sum_{n=0}^{N_p-1} b\,(t)\, c\,[n]\, \mathrm{e}^{j2\pi f_n t}, \quad t \in [-T_g, T] \tag{2.2}$$

where $b\,(t)$ is the information bearing signal, $c\,[n]$ is the nth component of the spreading signal. N_p is the total number of subcarriers which is equal to the length of the spreading code (i.e. processing gain), f_n is the frequency of the

nth subcarrier. In (2.2) T is the symbol duration and T_g is the length of the cyclic prefix. All subcarriers are assumed to be equally spaced in frequency with a minimum subcarrier separation of $1/T$ and hence the total bandwidth occupied by the MC-CDMA signal is $\frac{N_p}{T}$.

The received signal is decoded by the conventional correlation receiver described earlier with maximal-ratio combining. Let Z represent the receiver decision variable then

$$Z = \sum_{m=0}^{N_p-1} \frac{1}{T} \int_0^T G_m^* \, c[m] \mathrm{e}^{-j2\pi f_m t} \, r\left(t\right) \mathrm{d}t$$

where $r\left(t\right)$ is the receive signal and G_m^* is the complex conjugate of the channel transfer function of the mth subcarrier.

2.3.2 Multicarrier DS-CDMA

In multicarrier DS-CDMA symbols are first serial to parallel converted and then spread in the time domain [9, 17]. The multiple time-spread streams are then modulated on separate subcarriers. In this scheme the number of available subcarriers determine the number of substreams that the data is serial to parallel converted into. Fig. 2.7 shows the block diagram of one of the possible implementations of MC DS-CDMA transmitter and receiver [16]. At the receiver the received signal is demodulated by all subcarriers separately and then the whole spreading code is multiplied before taking a low pass filter. The outputs of the filters give the decision variables from which data is recovered in parallel and then converted serially.

The main difference between this scheme and MC-CDMA is that here the data is spread in time domain while in MC-CDMA it is spread in frequency domain. Since the spreading takes place in time domain it is limited by the spacing between

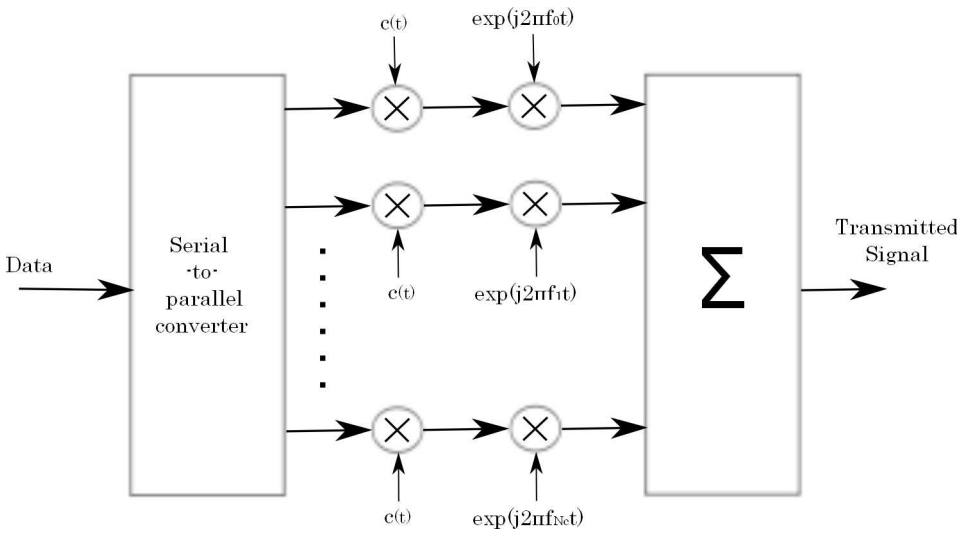

(a) Transmitter

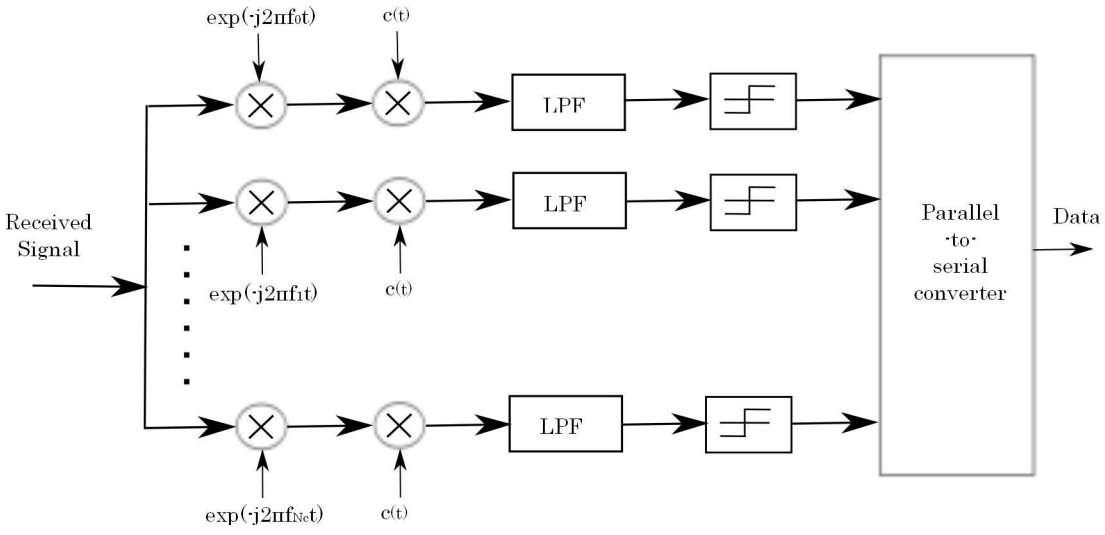

(b) Receiver

Figure 2.7: MC DS-CDMA transmitter and receiver block diagrams.

adjacent subcarriers so that the resulting spectrum of each subcarrier does not overlap and hence inter-carrier interference is avoided. This scheme can not benefit from frequency or time diversity as each subcarrier carries a different data signal and large spreading codes with rake receivers are not used.

The transmitted MC DS-CDMA signal can be represented during an arbitrary signaling interval as

$$s(t) = \sum_{l=1}^{N_c} b_l(t)\, c(t)\ \mathrm{e}^{j2\pi f_l t}, \quad t \in [-T_g, N_c T] \tag{2.3}$$

where N_c is the number of subcarriers which is not necessarily equal to the length of the spreading code N_p. Also note that the signal interval has increased from T to $N_c T$, this is because of the serial to parallel conversion. The frequency separation between adjacent subcarriers is atleast $\frac{1}{T_c}$, where T_c is the chip duration, in terms of symbol duration T, it is $\frac{N_p}{N_c T}$, this is to avoid intercarrier interference as discussed earlier. With this frequency separation the total bandwidth occupied by the MC DS-CDMA signal becomes $\frac{N_p}{T}$.

The received signal $r(t)$ is decoded by the conventional correlation receiver described earlier with maximal-ratio combining. Let Z_1 represent the receiver decision variable for the first subcarrier stream then

$$Z_1 = \frac{1}{N_c T} \int_0^{N_c T} G_1^* c(t)\, \mathrm{e}^{-j2\pi f_1 t}\, r(t)\, \mathrm{d}t.$$

Note that the desired output of this decision variable is the first symbol. The decision variable for the other subcarriers will be similar and is avoided for brevity.

2.3.3 Multi-Tone CDMA

Multitone CDMA transmitter is very similar to that of MC DS-CDMA transmitter where symbols are first serial to parallel converted and then spread in the time domain [9, 17]. The multiple time-spread streams are then modulated on separate subcarriers. In this scheme the frequency separation between subcarriers is selected such that the spectrum of each subcarrier satisfies the orthogonality condition before spreading is performed. The orthogonality condition does not satisfy after spreading is performed hence much longer spreading codes can be used to accommodate more users but this also results in intercarrier interference at the receiver. Fig.2.8 shows the block diagram of one of the possible implementations of multitone CDMA transmitter and receiver [16]. At the receiver the received signal is demodulated by all subcarriers separately and then rake combiner is applied separately. The outputs of the rake combiners give the decision variables from which data is recovered in parallel and then converted serially.

This scheme can accommodate more users than MC DS-CDMA due to the use of longer spreading codes and reduces multiple access interference. Another benefit of using longer spreading codes is that rake combiners can be used at the receiver giving diversity gain.

The transmitted MT CDMA signal can be represented during an arbitrary signaling interval as

$$s(t) = \sum_{l=1}^{N_c} b_l(t)\, c(t)\, \mathrm{e}^{j2\pi f_l t}, \quad t \in [-T_g, N_c T] \tag{2.4}$$

which is the same as (3.8). The frequency separation between adjacent subcarriers is however different and is atleast $\frac{1}{N_c T}$ which is equal to $\frac{1}{N_p T_c}$. The total bandwidth occupied by the MT CDMA signal is also different than MC DS-CDMA and is equal to $\frac{N_c+N_p-1}{N_c T}$.

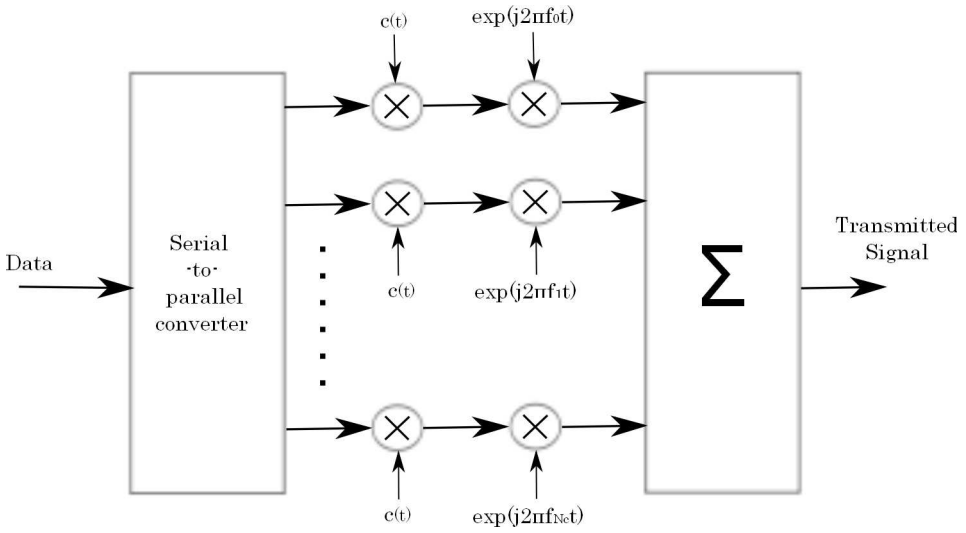

(a) Transmitter

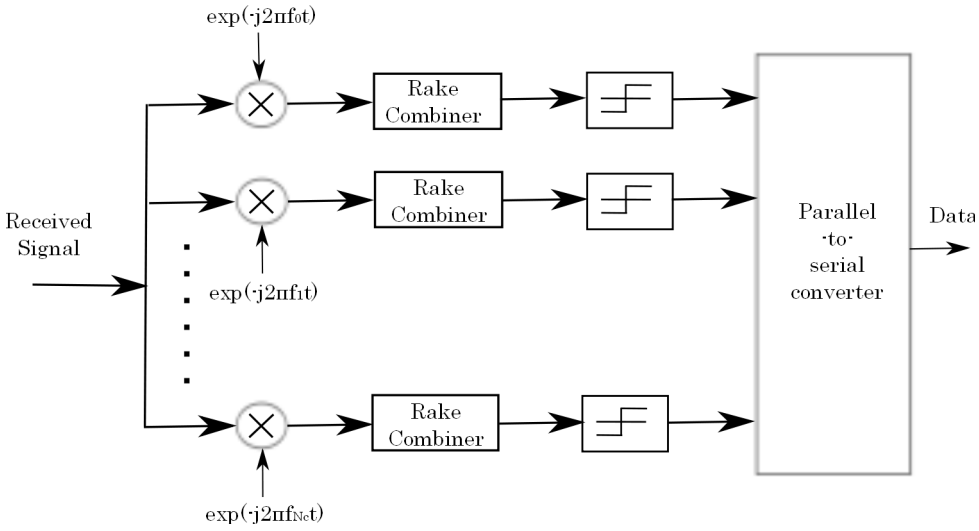

(b) Receiver

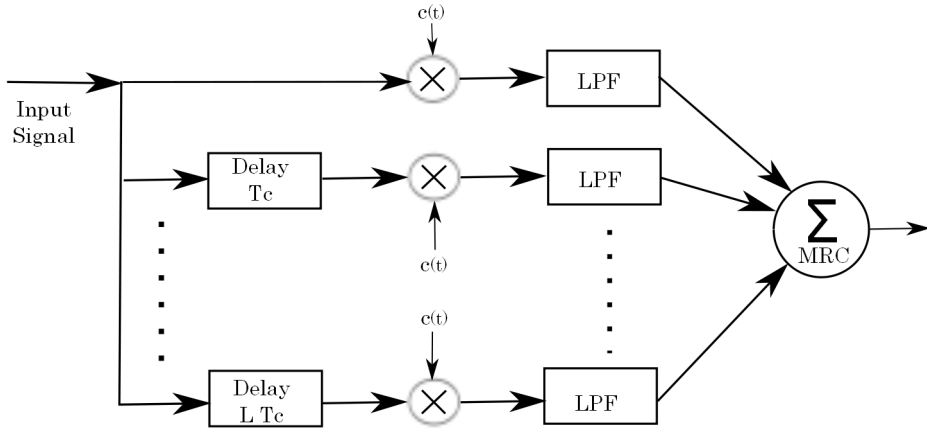

(c) Rake Combiner

Figure 2.8: Multitone CDMA transmitter and receiver block diagrams.

The received signal is decoded by the rake receivers after being demodulated. The receiver decision variable for the first symbol Z_1 that was modulating the first subcarrier becomes

$$Z_1 = \sum_{m=0}^{L_F-1} \frac{1}{N_c T} \int_0^{N_c T} g_m^* c(t - m\tau) \mathrm{e}^{-j2\pi f_1 t} r(t) \mathrm{d}t$$

where L_F is the number of fingers in the rake receiver.

2.4 Spectral Efficiency of Wireless Networks

The capacity ($\mathrm{C_p}$) of an additive white Gaussian noise (AWGN) wireless channel of bandwidth B can be found using Shannon's well known as [18, 19]:

$$\mathrm{C_p} = B \log_2 (1 + \mathrm{SNR}) \tag{2.5}$$

where SNR stands for signal to noise ratio and the units of $\mathrm{C_p}$ are bits per sec (bits/sec). Shannon's theorem proves that a code exists that can achieve a data rate that is arbitrarily close to $\mathrm{C_p}$ with small probability of bit error, furthermore, a data rate higher than $\mathrm{C_p}$ would have arbitrarily high probability of bit error. A practical coding method would fall short of the Shannon's limit in (2.5) and this is captured by Γ namely "SNR gap" [20, 21] and the capacity expression with Γ is given by $\mathrm{C_p} = B \log_2 \left(1 + \frac{\mathrm{SNR}}{\Gamma}\right)$.

In our analysis we use spectral efficiency, which gives the data rate per unit time and frequency, it is measured in bits/sec/Hz. The spectral efficiency of a system can be given as $\mathrm{C} = \log_2 \left(1 + \frac{\mathrm{SNR}}{\Gamma}\right)$. In our analysis we consider $\Gamma = 1$ for simplicity. In the presence of other impairments like Gaussian interference the spectral efficiency can be taken as [22] $\mathrm{C} = \log_2 (1 + \mathrm{SINR})$, where SINR stands for signal to interference and noise ratio. In a multicarrier CDMA system

with processing gain and number of carriers equal to N_p we measure the spectral efficiency as $\mathrm{C} = \frac{1}{N_p}\log_2(1+\mathrm{SINR})$ [22], the term $\frac{1}{N_p}$ appears because the signal is spread N_p times as compared to an unspread signal.

Spectral efficiency is an important measure of the performance of a communication system. This importance comes from the scarcity and cost of the available radio spectrum. Any new communication strategy has to be able to use this spectrum in the most efficient way and spectral efficiency is the measure of it.

2.5 Ad-hoc Networks

Ad-hoc networks are the networks that do not have a specific structure. They are made up of nodes that happen to be in the vicinity of each other without any pre planning or organization for either a short period of time or permanently. Nodes communicate with each other and help each other to communicate outside their immediate neighborhood. These are battery powered nodes performing a single or multiple functions with ability to send and receive data wirelessly. Mobile ad-hoc networks are receiving an ever increasing interest from the research community. It has military as well as commercial applications [23] in sensor networks, voice and video communications. Most of the work has been directed towards Quality of Services (QoS) and routing [24] with few researchers interested in capacity. Most of the research in the estimation of network capacity or performance evaluation parameters is centered on the performance of a transmitter receiver pair in an ad-hoc network in the presence of similar transmitters (interferers). Poisson and uniform distribution models are widely used for the distribution of the interferers around the receiver e.g. [25], [26] and [24]. The transmission loss is commonly characterized by a path-loss model according to which median path loss at a distance r from the transmitter is $r^{-\beta}$, where β is the path-loss exponent. Haykin [6] gives a table of sample path loss exponent values, where it has a value of 2 for

free space, 4 for suburban, low noise and 4.5 for dense urban areas. Log-normal model is also used for the transmission loss characterization [27] and [28], however we will use the path-loss model for simplicity. For the power loss parameter of 4 probability density function for signal to interference ratio is known [29], so performance evaluation statistics can be calculated for all transmission types. Probably because of this reason most researchers have used this exponent value. For example Sousa [30] found equations for moment generating function of the sum of interference power ($\sum_{r_i \leq a} g(r_i)$ where $g(.)$ is the power output of a single interfere and a is the radius of the disk, centered at the receiver and containing all the interferers) and calculated probability of error for different spread spectrum schemes. Similarly Liu [26] has also calculated probability of success only for the path-loss parameter of 4.

Significant research in ad-hoc sensor networks in the past few years has resulted in a number of civil and military applications. Below are some of the important applications [31]:

- **Communication during disaster recovery** Disaster struck areas can have all or most of the communication network destroyed. An ad-hoc network can be used to provide crisis management services applications when resorting communication is crucial but wired line communication would take long.

- **Surveillance networks** Small battery powered video cameras can be used by military, law enforcement agencies and others to monitor borders, public events, private properties and other areas.

- **Storage of potentially important activities** Activities such as thefts, car accidents, traffic violations etc can be stored by a distributed video network for future legal and other usage.

- **Traffic avoidance and enforcement** A distributed network of cameras can be used on highways to detection and rerouting of traffic to avoid congestion. Parking space monitoring and automated parking advices can be generated. Traffic violations can also be stored and transmitted to the law enforcement agencies.

- **Advanced health care** Telemedicine sensor networks integrated with 3G mobile networks can be used for health care services. Patients carrying sensors for body temperature, blood pressure, pulse, ECG, breathing activities etc can be fed into remote medical centers for advanced remote monitoring.

- **Assistance for the elderly** Multimedia sensors can be used for monitoring of the elderly. Emergency situations can be detected and assistance called in a timely fashion.

- **Environmental monitoring** Several projects on habitat monitoring are possible. For example an array of video cameras is being used by the oceanographers to determine the evolution of sandbars.

- **Person locator** Video streams and still images can be used to locate missing persons and/or identify criminals.

- **Industrial process control** Multimedia content along with other sensors of temperature, pressure etc can be used for time-critical industrial process control.

- **Target tracking** A distributed array of sensor networks can track a target over an increased range and with higher precision [32]. The results can be fed back to the user in real time.

Wireless sensor networks with video sensors offer new challenges that are above and beyond those in the traditional sensor networks. Video processing requires

high computational complexity and results in high data rates [33]. Consequently it uses more energy; which is the dearest resource in most of the wireless sensor networks.

Multiple parameters have been studied to characterize the performance of ad-hoc networks. This includes, but not limited to, lifetime of the network, the packet success probability as experienced by any node in the network and the throughput of the network. We will now define these parameters in the following sections and in depth analysis of these parameters will follow in the next chapters.

Chapter 3

Spectral Efficiency of Multicarrier CDMA in Noise and Multipath Fading Environment

In this chapter we investigate the performance of MC-CDMA, MC DS-CDMA and MT-CDMA in terms of spectral efficiency in additive white Gaussian noise and multipath Rayleigh fading environment and the absence of any other impairment. We assume a transmitter receiver pair communicating in the absence of any other transmitter in the area. The three multicarrier CDMA schemes are analyzed separately.

3.1 MC-CDMA

The transmitted multicarrier CDMA signal during an arbitrary signaling interval is given in (2.2) and is reproduced below as

$$s(t) = \frac{1}{\sqrt{N_p}} \sum_{n=0}^{N_p-1} b\,(t)\, c\,[n]\, \mathrm{e}^{j2\pi f_n t}, \quad t \in [-T_g, T] \tag{3.1}$$

where $b(t)$ is the information bearing signal, we assume it to be a zero-mean complex valued random variable with signal energy E_s, $c[n]$ is the nth component of the spreading signal. For the sake of analysis, we assume that $c[n]$ takes values in $\{-1, 1\}$ with equal probability. N_p is the total number of subcarriers which is equal to the length of the spreading code (i.e. processing gain), f_n is the frequency of the nth subcarrier where all subcarriers are assumed to be equally spaced in frequency giving $f_n - f_m = (n-m)/T$ where T is the symbol duration and T_g in (3.11) is the length of the cyclic prefix.

The transmitted signal is subjected to a frequency-selective multipath Rayleigh fading channel as described in section 2.1.2 with transfer function given as

$$G_n = \sum_{l=0}^{L-1} g_l \mathrm{e}^{-j2\pi f_n \tau_l} \tag{3.2}$$

where L is the total number of resolvable propagation paths, g_l and τ_l are the complex amplitude and propagation delay of the lth path and $\tau_0 \leq \tau_1 \leq \ldots \leq \tau_{L-1}$. We assume that all g_l, where $l \in [0, L-1]$, are zero mean uncorrelated complex Gaussian random variables with normalized power such that $\sum_{l=0}^{L-1} \mathbb{E}\left[|g_l|^2\right] = 1$, where $\mathbb{E}$ is the expectation operator. Therefore $G_0, G_1, \ldots, G_{N_p-1}$ are jointly complex Gaussian random variables. We also assume that the channel is slowly varying and can be considered constant over the duration of a symbol. Our analysis is valid for any delay profile model. However, for numerical results, to account for the non-zero cross correlation between fading experienced by the subcarriers we adopt Jakes' model [34] while assuming zero Doppler frequency and channel delay spread of α, we have

$$\mathbb{E}\left[G_i G_j^*\right] = \frac{1}{1 + j2\pi\alpha(f_i - f_j)}. \tag{3.3}$$

We also assume that intersymbol interference is completely avoided by selecting cyclic prefix duration $T_g > \tau_{L-1}$ and perfect time synchronization is achieved. The received signal $r(t)$ after removing the cyclic prefix is given by

$$r(t) = \frac{1}{\sqrt{N_p}} \sum_{n=0}^{N_p-1} G_n \, b\,(t) \, c[n] \mathrm{e}^{j2\pi f_n t} + \eta\,(t)$$

where $\eta\,(t)$ represents additive white Gaussian noise (AWGN) with two sided power spectral density of N_0. Note that the received signal does not include any contribution from any other transmitter since we only consider a single transmitter receiver pair. The effects of interference from other transmitters is analyzed in Chapter 5.

The received signal is decoded by the conventional correlation receiver described earlier with maximal-ratio combining. Let Z represent the receiver decision variable then

$$Z = \sum_{m=0}^{N_p-1} \frac{1}{T} \int_0^T G_m^* \, c[m] \mathrm{e}^{-j2\pi f_m t} \, r(t) \mathrm{d}t$$

where G_m^* is the complex conjugate of the channel transfer function of the mth subcarrier. We assume perfect frequency synchronization between the transmitter and receiver and hence zero frequency offset (i.e. $f_m = f_n$). Performance degradation due to frequency offset is analyzed in Chapter 4.

The decision variable Z at the receiver can be written as

$$Z = \sum_{m=0}^{N_p-1} \frac{1}{T} \int_0^T G_m^* \, c[m] \mathrm{e}^{-j2\pi f_m t} \left(\frac{1}{\sqrt{N_p}} \sum_{n=0}^{N_p-1} G_n \, b\,(t) \, c[n] \mathrm{e}^{j2\pi f_n t} \mathrm{e}^{j\phi} + \eta\,(t) \right) \mathrm{d}t$$

where ϕ is the phase difference between transmitter and receiver's oscillator. The decision variable can be separated into three distinct components $Z = S + I + N$, where S is the desired signal component, I is the interference component and N

is the noise component, these are given as

$$S = b\left(t\right)\frac{1}{\sqrt{N_p}}\mathrm{e}^{j\phi}\sum_{m=0}^{N_p-1}\left|G_m\right|^2$$

$$I = \sum_{m=0}^{N_p-1}\frac{1}{T}G_m^*\,c[m]\frac{1}{\sqrt{N_p}}\sum_{n=0,n\neq m}^{N_p-1}G_n\,b\left(t\right)c[n]\mathrm{e}^{j\phi}\int_0^T\mathrm{e}^{j2\pi(f_n-f_m)t}\mathrm{d}t$$

$$N = \sum_{m=0}^{N_p-1}G_m^*\,c[m]\frac{1}{T}\int_0^T\mathrm{e}^{-j2\pi f_m t}\eta\left(t\right)\mathrm{d}t$$

where it was possible to take the channel gains $\left(G_0,\ldots,G_{N_p-1}\right)$ out of the integrals due to the slowly varying channel assumption.

The interference component I is always zero because the integral

$$\int_0^T\mathrm{e}^{j2\pi(f_n-f_m)t}\mathrm{d}t\to 0$$

as subcarriers are orthogonal to each other and there is no frequency offset.

When we condition on $G_0,\ldots G_{N_p-1}$ then Z becomes a conditional Gaussian random variable and the conditional mean is

$$\mathbb{E}\left[Z|G_0,\ldots,G_{N_p-1}\right] = \sqrt{\frac{E_s}{TN_p}}\left(\sum_{m=0}^{N_p-1}\left|G_m\right|^2\right).$$

The conditional variance of Z can be shown as $\sum_{m=0}^{N_p-1}\left|G_m\right|^2\frac{N_0}{T}$. The instantaneous SINR is then

$$\mathrm{SINR} = \frac{\frac{E_s}{TN_p}\left(\sum_{m=0}^{N_p-1}\left|G_m\right|^2\right)^2}{\sum_{m=0}^{N_p-1}\left|G_m\right|^2\frac{N_0}{T}}$$

which can be simplified into

$$\mathrm{SINR} = \frac{E_s}{N_p N_0} \sum_{m=0}^{N_p-1} |G_m|^2. \tag{3.4}$$

The signal to interference and noise ratio in (3.4) can now be used to find the spectral efficiency.

3.1.1 Spectral Efficiency Analysis

The spectral efficiency of the system can be found using (3.4) as

$$\mathrm{C} = \frac{1}{N_p} \mathbb{E}\left[\log_2\left(1 + \frac{E_s}{N_p N_0} \sum_{m=0}^{N_p-1} |G_m|^2\right)\right] \tag{3.5}$$

where the expectation is over $\mathbf{G} = \left[G_0, \ldots, G_{N_p-1}\right]^{\mathrm{T}}$ and $\mathbf{G}$ is a complex random vector that represents complex correlated channel gains. Since we are assuming Rayleigh fading $\mathbf{G}$ is a zero-mean complex Gaussian random vector having pdf

$$f(\mathbf{G}) = \frac{1}{\pi^{N_p} |\mathbf{\Lambda}|} \mathrm{e}^{-\mathbf{G}^h \mathbf{\Lambda}^{-1} \mathbf{G}}$$

where $\mathbf{\Lambda} = \mathbb{E}\left[\mathbf{G}^h \mathbf{G}\right]$ is the $N_p \times N_p$ complex covariance matrix and the superscript h denotes Hermitian transposition, the entries of this matrix are given in (3.3). The term $\frac{1}{N_p}$ in (3.5) appears because the MC-CDMA signal takes N_p times more bandwidth than an unspread signal.

The direct method to solve (3.5) would require finding pdf of the sum $\sum_{m=0}^{N_p-1} |G_m|^2$ while this summation can not be considered as chi square distributed because of the correlation that exists between G_m's. Furthermore, even if the pdf of the summation is known it would require N_p-fold integrations making it too complex. However, we can invoke [35, Lemma 1] to rewrite (3.5) in a more desirable

form as

$$\mathrm{C} = \frac{\log_2 \mathrm{e}}{N_p} \int_0^\infty \frac{1}{z} \left(1 - \mathbb{E} \left[\exp \left(-z \frac{E_s}{N_p N_0} \sum_{m=0}^{N_p-1} |G_m|^2 \right) \right] \right) \mathrm{e}^{-z} \mathrm{d}z$$

where the Gaussian quadratic forms $\sum_{m=0}^{N_p-1} |G_m|^2$ appear only in the exponent. The integration was shown in [35] to be converging as the integrand is always bounded, non-negative and continuous in the range of integration. Now, known results for the MGF of the Gaussian quadratic forms [36, eq. (4a)] can be applied to obtain the following explicit expression for the spectral efficiency of the multicarrier CDMA

$$\mathrm{C} = \frac{\log_2 \mathrm{e}}{N_p} \int_0^\infty \frac{1}{z} \left(1 - \frac{1}{\left| \mathbf{I}_{N_p} + z \frac{E_s}{N_p N_0} \mathbf{\Lambda} \right|} \right) \mathrm{e}^{-z} \mathrm{d}z \tag{3.6}$$

where $\mathbf{I}_{N_p}$ is $N_p \times N_p$ identity matrix.

3.1.2 Numerical Results

In Fig. 3.1 numerical calculation of spectral efficiency are shown, analysis results were computed using (3.6). In order to validate these new results we also include Monte Carlo simulation using (3.5) with 10^5 iterations. A 312.5 kHz frequency separation between neighboring subcarriers (IEEE 802.11a [37]) and channel delay spread (α) of 0.1μs is used. The results show that spectral efficiency decreases with N_p, this is expected as higher N_p means more spreading, which results in more bandwidth consumption and in the absence of any other transmitter this results in reduction of spectral efficiency.

Fig. 3.2 shows the effects of normalized delay spread (σ) on spectral efficiency for 64 number of subcarriers and E_s/N_o of 20dB, where the delay spread is normalized to the symbol time i.e. $\sigma = \alpha/T$. Higher values of σ result in smaller coherence bandwidth and hence lower correlation between subcarriers, resulting

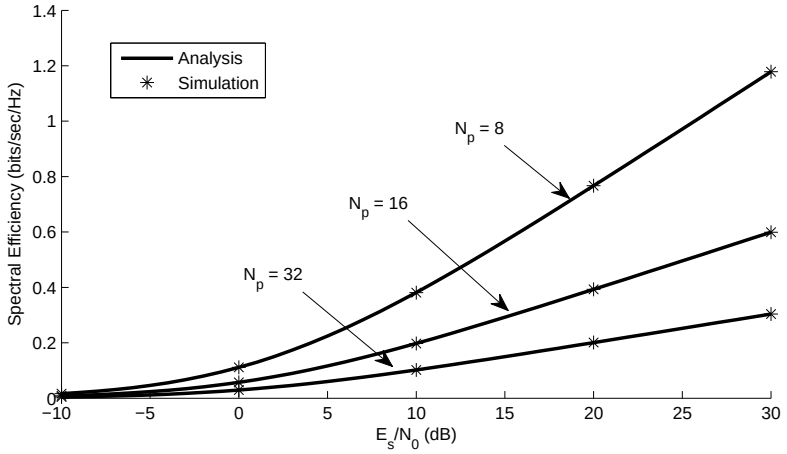

Figure 3.1: Spectral Efficiency of MC-CDMA versus E_s/N_o for some values of $N_p = N_c$.

in better spectral efficiency. This shows correlation between subcarriers reduces the spectral efficiency of the system. This confirms known results that in Rayleigh fading correlation reduces capacity [38, 39].

3.2 Multi-Carrier DS-CDMA

The transmitted MC DS-CDMA signal can be represented during an arbitrary signaling interval as

$$s(t) = \sum_{l=1}^{N_c} b_l(t)\, c(t)\, \mathrm{e}^{j2\pi f_l t}, \quad t \in [-T_g, N_c T] \tag{3.7}$$

where N_c is the number of subcarriers which is not necessarily equal to the length of the spreading code N_p. Also note that the signal interval has increased from T to $N_c T$, this is because of the serial to parallel conversion. The frequency separation between adjacent subcarriers is atleast $\frac{1}{T_c}$, where T_c is the chip duration, in terms of symbol duration T, it is $\frac{N_p}{N_c T}$, this is to avoid intercarrier interference as discussed earlier.

The transmitted signal is subjected to multipath fading environment given in

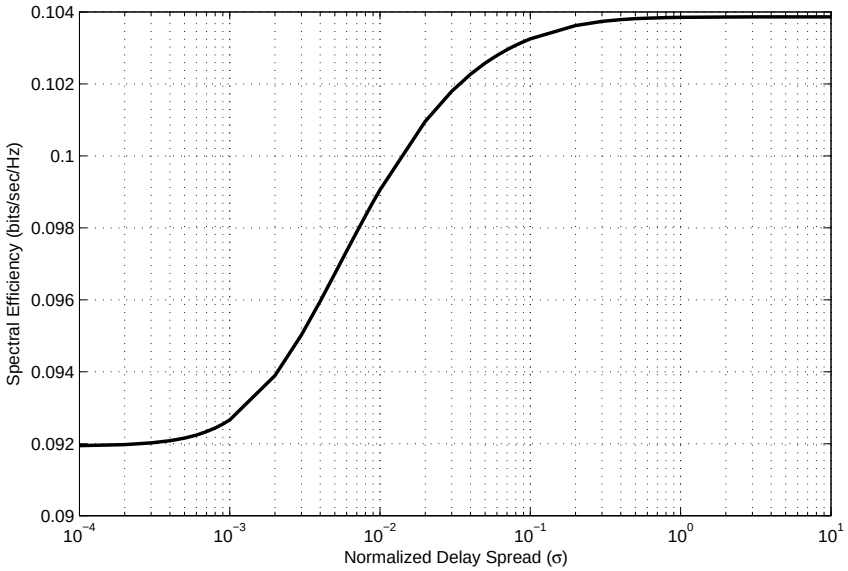

Figure 3.2: Spectral efficiency of MC-CDMA versus normalized delay spread (σ).

(3.2) and the resultant received signal after removing the cyclic prefix is given as

$$r(t) = \sum_{l=1}^{N_c} G_l \, b_l \, (t) \, c \, (t) \, \mathrm{e}^{j2\pi f_l t} + \eta \, (t) \, .$$

The received signal is decoded by the conventional correlation receiver described earlier with maximal-ratio combining. Let Z_1 represent the receiver decision variable for the first symbol of the first subcarrier then

$$Z_1 = \frac{1}{N_c T} \int_0^{N_c T} G_1^* c \, (t) \, \mathrm{e}^{-j2\pi f_1 t} \, r(t) \mathrm{d}t.$$

Note that the desired output of this decision variable is the first symbol. The decision variable for the other subcarriers will be similar and is avoided for brevity.

The decision variable Z_1 at the receiver is given as

$$Z_1 = \frac{1}{N_c T} \int_0^{N_c T} G_1^* c\left(t\right) \mathrm{e}^{-j2\pi f_1 t} \left(\sum_{l=1}^{N_c} G_l b_l\left(t\right) c\left(t\right) \mathrm{e}^{j2\pi f_l t} \mathrm{e}^{j\phi} + \eta\left(t\right) \right) \mathrm{d}t.$$

This decision variable can be separated into three distinct components

$$S = \frac{1}{N_c T} \int_0^{N_c T} G_1^* c\left(t\right) \mathrm{e}^{-j2\pi f_1 t} G_1\, b_1\left(t\right) c\left(t\right) \mathrm{e}^{j2\pi f_1 t} \mathrm{d}t$$

$$I = \frac{1}{N_c T} \int_0^{N_c T} G_1^* c\left(t\right) \mathrm{e}^{-j2\pi f_1 t} \sum_{l=2}^{N_c} G_l b_l\left(t\right) c\left(t\right) \mathrm{e}^{j2\pi f_l t} \mathrm{e}^{j\phi} \mathrm{d}t$$

$$N = \frac{1}{N_c T} G_1^* c\left(t\right) \int_0^{N_c T} \mathrm{e}^{-j2\pi f_1 t} \eta\left(t\right) \mathrm{d}t.$$

The desired signal component simplifies into

$$S = \left|G_1\right|^2 b_1\left(t\right) \tag{3.8}$$

while the interference component again disappears similar to MC-CDMA because the integration $\int_0^{N_c T} \mathrm{e}^{j2\pi(f_l - f_1)t} \mathrm{d}t \to 0$ as orthogonal subcarriers are used. When we condition on G_1, Z_1 becomes a Gaussian random variable with conditional mean $\sqrt{\frac{E_s}{N_c T}} \left|G_1\right|^2$ and the conditional variance $\frac{1}{N_c T} \left|G_1\right|^2 N_0$. Hence the instantaneous signal to interference and noise ratio becomes

$$\mathrm{SINR} = \frac{\frac{E_s}{N_c T} \left|G_1\right|^4}{\frac{1}{N_c T} \left|G_1\right|^2 N_0}$$

which simplifies into

$$\mathrm{SINR} = \frac{E_s \left|G_1\right|^2}{N_0}. \tag{3.9}$$

The signal to interference and noise ratio in (3.9) can now be used to analyze

the spectral efficiency.

3.2.1 Spectral Efficiency Analysis

The spectral efficiency of the system can be calculated using (3.9) as

$$\mathrm{C} = \frac{1}{N_p}\mathbb{E}\left[\log_2\left(1+\frac{E_s\left|G_1\right|^2}{N_0}\right)\right].$$

The expectation is over G_1 and since we are considering Rayleigh fading it is a zero mean complex Gaussian random variable and$|G_1|$ is a Rayleigh distributed random variable. The expectation can be solved in a similar way as for MC-CDMA to give for spectral efficiency

$$\mathrm{C} = \frac{1}{N_p}\log_2\mathrm{e}\int_0^\infty\left(\frac{1}{z+\frac{N_0}{E_s}}\right)\mathrm{e}^{-z}\mathrm{d}z. \tag{3.10}$$

We can now use (3.10) to calculate spectral efficiency numerically

3.2.2 Numerical Results

The spectral efficiency of MC DS-CDMA is plotted in (3.10) for some values of processing gain N_p against symbol energy to noise ratio E_s/N_0. The spectral efficiency monotonically increases with E_s/N_0 as expected. The decrease in spectral efficiency when N_p is increased is because MC DS-CDMA occupies more bandwidth when N_p is increased, without any increase in the capacity for a single user. However the benefit of increasing N_p, which can not be seen in this analysis, is that it can then support more concurrent users.

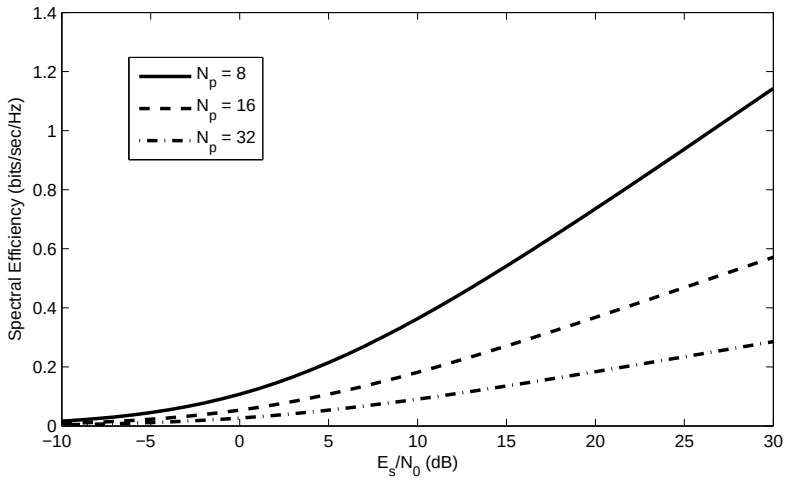

Figure 3.3: Spectral Efficiency of MC DS-CDMA versus E_s/N_o for some values of N_p.

3.3 Multi-Tone CDMA

The transmitted MT-CDMA signal can be represented during an arbitrary signaling interval as

$$s(t) = \sum_{l=1}^{N_c} b_l\,(t)\,c\,(t)\;\mathrm{e}^{j2\pi f_l t}, \quad t \in [-T_g, N_c T] \tag{3.11}$$

which is the same as (3.7). The frequency separation between adjacent subcarriers is however different and is atleast $\frac{1}{N_c T}$ which is equal to $\frac{1}{N_p T_c}$.

The transmitted signal is subjected to multipath fading given in (3.2) and the resultant received signal after removing the cyclic prefix is given as

$$r(t) = \sum_{l=1}^{N_c}\sum_{i=0}^{L-1} g_i\, b_l\,(t)\,c\,(t - i\tau)\,\mathrm{e}^{j2\pi f_l (t-i\tau)} + \eta\,(t)\,.$$

The received signal is decoded by the rake receivers after being demodulated. The receiver decision variable for the first symbol Z_1 that was modulating the first subcarrier can be shown as

$$Z_1 = \sum_{m=0}^{L_F-1} \frac{1}{N_c T} \int_0^{N_c T} g_m^* c(t - m\tau) \mathrm{e}^{-j2\pi f_1 t} r(t) \mathrm{d}t$$

where L_F is the number of fingers in the rake receiver. The decision variables for the subsequent symbols that modulate other subcarriers will be similar. In this thesis we only consider full rake receiver, which assigns a finger to each resolvable propagation path and hence $L_F = L$.

The decision variable Z_1 at the receiver is given as

$$Z_1 = \sum_{m=0}^{L-1} \frac{1}{N_c T} \int_0^{N_c T} g_m^* c(t-m\tau) \mathrm{e}^{-j2\pi f_1 t} \left(\sum_{l=1}^{N_c} \sum_{i=0}^{L-1} g_i \, b_l \left(t\right) c \left(t - i\tau\right) \mathrm{e}^{j2\pi f_l (t - i\tau)} + \eta \left(t\right) \right) \mathrm{d}t.$$

This decision variable can also be separated into four distinct components, desired signal (S), self interference of the rake combiner (I_1), intercarrier interference (I_2) and noise (N) given as

$$S = b_1 \left(t\right) \sum_{i=0}^{L-1} \left|g_i\right|^2$$

$$I_1 = b_1 \left(t\right) \sum_{k=0}^{L-1} g_k^* \sum_{l=0, l \neq k}^{L-1} g_l \frac{1}{N_p} \sum_{m=1}^{N_p} c \left[m\right] c \left[m + \left(m - l\right) \tau\right]$$

$$\begin{aligned} I_2 = & \sum_{i=2}^{N_c} b_i \left(t\right) \sum_{k=0}^{L-1} \left|g_k\right|^2 \frac{1}{N_c T} \int_0^{N_c T} \mathrm{e}^{-j2\pi (f_i - f_1) t} \mathrm{d}t \\ & + \sum_{i=2}^{N_c} b_i \left(t\right) \sum_{k=0}^{L-1} g_k^* \sum_{l=0, l \neq k}^{L-1} g_l \frac{1}{N_c T} \int_0^{N_c T} c(t) c(t + \left(k - l\right) \tau) \mathrm{e}^{-j2\pi (f_i - f_1) t} \mathrm{d}t \end{aligned}$$

$$N = \sum_{i=0}^{L-1} g_i^* \frac{1}{N_c T} \int_0^{N_c T} c(t) \mathrm{e}^{-j2\pi f_1 t} \eta \left(t\right) \mathrm{d}t.$$

Note that in I_1 the summation $\sum_{i=1}^{N_p} c[i]\, c[i+(i-k)\,\tau] \neq 0$ in general as there exists non-zero auto-correlation in the spreading signals. However, all terms in the summation are independent of each other and hence the summation as a whole can be considered as a Gaussian random variable with zero mean and variance of N_p. I_1 can not be considered as a Gaussian because of the correlation that exists in g_i's but when we condition on the channel gains (g_i) I_1 becomes a zero mean Gaussian random variable with conditional variance given as

$$\mathrm{Var}\left\{I_1|g_0,\ldots g_{L-1}\right\} = \frac{E_s}{N_cT}\sum_{k=0}^{L-1}|g_k|^2\sum_{l=0,l\neq k}^{L-1}|g_l|^2\,\frac{1}{N_p}.$$

To solve for I_2, note that the first term is always zero as the integration is over a complete cycle i.e.

$$\int_0^{N_cT}\mathrm{e}^{-j2\pi(f_i-f_1)t}\mathrm{d}t = \left.\frac{\mathrm{e}^{-j2\pi\left(\frac{i-1}{N_cT}\right)t}}{-j2\pi\left(\frac{i-1}{N_cT}\right)}\right|_0^{N_cT}$$
$$= \frac{\mathrm{e}^{-j2\pi i}-1}{-j2\pi\left(\frac{i-1}{N_cT}\right)} = \frac{1-1}{-j2\pi\left(\frac{i-1}{N_cT}\right)} = 0.$$

The integration in the second term can be divided into a summation of integrals over chip durations i.e.

$$\int_0^{N_cT} c(t)\, c(t+(k-l)\,\tau)\,\mathrm{e}^{-j2\pi(f_i-f_1)t}\mathrm{d}t = \sum_{i=1}^{Np} c(t)\, c(t+(k-l)\,\tau)\int_{(i-1)T_c}^{iT_c}\mathrm{e}^{-j2\pi\left(\frac{i-1}{N_cT}\right)t}\mathrm{d}t$$

the benefit of this division is that the integration on the right can now be solved easily. Please also note that the limits of summation and integrals are correct as $N_cT = N_pT_c$. We now have for I_2

$$I_2 = \sum_{i=2}^{N_c} b_i(t)\sum_{k=0}^{L-1} g_k^*\sum_{l=0,l\neq k}^{L-1} g_l c(t)c(t+(k-l)\,\tau)\mathrm{e}^{-j\frac{2\pi i}{N_p}(i-1)}\mathrm{e}^{j\frac{\pi}{N_p}(i-1)}\frac{1}{N_p}\mathrm{sinc}\left(\frac{\pi}{N_p}(i-1)\right).$$

The conditional variance of I_2 can be calculated as

$$\mathrm{Var}\left\{I_2|g_0,\ldots g_{L-1}\right\} = \frac{E_s}{N_cT}\sum_{i=2}^{N_c}\sum_{k=0}^{L-1}|g_k|^2\sum_{l=0,l\neq k}^{L-1}|g_l|^2\frac{1}{N_p}\mathrm{sinc}^2\left(\frac{\pi}{N_p}(i-1)\right).$$

The variance of I_1 and I_2 can be combined to give a single expression of

$$I = \frac{E_s}{N_cT}\sum_{i=1}^{N_c}\sum_{k=0}^{L-1}|g_k|^2\sum_{l=0,l\neq k}^{L-1}|g_l|^2\frac{1}{N_p}\mathrm{sinc}^2\left(\frac{\pi}{N_p}(i-1)\right)$$

where $I = I_1 + I_2$. We can now construct the instantaneous signal to interference and noise ratio as

$$\mathrm{SINR} = \frac{\frac{E_s}{N_cT}\left(\sum_{i=0}^{L-1}|g_i|^2\right)^2}{\frac{E_s}{N_cT}\sum_{i=1}^{N_c}\sum_{k=0}^{L-1}|g_k|^2\sum_{l=0,l\neq k}^{L-1}|g_l|^2\frac{1}{N_p}\mathrm{sinc}^2\left(\frac{\pi}{N_p}(i-1)\right)+\frac{N_0}{N_cT}\sum_{i=0}^{L-1}|g_i|^2}. \quad (3.12)$$

The spectral efficiency of the MT-CDMA system can now be calculated using the above instantaneous SINR expression and is analyzed in the next section.

3.3.1 Spectral Efficiency Analysis

The spectral efficiency of the system can now be calculated using (3.12) as

$$\mathrm{C} = \frac{N_c}{N_c+N_p-1}\mathbb{E}\left[\log_2\left(1+\left(\sum_{i=0}^{L-1}|g_i|^2\right)^2\left(\sum_{i=1}^{N_c}\sum_{k=0}^{L-1}|g_k|^2\sum_{l=0,l\neq k}^{L-1}|g_l|^2\frac{1}{N_p}\right.\right.\right.$$
$$\left.\left.\left.\times\mathrm{sinc}^2\left(\frac{\pi}{N_p}(i-1)\right)+\frac{N_0}{E_s}\sum_{i=0}^{L-1}|g_i|^2\right)^{-1}\right)\right] \quad (3.13)$$

where the expectation is over $g_0, g_1, \ldots, g_{L-1}$. The term $\frac{N_c}{N_c+N_p-1}$ appears because an MT-CDMA signal occupies $\frac{N_c+N_p-1}{N_c}$ times more bandwidth than an unspread signal. The direct method to solve (3.13) requires L-fold integrations making it

too complex. To simplify the analysis we apply Jensen inequality to (3.13) and rearrange terms in the denominator to get

$$\mathrm{C} \geq \frac{N_c}{N_c+N_p-1}\mathbb{E}\left[\log_2\left(1+\frac{\sum_{i=0}^{L-1}|g_i|^2}{\sum_{i=0}^{L-1}|g_i|^2\sum_{i=1}^{N_c}\frac{1}{N_p}\mathrm{sinc}^2\left(\frac{\pi}{N_p}(i-1)\right)\rho+\frac{N_0}{E_s}}\right)\right] \tag{3.14}$$

where

$$\rho=\mathbb{E}\left[\frac{\sum_{k=0}^{L-1}\sum_{l=0,l\neq k}^{L-1}|g_k|^2|g_l|^2}{\sum_{i=0}^{L-1}|g_i|^2\sum_{i=0}^{L-1}|g_i|^2}\right]$$

which is similar to the orthogonality factor in [40] where solution of the expectation is also given, which is reproduced here as

$$\rho=1-\int_0^{\infty}\left\{\sum_{k=0}^{L-1}\psi_k(z)\prod_{l=0,l\neq k}^{L-1}\phi_l(z)\right\}z\,\mathrm{d}z \tag{3.15}$$

and for Rayleigh fading with uniform delay profile, the integration in (3.15) can be solved to get [40, eq. (15)]

$$\rho=\frac{L-1}{L+1}.$$

We can now invoke [35, Lemma 1] to rewrite (3.14) in a more desirable form as

$$\mathrm{C}\geq\frac{\log_2\mathrm{e}\,N_c}{N_c+N_p-1}\int_0^{\infty}\frac{1}{z}\left(\mathbb{E}\left[\exp\left(-z\hat{\chi}\sum_{i=0}^{L-1}|g_i|^2\right)\right]-\mathbb{E}\left[\exp\left(-z\left(1+\hat{\chi}\right)\times\sum_{i=0}^{L-1}|g_i|^2\right)\right]\right)\exp\left(-z\frac{N_0}{E_s}\right)\mathrm{d}z$$

where

$$\hat{\chi} = \sum_{i=1}^{N_c} \frac{1}{N_p} \mathrm{sinc}^2 \left(\frac{\pi}{N_p} (i-1) \right) \rho.$$

Now known results for the MGF of the Gaussian quadratic forms [36, eq. (4a)] can be applied to obtain the following explicit expression for the lower bound on the spectral efficiency of the multitone CDMA

$$\mathrm{C} \geq \frac{\log_2 \mathrm{e}\, N_c}{N_c + N_p - 1} \int_0^\infty \frac{1}{z} \left(\frac{1}{|\mathbf{I}_L + z\hat{\chi}\mathbf{\Lambda}|} - \frac{1}{|\mathbf{I}_L + z\,(1+\hat{\chi})\,\mathbf{\Lambda}|} \right) \exp\left(-z \frac{N_0}{E_s} \right) \mathrm{d}z \tag{3.16}$$

where $\mathbf{I}_L$ is $L \times L$ identity matrix and $\mathbf{\Lambda}$ is $L \times L$ correlation matrix where a typical element is given by$\Lambda_{ij} = \mathrm{E}\left[|g_i|\,|g_j|\right]$. Since all g_k's are i.i.d random variables with zero mean $\mathbf{\Lambda} = \frac{1}{L}\mathbf{I}_L$, this simplifies (3.16) into

$$\mathrm{C} \geq \frac{\log_2 \mathrm{e}\, N_c}{N_c + N_p - 1} \int_0^\infty \frac{1}{z} \left(\frac{1}{\left(1 + \frac{z}{L}\hat{\chi}\right)^L} - \frac{1}{\left(1 + \frac{z}{L}\,(1+\hat{\chi})\right)^L} \right) \exp\left(-z \frac{N_0}{E_s} \right) \mathrm{d}z. \tag{3.17}$$

Equation (3.17) is the desired spectral efficiency expression for MT-CDMA in the presence of multipath fading and noise.

3.3.2 Numerical Results

The spectral efficiency bound in (3.17) is plotted in Fig. 3.4 along with Monte Carlo simulation of the exact spectral efficiency expression in (3.13). The results are calculated for $N_p = 1024$ and $L = 16$. The spectral efficiency monotonically increases with E_s/N_0 as expected. The spectral efficiency also increases when the number of subcarriers (N_c) is increased this is counter intuitive as intercarrier interference (ICI) increases with N_c and hence spectral efficiency should decrease. However, on a closer look, with more subcarriers the spectrum is getting better utilized and this is captured by the factor $\frac{N_c}{N_c+N_p-1}$, which increases with N_c and the increase is large enough to counter the decrease due to ICI.

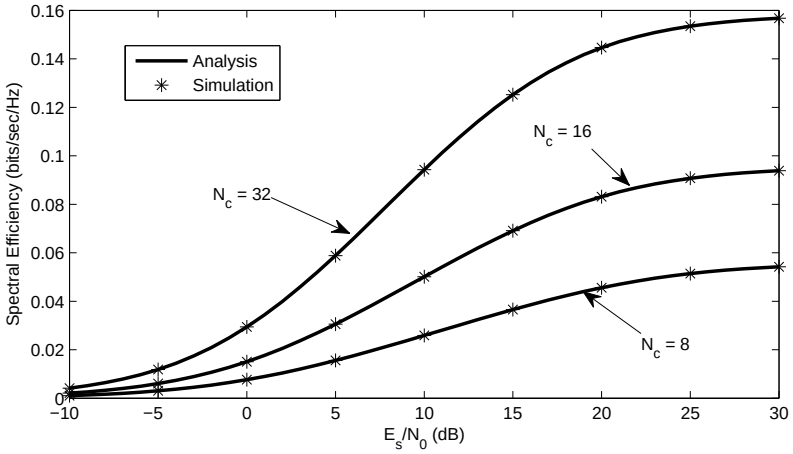

Figure 3.4: Spectral Efficiency of multitone CDMA versus E_s/N_o for some values of N_c.

3.4 Chapter Conclusion

In this chapter we found simple expressions for the spectral efficiency of the three multicarrier schemes. These are new expressions which are not available in the published literature. In the cases of MC-CDMA and MT-CDMA Jensen inequality was used to generate lower bounds to simplify the analysis, therefore we have also shown simulation results for those two schemes to confirm the tightness of the bound given by our expressions.

Fig. 3.5 shows a comparison of the three schemes against E_s/N_0 for $N_p = 8$, $N_c = 8$ and $L = 8$. MT-CDMA is the clear winner at most values of E_s/N_0 except at very high values i.e. $E_s/N_0 > 25$dB. This is due to the rake combiner in the MT-CDMA receiver which offers diversity combining of independent time-shifted paths while the diversity combining in MC-CDMA is of correlated frequency-shifted paths, furthermore, MT-CDMA gives a better spectrum utilization. However, at high values of E_s/N_0, MT-CDMA becomes an interference limited system as N_0/E_s becomes negligible in comparison to the interference component in (3.14), while in MC-CDMA and MC DS-CDMA there is no source

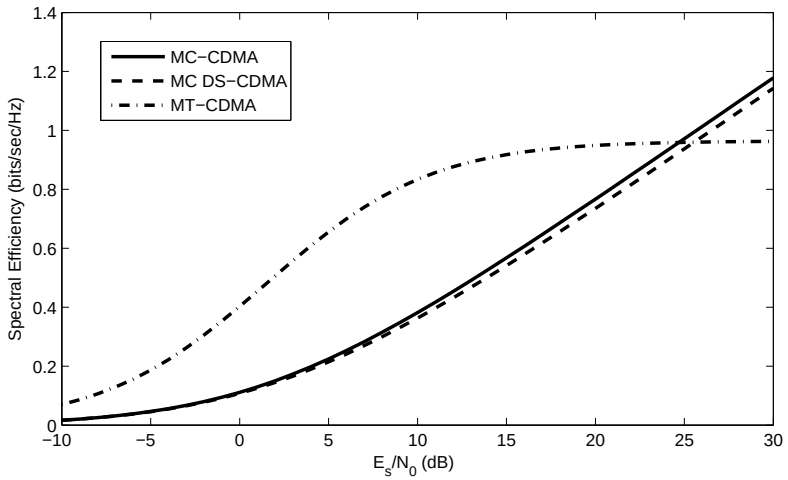

Figure 3.5: Spectral Efficiency of MC-CDMA, MC DS-CDMA and MT-CDMA versus E_s/N_0.

of interference. MC-CDMA also has higher spectral efficiency than MC DS-CDMA at all values of E_s/N_0 as it also offers frequency diversity while MC DS-CDMA offers no diversity. This result, however, is not a complete picture and we can not confirm MT-CDMA to be the best among the three schemes as we still have to see their robustness to carrier frequency offset and asynchronous interferers.

Chapter 4

Spectral Efficiency Degradation of Multicarrier CDMA due to Frequency Offset

A drawback of multicarrier CDMA systems is that they suffer from the inter-carrier interference (ICI) due to frequency offset. The frequency offset appears due to the difference in the frequency of the local oscillators in transmitter and receiver and the Doppler shift in frequency due to the motion of transmitter and/or receiver. Performance degradation due to the frequency offset has been extensively studied [41–50], where different methods have been proposed to estimate this offset [51–55] and to mitigate its effects [56–59]. In [41, 45–48, 60] expressions for bit error rate (BER) are calculated and in [44] BER is found with simulation. In [49, 50] the signal-to-noise (SNR) degradation is calculated while assuming ideal channel condition.

In most previous performance analyses the ICI is considered to be a purely Gaussian distributed random variable and uncorrelated with the useful signal component. However, this Gaussian approximation is not accurate due to the

correlation in fading experienced by the adjacent subcarriers and is known to over estimates the performance at high SNR values and when the number of subcarriers is small [41–43]. Furthermore, the resultant ICI due to the frequency offset is highly correlated with the useful signal component. This brings mathematical complexity in the analysis as the signal to interference and noise ratio (SINR) becomes a ratio of correlated random variables. Recently, in [41] conditional Gaussian approximation was used for ICI but their focus was on error rates. In this chapter we analyze the degradation in spectral efficiency due to frequency offset which to our knowledge has not been analyzed. We base our analysis on accurate conditional Gaussian approximation for ICI and derive a new simple expression for spectral efficiency while considering the fading experienced by the subcarriers to be correlated.

We follow the same model and assumptions as in Chapter 3, the transmitted signals for MC-CDMA, MC DS-CDMA and MT-CDMA schemes are the same as given in 2.2, 2.3 and 2.4 respectively. The spectral efficiency of the three multicarrier CDMA schemes are analyzed in detail in the following sections.

4.1 MC-CDMA

The receiver decision variable for MC-CDMA in AWGN is given as

$$Z = \sum_{m=0}^{N_p-1} \frac{1}{T} \int_0^T G_m^* \, c[m] \mathrm{e}^{-j2\pi f_m t} \left(\frac{1}{\sqrt{N_p}} \sum_{n=0}^{N_p-1} G_n \, b\left(t\right) c[n] \mathrm{e}^{j2\pi f_n t} \mathrm{e}^{j\phi} \mathrm{e}^{j2\pi \frac{\Delta}{T} t} + \eta\left(t\right) \right) \mathrm{d}t \tag{4.1}$$

where Δ is the carrier frequency offset normalized to the frequency separation between adjacent subcarriers, which, in the case of MC-CDMA is one over symbol duration i.e. $1/T$. In (4.1) $b\left(t\right)$ is the information bearing signal, $c\left[n\right]$ is the nth component of the spreading signal, N_p is the total number of subcarriers, f_n is the frequency of the nth subcarrier and $\eta\left(t\right)$ is the AWGN component. The decision

variable Z can be separated into three distinct components $Z = S + I + N$, where S is the desired signal component, I is the intercarrier interference (ICI) component and N is the noise component, these are given respectively as

$$S = b\left(t\right)\frac{1}{\sqrt{N_p}}\sum_{m=0}^{N_p-1}\left|G_m\right|^2\frac{1}{T}\int_0^T \mathrm{e}^{j2\pi\frac{\triangle}{T}t}\mathrm{d}t$$

$$I = b\left(t\right)\frac{1}{\sqrt{N_p}}\sum_{m=0}^{N_p-1}\sum_{n=0,n\neq m}^{N_p-1} c[m]c[n]\,G_m^* G_n\frac{1}{T}\int_0^T \mathrm{e}^{j2\pi\frac{(n-m)}{T}t}\mathrm{e}^{j2\pi\frac{\triangle}{T}t}\mathrm{d}t$$

$$N = \sum_{m=0}^{N_p-1} G_m^*\, c[m]\frac{1}{T}\int_0^T \mathrm{e}^{-j2\pi f_m t}\eta\left(t\right)\mathrm{d}t.$$

The integrations in the signal and interference components can be easily solved to give

$$S = \frac{b\left(t\right)}{\sqrt{N_p}}\sum_{m=0}^{N_p-1}\left|G_m\right|^2\mathrm{e}^{j\pi\triangle}\mathrm{sinc}\left(\pi\triangle\right)$$

$$I = \frac{b\left(t\right)}{\sqrt{N_p}}\sum_{m=0}^{N_p-1}\sum_{n=0,n\neq m}^{N_p-1} c[m]c[n]\,G_m^* G_n\mathrm{e}^{j\pi(n-m+\triangle)}\mathrm{sinc}\left(\pi\left(n-m+\triangle\right)\right). \quad (4.2)$$

Note that the ICI component is due to the frequency offset Δ only and it can be easily shown that I goes to zero in (4.2) when $\Delta = 0$. As far as the statistics of the ICI in (4.2) are concerned note that it is a large sum of correlated random variables and because of the correlation the central limit theorem can not be applied hence the assumption of I being a Gaussian random variable can not be justified. However if we condition on $G_0, \ldots G_{N_p-1}$ then the central limit theorem is applicable as $c[m]$ and $c[n]$ are independent random variables. We therefore approximate Z as a conditional Gaussian random variable, conditioned on $G_0, \ldots G_{N_p-1}$ and the conditional mean is

$$\mathbb{E}\left[Z|G_0,\ldots,G_{N_p-1}\right] = \sqrt{\frac{E_s}{T\,N_p}}\sum_{m=0}^{N_p-1}|G_m|^2\,\mathrm{sinc}(\pi\triangle)$$

and the conditional variance of Z can be calculated as

$$\mathrm{Var}\left[Z|G_0,\ldots,G_{N_p-1}\right] = \sum_{m=0}^{N_p-1}\sum_{n=0,n\neq m}^{N_p-1}\frac{E_s}{T\,N_p}|G_m|^2|G_n|^2\,\mathrm{sinc}^2\left(\pi\left(n-m+\triangle\right)\right) + \sum_{m=0}^{N_p-1}|G_m|^2\frac{N_0}{T}.$$

The instantaneous SINR is therefore a random variable given by the ratio

$$\mathrm{SINR} = \frac{\frac{E_s}{T\,N_p}\left(\mathrm{sinc}(\pi\triangle)\sum_{m=0}^{N_p-1}|G_m|^2\right)^2}{\sum_{m=0}^{N_p-1}\sum_{n=0,n\neq m}^{N_p-1}\frac{E_s}{T\,N_p}|G_m|^2|G_n|^2\,\mathrm{sinc}^2\left(\pi\left(n-m+\triangle\right)\right) + \sum_{m=0}^{N_p-1}|G_m|^2\frac{N_0}{T}}$$

which can be simplified into

$$\mathrm{SINR} = \frac{\left(\sum_{m=0}^{N_p-1}|G_m|^2\right)^2}{\sum_{m=0}^{N_p-1}\sum_{n=0,n\neq m}^{N_p-1}|G_m|^2|G_n|^2\left(\frac{\Delta}{n-m+\Delta}\right)^2 + \frac{N_0}{E_s}N_p\left(\frac{\pi\triangle}{\sin(\pi\triangle)}\right)^2\sum_{m=0}^{N_p-1}|G_m|^2}. \quad (4.3)$$

The spectral efficiency of the system depends on the SINR in (4.3) and is analyzed in the next section.

4.1.1 Spectral Efficiency Analysis

The spectral efficiency can be evaluated by using (4.3) and the well known Shannon's capacity expression as

$$\mathrm{C} = \frac{1}{N_p}\mathbb{E}\left[\log_2\left(1+\left(\sum_{m=0}^{N_p-1}|G_m|^2\right)^2\left(\sum_{m=0}^{N_p-1}\sum_{n=0,n\neq m}^{N_p-1}|G_m|^2|G_n|^2\left(\frac{\Delta}{n-m+\Delta}\right)^2 + \frac{N_0N_p}{E_s}\left(\frac{\pi\triangle}{\sin(\pi\triangle)}\right)^2\left(\sum_{m=0}^{N_p-1}|G_m|^2\right)\right)^{-1}\right)\right]. \quad (4.4)$$

The direct method to solve (4.4) would require N_p-fold integrations making it too complex. In [41, eq. (25)] the pdf of multiple access interference and ICI from a single transmitter is derived which requires $2N_p$ summations of $2N_p$ multiplications of binomial coefficients but subcarrier channel dependence was not considered which would make it even more complex. Gaussian approximation of the interference in the denominator, though incorrect due to the correlation between the numerator and the denominator would still require finding pdf of the sum $\sum_{m=0}^{N_p-1}|G_m|^2$. Furthermore the summation $\sum_{m=0}^{N_p-1}|G_m|^2$ can not be considered as chi square distributed because of the correlation that exists between G_m's.

We derive a new tight lower bound for the average in (4.4). Let

$$\chi = \sum_{m=0}^{N_p-1}\sum_{n=0,n\neq m}^{N_p-1}\frac{|G_m|^2}{\sum_{m=0}^{N_p-1}|G_m|^2}\frac{|G_n|^2}{\sum_{m=0}^{N_p-1}|G_m|^2}\left(\frac{\Delta}{n-m+\Delta}\right)^2.$$

Then (4.4) can be rewritten as

$$\mathrm{C} = \frac{1}{N_p}\mathbb{E}\left[\log_2\left(1+\frac{\sum_{m=0}^{N_p-1}|G_m|^2}{\chi\sum_{m=0}^{N_p-1}|G_m|^2+\frac{N_0N_p}{E_s}\left(\frac{\pi\triangle}{\sin(\pi\triangle)}\right)^2}\right)\right].$$

Now, Jensen inequality asserts that

$$\mathrm{C} \geq \frac{1}{N_p}\mathbb{E}\left[\log_2\left(1+\frac{\sum_{m=0}^{N_p-1}|G_m|^2}{\hat{\chi}\sum_{m=0}^{N_p-1}|G_m|^2+\frac{N_0N_p}{E_s}\left(\frac{\pi\triangle}{\sin(\pi\triangle)}\right)^2}\right)\right] \tag{4.5}$$

where $\hat{\chi}=\mathbb{E}\left[\chi|\sum_{m=0}^{N_p-1}|G_m|^2\right]$.

As far as the statistics of $\hat{\chi}$ are concerned, note firstly that when $\sigma=0$ then $\hat{\chi}$ is independent of the sum $\sum_{m=0}^{N_p-1}|G_m|^2$. Furthermore, it can also be verified (by the using [61, The. 1.5.6]) that when $\sigma\gg 1$ then the random vector $\left\{\frac{G_0}{\sum_{m=0}^{N_p-1}|G_m|^2},\frac{G_1}{\sum_{m=0}^{N_p-1}|G_m|^2},\ldots,\frac{G_{N_p-1}}{\sum_{m=0}^{N_p-1}|G_m|^2}\right\}$ becomes independent of the sum $\sum_{m=0}^{N_p-1}|G_m|^2$ and hence $\hat{\chi}=\mathbb{E}\left[\chi|\sum_{m=0}^{N_p-1}|G_m|^2\right]=\mathbb{E}[\chi]$ (independently of the sum $\sum_{m=0}^{N_p-1}|G_m|^2$). Therefore we conjecture that only marginal errors might be introduced if we replace the conditional average $\mathbb{E}\left[\chi|\sum_{m=0}^{N_p-1}|G_m|^2\right]$ by the unconditional average $\mathbb{E}[\chi]$ in (4.5).

We now find expression for the unconditional average $\mathbb{E}[\chi]$. Let

$$\zeta=\mathbb{E}\left[\frac{|G_m|^2}{\sum_{m=0}^{N_p-1}|G_m|^2}\frac{|G_n|^2}{\sum_{m=0}^{N_p-1}|G_m|^2}\right] \tag{4.6}$$

which can be simplified by first considering the well known mathematical identity

$$\frac{1}{y^c}=\int_0^\infty \frac{x^{c-1}}{\Gamma(c)}\exp(-yx)\,\mathrm{d}x,\quad \forall y,c>0$$

using $c=2$ and $y=\sum_{l=0}^{N_p-1}|G_m|^2$ we get

$$\zeta=\mathbb{E}\left[|G_m|^2|G_n|^2\int_0^\infty \exp\left(-x\sum_{l=0}^{N_p-1}|G_l|^2\right)x\,\mathrm{d}x\right].$$

Let

$$\phi\left(x_1, x_2, \ldots, x_{N_p}\right) = \mathbb{E}\left[\exp\left(-\sum_{m=1}^{N_p} x_m |G_m|^2\right)\right]$$

then

$$\zeta = \int_0^\infty \frac{\partial}{\partial x_m}\frac{\partial}{\partial x_n}\phi\left(x_1, x_2, \ldots, x_{N_p}\right) x \, \mathrm{d}x \tag{4.7}$$

from [36, eq. (4a)] for the MGF of the Gaussian quadratic forms we know that

$$\phi\left(x_1, x_2, \ldots, x_{N_p}\right) = \frac{1}{\left|\mathbf{I}_{N_p} + \mathrm{diag}\left(x_1, x_2, \ldots, x_{N_p}\right)\mathbf{\Lambda}\right|}$$

where $\mathbf{I}_{N_p}$ is the $N_p \times N_p$ identity matrix and Λ is $N_p \times N_p$ correlation matrix where a typical element is given by $\Lambda_{ij} = \mathrm{E}\left[G_i G_j^*\right]$. We now have to find its partial derivatives. The first partial derivative is given as [62, eq. (29)]

$$\frac{\partial}{\partial x_n}\phi\left(x_1, x_2, \ldots, x_{N_p}\right) = \frac{-\left|\mathrm{diag}\left(1, \ldots, 0_n, \ldots, 1\right) + \mathrm{diag}\left(x_1, \ldots, 1_n, \ldots, x_{N_p}\right)\mathbf{\Lambda}\right|}{\left|\mathbf{I}_{N_p} + \mathrm{diag}\left(x_1, x_2, \ldots, x_{N_p}\right)\mathbf{\Lambda}\right|^2}. \tag{4.8}$$

The second partial derivative of (4.8) can similarly be found and is given as

$$\begin{aligned}\frac{\partial}{\partial x_m}\frac{\partial}{\partial x_n}\phi\left(x_1, x_2, \ldots, x_{N_p}\right) = &\left(\frac{2\left|\mathrm{diag}(1,\ldots,0_n,\ldots,1)+\mathrm{diag}\left(x_1,\ldots,1_n,\ldots,x_{N_p}\right)\mathbf{\Lambda}\right|}{\left|\mathbf{I}_{N_p}+\mathrm{diag}\left(x_1,x_2,\ldots,x_{N_p}\right)\mathbf{\Lambda}\right|^3}\right) \\ &\times\left|\mathrm{diag}\left(1,\ldots,0_m,\ldots,1\right)+\mathrm{diag}\left(x_1,\ldots,1_m,\ldots,x_{N_p}\right)\mathbf{\Lambda}\right| \\ &-\frac{\left|\mathrm{diag}(1,\ldots,0_m,\ldots,0_n,\ldots,1)+\mathrm{diag}\left(x_1,\ldots,1_m,\ldots,1_m,\ldots,x_{Np}\right)\mathbf{\Lambda}\right|}{\left|\mathbf{I}_{N_p}+\mathrm{diag}\left(x_1,x_2,\ldots,x_{N_p}\right)\mathbf{\Lambda}\right|^2}.\end{aligned} \tag{4.9}$$

Using (4.9) and (4.7) we can find the value of ζ and hence an exact expression for $\hat{\chi} = \sum_{m=0}^{N_p-1}\sum_{n=0,n\neq m}^{N_p-1}\zeta\left(\frac{\Delta}{n-m+\Delta}\right)^2$ can be found. However, our numerical results suggest that only marginal errors might be introduced when the following

approximate expression is used instead for reduced computational complexity

$$\hat{\chi} = \frac{1}{N_p^2} \sum_{m=0}^{N_p-1} \sum_{n=0, n\neq m}^{N_p-1} \left(\frac{\Delta}{n-m+\Delta} \right)^2. \tag{4.10}$$

We now find an expression for the spectral efficiency using lemma 1 in [35] we can write (4.5) as

$$\mathrm{C} \geq \frac{\log_2 \mathrm{e}}{N_p} \int_0^\infty \frac{1}{z} \left(\mathbb{E}\left[\exp\left(-z\hat{\chi} \sum_{m=0}^{N_p-1} |G_m|^2 \right) \right] - \mathbb{E}\left[\exp\left(-z\left(1+\hat{\chi}\right) \times \sum_{m=0}^{N_p-1} |G_m|^2 \right) \right] \right) \exp\left(-\frac{z N_0 N_p \left(\pi\triangle\right)^2}{E_s \sin^2(\pi\triangle)} \right) \mathrm{d}z \tag{4.11}$$

where the Gaussian quadratic forms $\sum_{m=0}^{N_p-1} |G_m|^2$ appear only in the exponent. Therefore, known results for the MGF of the Gaussian quadratic forms [36, eq. (4a)] can be applied to obtain the following explicit expression for the lower bound on the spectral efficiency of the multicarrier CDMA in the presence of frequency offset

$$\mathrm{C} \geq \frac{\log_2 \mathrm{e}}{N_p} \int_0^\infty \frac{1}{z} \left(\frac{1}{\left|\mathbf{I}_{N_p} + z\hat{\chi}\left(\triangle\right)\mathbf{\Lambda}\right|} - \frac{1}{\left|\mathbf{I}_{N_p} + z\left(1+\hat{\chi}\left(\Delta\right)\right)\mathbf{\Lambda}\right|} \right) \times \exp\left(\frac{-z N_0 N_p}{E_s} \left(\frac{\pi\triangle}{\sin(\pi\triangle)} \right)^2 \right) \mathrm{d}z \tag{4.12}$$

where $\mathbf{I}_{N_p}$ is the $N_p \times N_p$ identity matrix and Λ is $N_p \times N_p$ correlation matrix where a typical element is given by $\Lambda_{ij} = \mathbb{E}\left[G_i G_j^*\right]$. Equation (4.12) is the desired expression for the spectral efficiency with frequency offset. Please note that (4.12) requires a single integration as compared to N_p+1 integrations in the direct method.

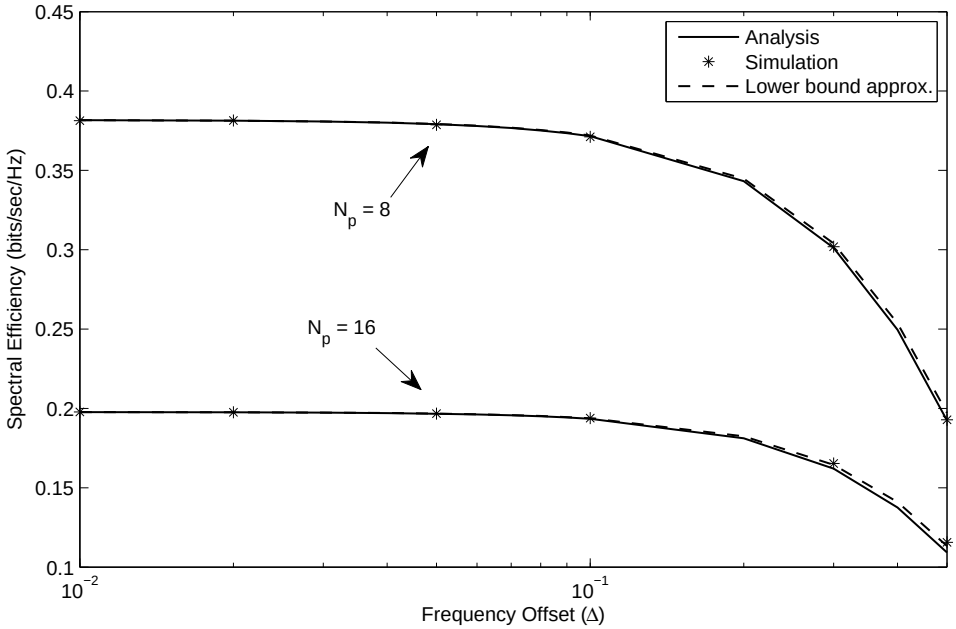

Figure 4.1: Degradation in spectral efficiency due to frequency offset for 8 and 16 subcarriers

4.1.2 Numerical Results

In this section we present some numerical and simulation results which show the tightness of the spectral efficiency bound. In Fig. 4.1 spectral efficiency using (4.12) is plotted against frequency offset (Δ), the simulation result was generated using (4.4) with 10^5 iterations and the lower bound approximation result was generated using (4.10) in (4.12). We used E_s/N_0 of 10dB and the results are shown for 8 and 16 number of subcarriers (N_p). A 312.5 kHz frequency separation ($1/T$) between neighboring subcarriers (IEEE 802.11a [37]) and channel delay spread (α) of 0.1μs is used. It can be clearly seen that our analysis provides a tight lower bound and the approximation using (4.10) follows the analysis and simulation very closely. Fig. 4.2 shows that the degradation in spectral efficiency is small for $\Delta < 0.1$ but sharply increases at higher values meaning small values of frequency offset do not degrade performance.

In Fig. 4.3 spectral efficiency versus E_s/N_0 calculated with our analysis is

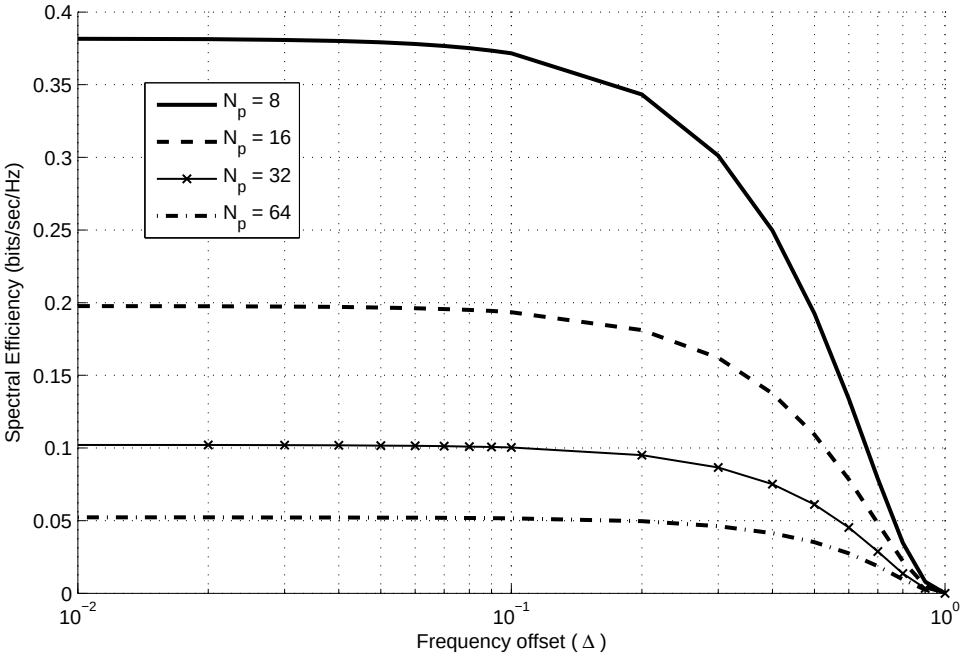

Figure 4.2: Spectral efficiency versus frequency offset (Δ) for some number of subcarriers

compared against those obtained with approximation and simulation. Our analysis results are very close to the simulation results again showing the tightness of the bound, the approximation results are also very close and show small deviation at higher values of E_s/N_0. In Fig. 4.4 spectral efficiency curves versus E_s/N_0 are drawn for different values of the frequency offset (Δ), the spectral efficiency increases with E_s/N_0 as expected and the decrease in spectral efficiency with increasing frequency offset is also evident. Furthermore it can be observed that the difference between spectral efficiency at different frequency offset values increases with increasing E_s/N_0 meaning the spectral efficiency is more sensitive to frequency offset at higher SNR than at lower SNR.

Fig. 4.5 shows the degradation in spectral efficiency against normalized delay spread (σ). Larger values of σ result in smaller coherence bandwidth and hence lower correlation between subcarriers, resulting in better spectral efficiency. This

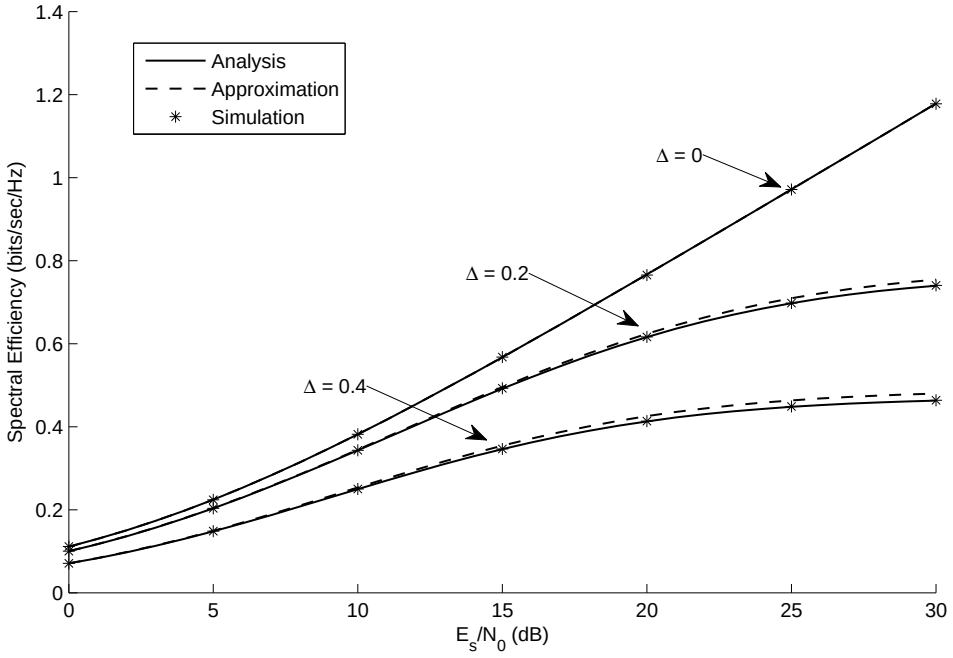

Figure 4.3: Spectral Efficiency versus E_s/N_0 for frequency offsets (Δ) of 0, 0.2 and 0.4

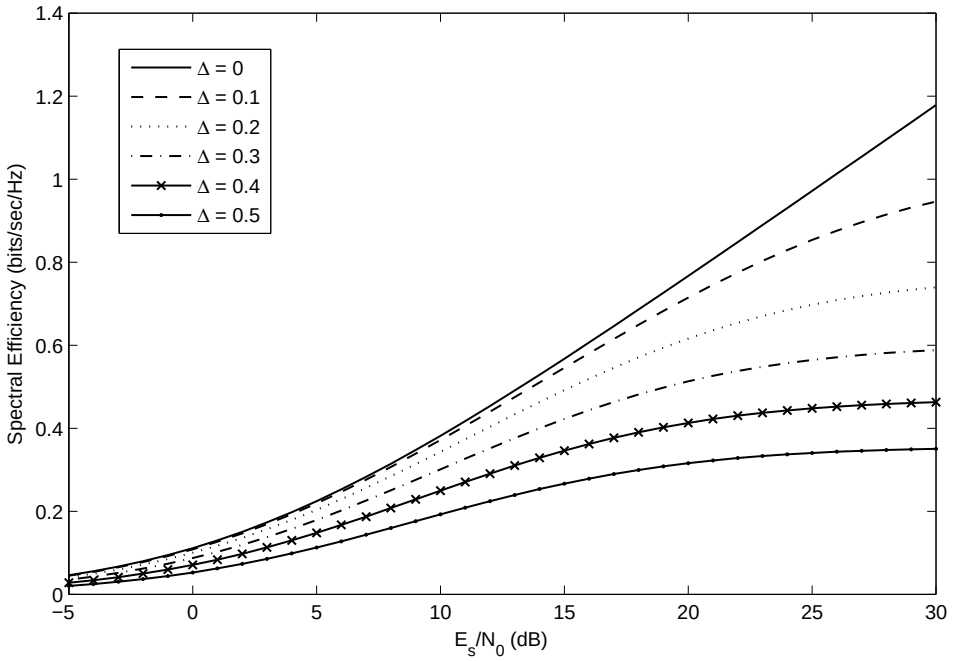

Figure 4.4: Spectral Efficiency versus E_s/N_0 for some frequency offsets (Δ)

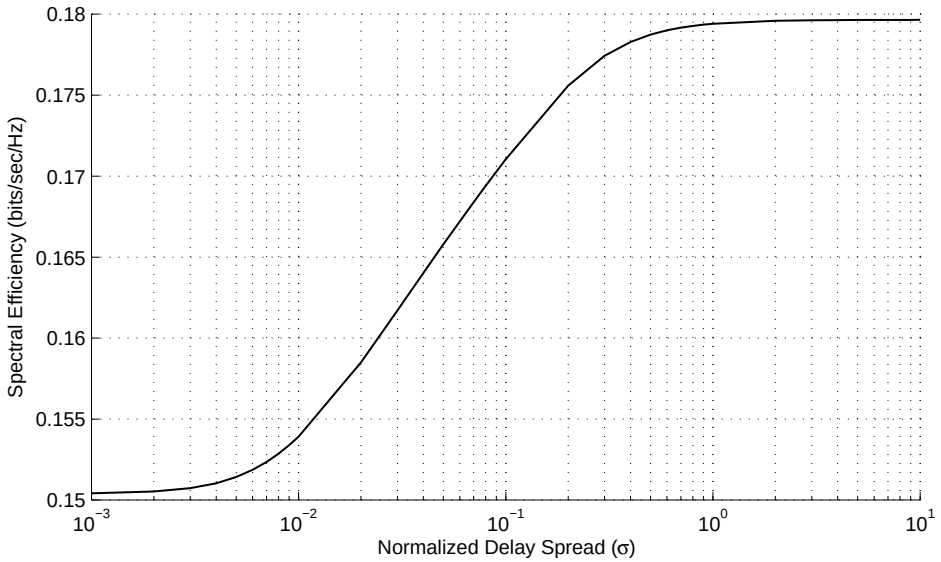

Figure 4.5: Spectral efficiency versus normalized delay spread (σ) for $\Delta = 0.3$.

is because the correlation between subcarriers reduces the diversity gain. The correlation between subcarriers decays faster when the normalized delay spread is increased, as shown in Fig. 4.6.

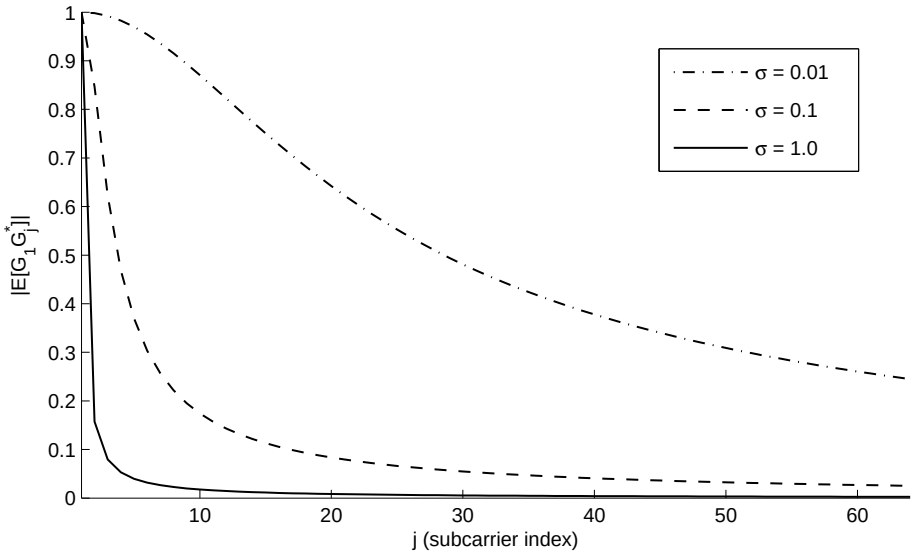

Figure 4.6: Magnitude of the cross-correlation between first subcarrier and other subcarriers for some values of normalized delay spread

4.2 Multi-Carrier DS-CDMA

In MC DS-CDMA the data stream is first serial to parallel converted before transmission, hence N_c number of symbols are received in parallel. We only analyze the first symbol which is transmitted over the first subcarrier, the analysis for other symbols is similar and is not required for spectral efficiency.

The receiver decision variable of MC DS-CDMA for the first symbol is given as

$$Z_1 = \frac{1}{N_c T} \int_0^{N_c T} G_1^* c\left(t\right) \mathrm{e}^{-j2\pi f_1 t} \left(\sum_{l=1}^{N_c} G_l b_l\left(t\right) c\left(t\right) \mathrm{e}^{j2\pi(f_l+\Delta f)t} \mathrm{e}^{j\phi} \mathrm{d}t + \eta\left(t\right) \right)$$

where Δf is the frequency offset. Let $\Delta = \Delta f \frac{N_c}{N_p} T$ where Δ is the frequency offset normalized to the frequency separation between adjacent subcarriers, the frequency separation between adjacent subcarriers is given as $\frac{N_p}{N_c T}$. The decision variable Z_1 can be separated into three distinct components $Z_1 = S + I + N$,

where S is the desired signal component, I is the ICI component and N is the noise component, these are given respectively as

$$S = |G_1|^2 b_1(t) \frac{1}{N_c T} \int_0^{N_c T} \mathrm{e}^{j2\pi \frac{\Delta N_p}{N_c T} t} \mathrm{d}t$$

$$I = \frac{1}{N_c T} G_1^* \sum_{l=2}^{N_c} G_l b_l(t) \mathrm{e}^{j\phi} \int_0^{N_c T} \mathrm{e}^{j2\pi (f_l - f_1)t} \mathrm{e}^{j2\pi \frac{\Delta N_p}{N_c T} t} \mathrm{d}t$$

$$N = \frac{1}{N_c T} G_1^* c(t) \int_0^{N_c T} \mathrm{e}^{-j2\pi f_1 t} \eta(t) \, \mathrm{d}t.$$

The integrations in the signal and interference components can be easily solved to give

$$S = |G_1|^2 b_1(t) \mathrm{e}^{j\pi N_p \Delta} \mathrm{sinc}(\pi N_p \Delta)$$

$$I = G_1^* \sum_{l=2}^{N_c} G_l b_l(t) \mathrm{e}^{j\phi} \mathrm{e}^{j\pi N_p (l-1+\Delta)} \mathrm{sinc}(\pi N_p (l-1+\Delta)).$$

Note that the interference component is due to the frequency offset Δ only and it can be easily shown that I goes to zero when $\Delta = 0$. We approximate Z_1 as a conditional Gaussian random variable, conditioned on $G_0, \ldots G_{N_p-1}$ and the conditional mean is

$$\mathbb{E}\left[Z_1 | G_0, \ldots, G_{N_p-1}\right] = |G_1|^2 \sqrt{\frac{E_s}{N_c T}} \mathrm{sinc}(\pi N_p \Delta). \tag{4.13}$$

The conditional variance of Z_1 can be calculated as

$$\mathrm{Var}\left[Z_1 | G_0, \ldots, G_{N_p-1}\right] = |G_1|^2 \frac{E_s}{N_c T} \sum_{l=2}^{N_c} |G_l|^2 \mathrm{sinc}^2(\pi N_p (l-1+\Delta)) + \frac{1}{N_c T} |G_1|^2 N_0.$$

The instantaneous SINR is therefore a random variable given by the ratio

$$\mathrm{SINR} = \frac{|G_1|^4 \frac{E_s}{N_c T} \mathrm{sinc}^2(\pi N_p \Delta)}{|G_1|^2 \frac{E_s}{N_c T} \sum_{l=2}^{N_c} |G_l|^2 \mathrm{sinc}^2(\pi N_p (l-1+\Delta)) + \frac{1}{N_c T} |G_1|^2 N_0} \tag{4.14}$$

which can be simplified into

$$\mathrm{SINR} = \frac{|G_1|^2}{\sum_{l=2}^{N_c} |G_l|^2 \frac{\Delta^2}{(l-1+\Delta)^2} + \frac{1}{\mathrm{sinc}^2(\pi N_p \Delta)} \frac{N_0}{E_s}}. \tag{4.15}$$

The spectral efficiency of the system depends on the instantaneous SINR in (4.15) and can be evaluated by using the well known Shannon's capacity and is analyzed in the next section.

4.2.1 Spectral Efficiency Analysis

The spectral efficiency can be found using (4.15) as

$$\mathrm{C} = \frac{1}{N_p} \log_2 \left(1 + \frac{|G_1|^2}{\sum_{l=2}^{N_c} |G_l|^2 \frac{\Delta^2}{(l-1+\Delta)^2} + \frac{1}{\mathrm{sinc}^2(\pi N_p \Delta)} \frac{N_0}{E_s}} \right). \tag{4.16}$$

Classical techniques can not be used to solve (4.16) due to the correlation between numerator and denominator, however, we can use lemma 1 in [35] to rewrite (4.16) as

$$\mathrm{C} = \frac{\log_2 \mathrm{e}}{N_p} \int_0^\infty \frac{1}{z} \left(\mathbb{E}\left[\mathrm{e}^{\left(-z \sum_{l=2}^{N_c} |G_l|^2 \frac{\Delta^2}{(l-1+\Delta)^2} \right)} \right] - \mathbb{E}\left[\mathrm{e}^{\left(-z \sum_{l=1}^{N_c} |G_l|^2 \frac{\Delta^2}{(l-1+\Delta)^2} \right)} \right] \right) \times \mathrm{e}^{-\frac{z}{\mathrm{sinc}^2(\pi N_p \Delta)} \frac{N_0}{E_s}} \mathrm{d}z.$$

We can now apply the known results for the MGF of the Gaussian quadratic

forms [36, eq. (4a)] to obtain the following explicit expression for the lower bound on the spectral efficiency of the multicarrier DS-CDMA in the presence of frequency offset

$$\mathrm{C} = \frac{\log_2 \mathrm{e}}{N_p} \int_0^\infty \frac{1}{z} \left(\frac{1}{|\mathbf{I}_{N_c-1} + z\mathbf{\Lambda_1}|} - \frac{1}{|\mathbf{I}_{N_c} + z\mathbf{\Lambda_2}|} \right) \mathrm{e}^{-\frac{z}{\mathrm{sinc}^2(\pi N_p \Delta)} \frac{N_0}{E_s}} \mathrm{d}z \qquad (4.17)$$

where $\mathbf{I}_{N_c-1}$ is $(N_c-1) \times (N_c-1)$ identity matrix and similarly $\mathbf{I}_{N_c}$ is $\mathbf{I}_{N_c} \times \mathbf{I}_{N_c}$ identity matrix, Λ_1 is $(N_c-1) \times (N_c-1)$ and Λ_2 is $N_c \times N_c$ correlation matrix where a typical element is given by $\Lambda_{ij} = \mathrm{E}\left[G_i G_j^*\right] \frac{\Delta^2}{(i-1+\Delta)(j-1+\Delta)}$ where for Λ_1, $(i,j) \in [2, N_c]$ and for Λ_2, $(i,j) \in [1, N_c]$.

4.2.2 Numerical Results

In this section we present some numerical and simulation results which show the accuracy of the analysis. In Fig. 4.7 spectral efficiency using (4.17) is plotted against frequency offset (Δ), the simulation result was generated using (4.16) with 10^6 iterations. We used 8 number of subcarriers (N_c) and processing gain (N_p) is also 8. A 312.5 kHz frequency separation ($1/T$) between neighboring subcarriers (IEEE 802.11a [37]) and channel delay spread (α) of 0.1μs is used. The results are shown for E_s/N_0 of 0, 10, 20 and 30 dB. It can be clearly seen that our analysis provides a tight lower bound. An important result is that the spectral efficiency decays to zero much faster than MC-CDMA, in MC-CDMA it always decays to zero when the normalized frequency offset is 1, however in MC DS-CDMA it decays to zero when normalized frequency offset approaches $1/N_p$. The reason of this sensitivity can easily be seen in (4.14), the instantaneous SINR goes to zero as Δ approaches $1/N_p$ due to $\mathrm{sinc}\,(\pi N_p \Delta)$ in the numerator. In order to compare the performance at different values of N_p, in Fig. 4.8 we plot spectral efficiency with respect to frequency offset normalized to the symbol rate instead of frequency separation. This was necessary because the frequency separation

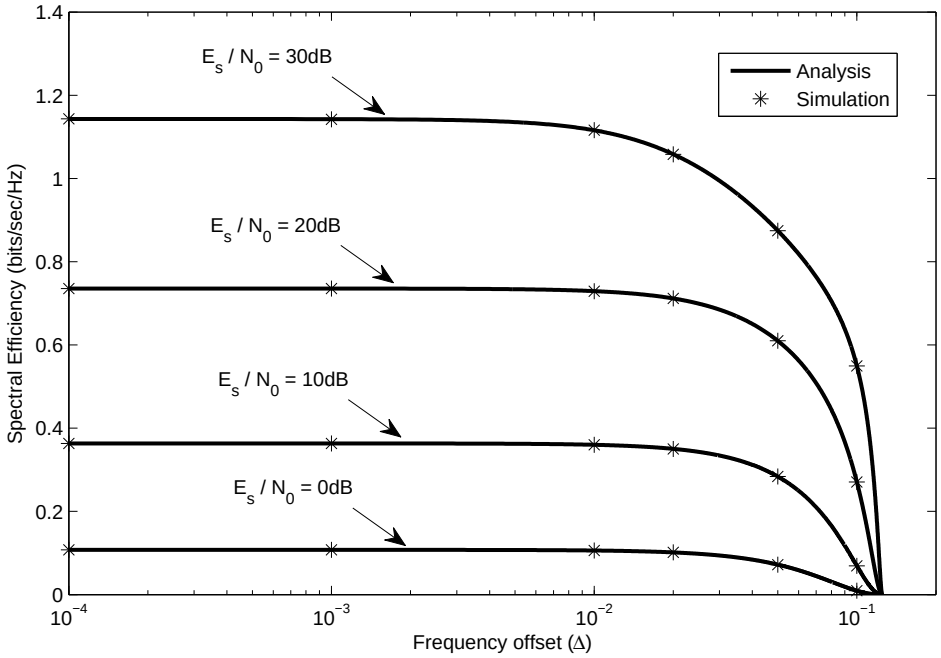

Figure 4.7: Spectral Efficiency versus Δ for E_s/N_0 of 0, 10, 20 and 30 dB.

between adjacent subcarriers changes with N_p. As seen in the figure the spectral efficiency for processing gain (N_p) values of 8, 16, 32 and 64 decay to zero at the same normalized frequency of $1/N_c$, where the number of subcarriers (N_c) was selected as 8. This shows that MC DS-CDMA is much more sensitive to carrier frequency offset than MC-CDMA and this sensitivity increases with increasing number of subcarriers, it is because the frequency separation decreases as N_c is increased.

In Fig. 4.9 spectral efficiency versus E_s/N_0 curves calculated with our analysis are compared with those obtained with simulation. Our analysis results are very close to the simulation results again showing the accuracy of the analysis. The results are drawn for different values of the frequency offset (Δ), the spectral efficiency increases with E_s/N_0 as expected and the decrease in spectral efficiency with increasing frequency offset is also clear.

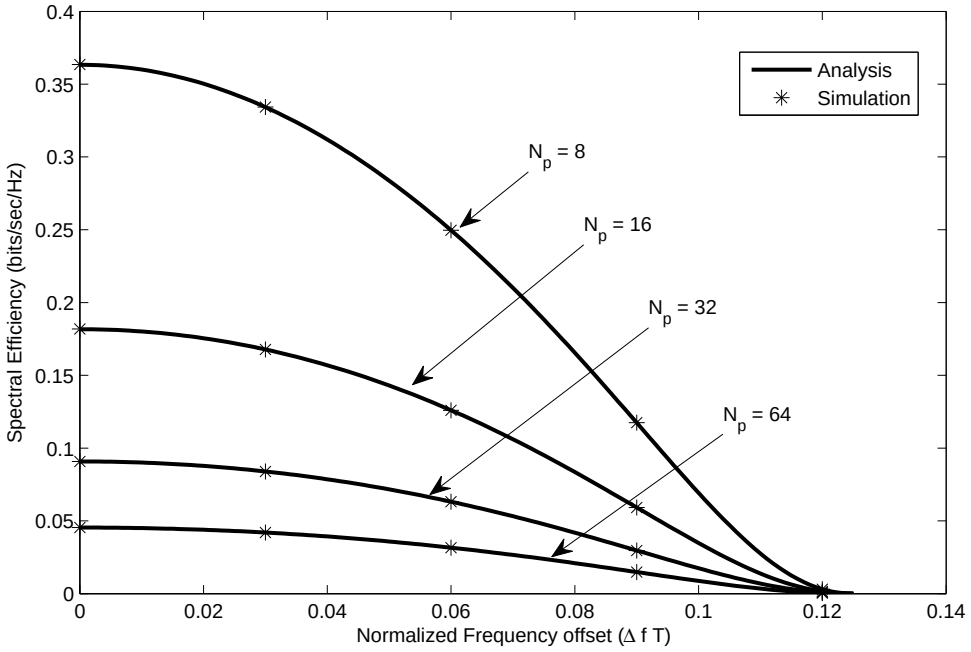

Figure 4.8: Spectral Efficiency versus $\Delta f\, T$ for processing gain (N_p) values of 8, 16, 32 and 64.

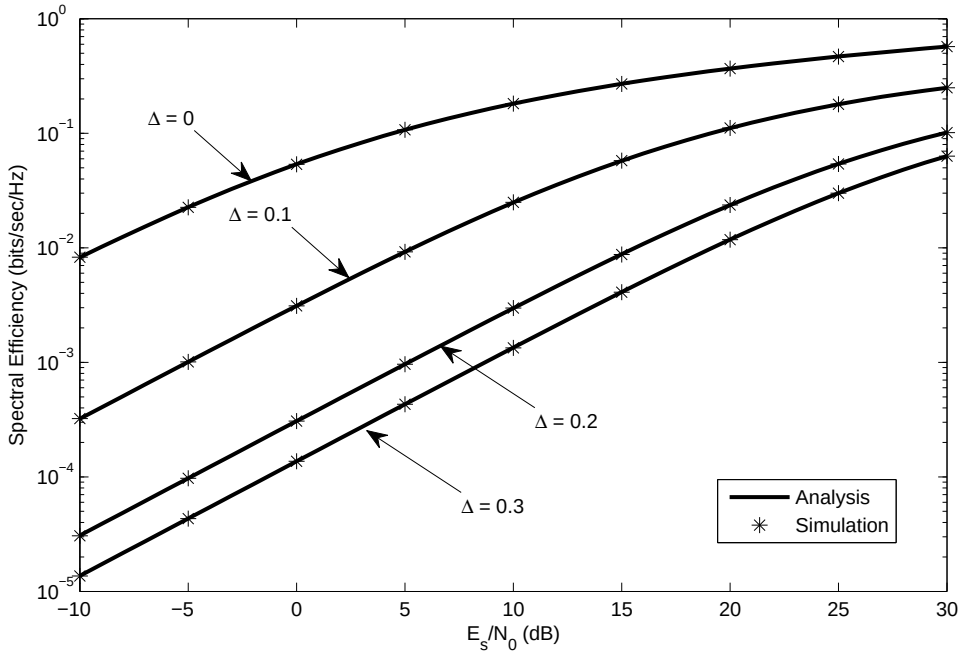

Figure 4.9: Spectral Efficiency versus E_s/N_0 for frequency offsets (Δ) of 0, 0.1, 0.2 and 0.3.

4.3 Multi-Tone CDMA

In MT-CDMA, similar to MC DS-CDMA, N_c number of symbols are transmitted in parallel and analyzing the first symbol is sufficient for spectral efficiency analysis. The receiver decision variable for the first symbol is given as

$$Z_1 = \sum_{m=0}^{L-1} \frac{1}{N_c T} \int_0^{N_c T} g_m^* c(t - m\tau) \mathrm{e}^{-j2\pi f_1 t} \left(\sum_{l=1}^{N_c} \sum_{i=0}^{L-1} g_i \, b_l(t) \, c(t - i\tau) \, \mathrm{e}^{j2\pi (f_l + \Delta f)(t - i\tau)} + \eta(t) \right) \mathrm{d}t$$

where L is the total number of resolvable propagation paths and the number of fingers in the rake receiver. Let $\Delta = \Delta f \, N_c T$ where Δ is the frequency offset normalized to the frequency separation between adjacent subcarriers, the frequency separation between adjacent subcarriers is given as $\frac{1}{N_c T}$. The decision variable Z_1 can be separated into four distinct components $Z = S + I_1 + I_2 + N$, where S is the desired signal component, I_1 is the self interference of the rake receiver, I_2 is the ICI component and N is the noise component, these are given respectively as

$$S = b_1(t) \sum_{i=0}^{L-1} |g_i|^2 \frac{1}{N_c T} \int_0^{N_c T} \mathrm{e}^{j2\pi \frac{\Delta}{N_c T} t} \mathrm{d}t$$

$$I_1 = b_1(t) \sum_{k=0}^{L-1} g_k^* \sum_{l=0, l \neq k}^{L-1} g_l \frac{1}{N_c T} \int_0^{N_c T} c(t) c(t - \tau) \, \mathrm{e}^{j2\pi \frac{\Delta}{N_c T} t} \mathrm{d}t$$

$$I_2 = \sum_{i=2}^{N_c} b_i(t) \sum_{k=0}^{L-1} |g_k|^2 \frac{1}{N_c T} \int_0^{N_c T} \mathrm{e}^{-j2\pi \frac{i-1+\Delta}{N_c T} t} \mathrm{d}t + \sum_{i=2}^{N_c} b_i(t) \sum_{k=0}^{L-1} g_k^* \sum_{l=0, l\neq k}^{L-1} g_l \frac{1}{N_c T} \times \int_0^{N_c T} c(t) c(t + (k-l)\tau) \mathrm{e}^{-j2\pi \frac{i-1+\Delta}{N_c T} t} \mathrm{d}t$$

$$N = \sum_{i=0}^{L-1} g_i^* \frac{1}{N_c T} \int_0^{N_c T} c(t) \mathrm{e}^{-j2\pi f_1 t} \eta(t)\, \mathrm{d}t.$$

When we condition on $g_0, \ldots, g_{L-1}$, Z_1 can be considered as a Gaussian random variable with conditional mean given as

$$\mathbb{E}\left[Z_1 | g_0, \ldots, g_{L-1}\right] = \sqrt{\frac{E_s}{N_c T}} \sum_{l=0}^{L-1} |g_l|^2 \, \mathrm{sinc}(\pi \triangle) \tag{4.18}$$

and the conditional variance of Z_1 can be calculated as

$$\mathrm{Var}\left[Z_1 | g_0, \ldots, g_{L-1}\right] = \frac{E_s}{T N_c N_p} \left(\sum_{k=1}^{N_c} \mathrm{sinc}^2 \left(\frac{\pi (k - 1 + \triangle)}{N_p} \right) \right) \left(\sum_{l=0}^{L-1} |g_l|^2 \times \sum_{m=0, m\neq l}^{L-1} |g_m|^2 \right) + \frac{E_s}{T N_c} \left(\sum_{m=2}^{N_c} \mathrm{sinc}^2 \left(\pi (m - 1 + \Delta) \right) \right) \left(\sum_{n=0}^{L-1} |g_n|^2 \right)^2 + \frac{N_0}{N_c T} \left(\sum_{l=0}^{L-1} |g_l|^2 \right)$$

where the first term is due to I_1, second due to I_2 and third due to N. The instantaneous SINR is a random variable given by

$$\mathrm{SINR} = \mathrm{sinc}^2(\pi \triangle) \left(\sum_{l=0}^{L-1} |g_l|^2 \right)^2 \left[\frac{1}{N_p} \left(\sum_{k=1}^{N_c} \mathrm{sinc}^2 \left(\frac{\pi (k - 1 + \triangle)}{N_p} \right) \right) \left(\sum_{l=0}^{L-1} |g_l|^2 \times \sum_{m=0, m\neq l}^{L-1} |g_m|^2 \right) + \left(\sum_{m=2}^{N_c} \mathrm{sinc}^2 \left(\pi (m - 1 + \Delta) \right) \right) \left(\sum_{n=0}^{L-1} |g_n|^2 \right)^2 + \frac{N_0}{E_s} \left(\sum_{l=0}^{L-1} |g_l|^2 \right) \right]^{-1}. \tag{4.19}$$

The instantaneous SINR in (4.19) can now be used to find the spectral efficiency of the system.

4.3.1 Spectral Efficiency Analysis

The spectral efficiency of the system depends on the SINR in (4.19) and can be evaluated by using the well known Shannon's capacity expression as

$$\mathrm{C} = \frac{N_c}{N_c+N_p-1}\mathbb{E}\left[\log_2\left(1+\mathrm{sinc}^2\left(\pi\triangle\right)\left(\sum_{l=0}^{L-1}|g_l|^2\right)^2 \times\left[\frac{1}{N_p}\left(\sum_{k=1}^{N_c}\mathrm{sinc}^2\left(\frac{\pi\left(k-1+\triangle\right)}{N_p}\right)\right)\left(\sum_{l=0}^{L-1}|g_l|^2\sum_{m=0,m\neq l}^{L-1}|g_m|^2\right)+\left(\sum_{m=2}^{N_c}\mathrm{sinc}^2\left(\pi\left(m-1+\Delta\right)\right)\right)\left(\sum_{n=0}^{L-1}|g_n|^2\right)^2+\frac{N_0}{E_s}\left(\sum_{l=0}^{L-1}|g_l|^2\right)\right]^{-1}\right). \quad (4.20)$$

The direct method to solve (4.20) requires L-fold integrations making it too complex. To simplify the analysis let

$$\rho\left(m,l\right)=\mathbb{E}\left[\frac{|g_l|^2}{\sum_{l=0}^{L-1}|g_l|^2}\frac{|g_m|^2}{\sum_{m=0}^{L-1}|g_m|^2}\right]$$

where ρ is similar to ζ in (4.6) and the analysis of ρ is the same as for ζ in section 4.1. Now Jensen inequality asserts that

$$\mathrm{C}\geq\frac{N_c}{N_c+N_p-1}\mathbb{E}\left[\log_2\left(1+\mathrm{sinc}^2\left(\pi\triangle\right)\sum_{l=0}^{L-1}|g_l|^2 \times\left[\sum_{l=0}^{L-1}|g_l|^2\left(\frac{1}{N_p}\left(\sum_{k=1}^{N_c}\mathrm{sinc}^2\left(\frac{\pi}{N_p}\left(k-1+\triangle\right)\right)\right)\sum_{l=0}^{L-1}\sum_{m=0,m\neq l}^{L-1}\rho\left(m,l\right) +\left(\sum_{m=2}^{N_c}\mathrm{sinc}^2\left(\pi\left(m-1+\Delta\right)\right)\right)\right)+\frac{N_0}{E_s}\right]^{-1}\right). \quad (4.21)$$

Let

$$\hat{\chi}(\triangle) = \frac{1}{N_p}\left(\sum_{k=1}^{N_c}\mathrm{sinc}^2\left(\frac{\pi}{N_p}(k-1+\triangle)\right)\right)\sum_{l=0}^{L-1}\sum_{m=0,m\neq l}^{L-1}\rho(m,l) + \left(\sum_{m=2}^{N_c}\mathrm{sinc}^2(\pi(m-1+\Delta))\right)$$

where $\hat{\chi}(\triangle)$ is a deterministic value. Now (4.21) can be simplified as

$$\mathrm{C} \geq \frac{N_c}{N_c+N_p-1}\mathbb{E}\left[\log_2\left(1+\frac{\mathrm{sinc}^2(\pi\Delta)\sum_{l=0}^{L-1}|g_l|^2}{\left(\sum_{l=0}^{L-1}|g_l|^2\right)\hat{\chi}(\triangle)+\frac{N_0}{E_s}}\right)\right].$$

Following similar analysis as in section 4.1 we get for the spectral efficiency of MT-CDMA

$$\mathrm{C} \geq \frac{N_c\log_2\mathrm{e}}{N_c+N_p-1}\int_0^\infty \frac{1}{z}\left(\frac{1}{|\mathbf{I}_L+z\hat{\chi}(\triangle)\,\mathbf{\Lambda}|}-\frac{1}{|\mathbf{I}_L+z\left(\mathrm{sinc}^2(\pi\Delta)+\hat{\chi}(\triangle)\right)\mathbf{\Lambda}|}\right) \times \exp\left(-z\frac{N_0}{E_s}\right)\mathrm{d}z \quad (4.22)$$

where $\mathbf{I}_L$ is $L\times L$ identity matrix.

4.3.2 Numerical Results

In this section we present some numerical and simulation results which show the accuracy of the analysis. In Fig. 4.10 spectral efficiency versus E_s/N_0 calculated with our analysis is compared against those obtained with simulation. The results were calculated for $N_c = 16$, $N_p = 1024$ and $L = 16$. Our analysis results are very close to the simulation results showing the accuracy of the analysis. The results are shown for frequency offset (Δ) values of 0, 0.2 and 0.4. The spectral efficiency increases with E_s/N_0 as expected and the decrease in spectral efficiency

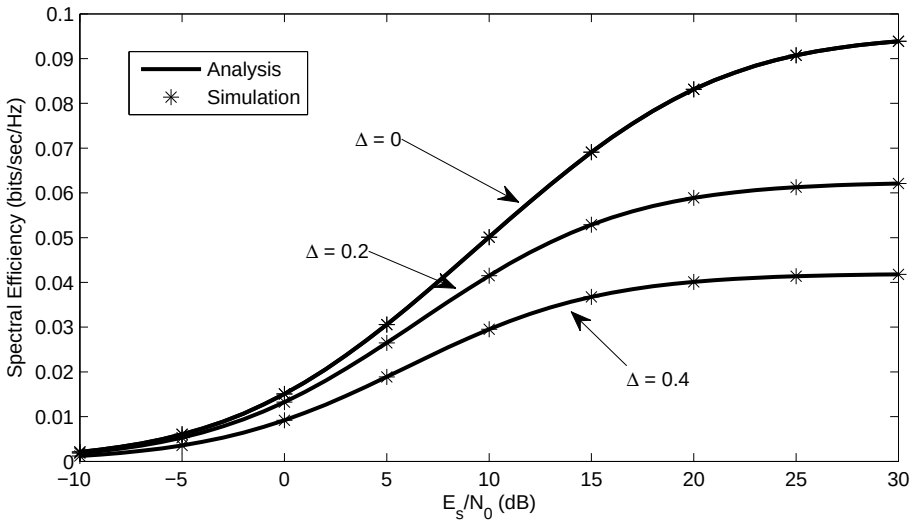

Figure 4.10: Spectral Efficiency versus E_s/N_0 for frequency offsets (Δ) of 0, 0.2 and 0.4.

with increasing frequency offset is also clear.

In Fig. 4.11 spectral efficiency using (4.22) is plotted against frequency offset (Δ), the simulation result was generated using (4.20) with 10^5 iterations. We used 16 number of subcarriers (N_c), the processing gain (N_p) is 1024 and the rake receiver used 16 fingers. A 312.5 kHz frequency separation ($1/T$) between neighboring subcarriers (IEEE 802.11a [37]) and channel delay spread (α) of 0.1μs is used. The results are shown for E_s/N_0 of 0, 10 and 20 dB. It can be clearly seen that our analysis provides a tight lower bound.

4.4 Chapter Conclusion

We have presented new expressions for the lower bound of spectral efficiency of MC-CDMA, MC DS-CDMA and MT-CDMA transmission in the presence of frequency offset. Numerical results show that the bounds are tight and a close approximation of the spectral efficiency. In the case of MC-CDMA we also present an approximation to the lower bound that reduces the computational complexity

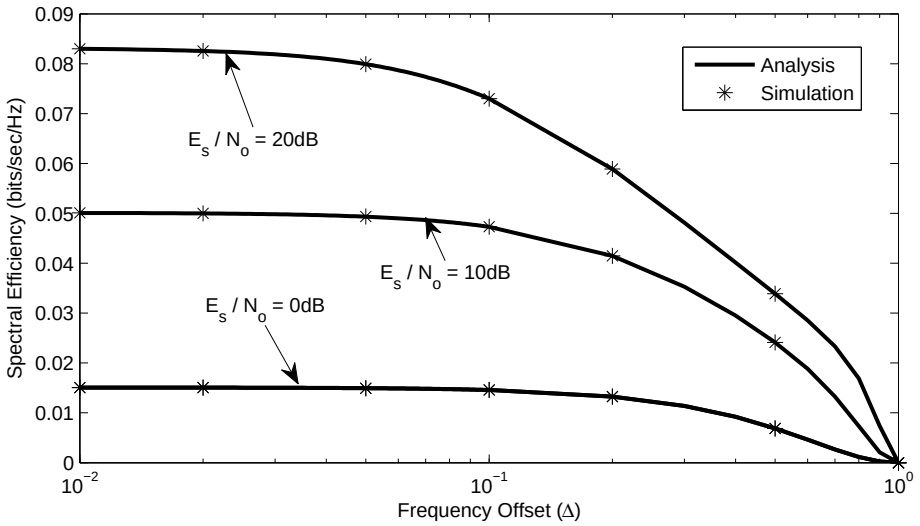

Figure 4.11: Spectral Efficiency versus frequency offsets (Δ) for E_s/N_0 of 0dB, 10dB and 20dB.

but still closely follow the exact solution.

In Fig. 4.12 we compare the performance of the three multicarrier schemes for $N_p = 8$, $N_c = 8$, $L = 8$ and for E_s/N_0 of 10dB. In order to have a fair comparison of the three multicarrier schemes we plot spectral efficiency with respect to frequency offset normalized to the symbol time i.e. horizontal axis is $\Delta f\, T$ instead of frequency separation. This was necessary because the frequency separation between adjacent subcarriers is different for the three schemes. The results show the advantage of MT-CDMA when there is no offset or when the offset is small. When the frequency offset increases the spectral efficiency for MC DS-CDMA and MT-CDMA erodes to zero much faster than MC-CDMA. In fact the spectral efficiency goes to zero when the offset approaches $1/N_c$ this is because of the S/P converter in both MC DS-CDMA and MT-CDMA that reduces the frequency separation between adjacent subcarriers.

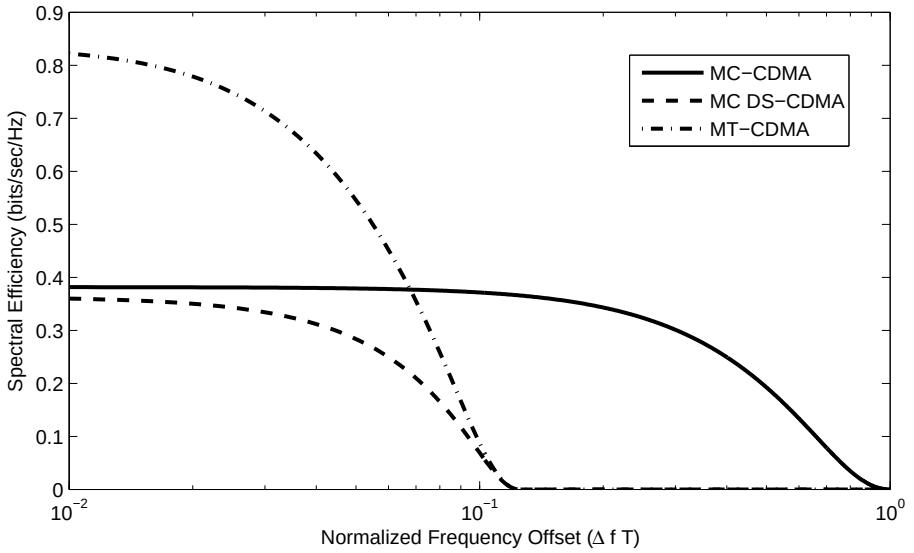

Figure 4.12: Spectral Efficiency versus normalized frequency offsets ($\Delta f\, T$) for the three multicarrier schemes.

Chapter 5

Spectral Efficiency of Multicarrier CDMA in Uncoordinated Ad-hoc Network

In an uncoordinated ad-hoc network all nodes are asynchronous to each other i.e. their symbol start time is random and uncoordinated. Furthermore due to the lack of central control there is no centralized media access control strategy and all nodes transmit at will. In such an environment multiple access interference (MAI) becomes the dominant factor that determines performance. In the literature, the performance of multicarrier CDMA has usually been investigated under two assumptions

- The MAI is pure Gaussian [60, 63–65] .
- The fading among different subcarriers is independent [66–68].

However, these assumptions are not valid when the number of users is small [69] or frequency separation among adjacent subcarriers is insufficient [70]. The problem of correlated fading brings some mathematical complexities which have only been addressed by a few reports. In [60, 63–65], bit error rate (BER) for maximal

ratio combining (MRC) and in [71] for equal gain combining (EGC) is derived considering dependent fading, however, Gaussian approximation (GA) is used for MAI. In [69, 70, 72] no assumption is made regarding the statistics of MAI, where [72] assumes independent fading and in [69, 70] numerical calculations require K summations of residue polynomial where K is the number of interferers. In [73] a lower bound to BER considering both independent and correlated fading for MRC and EGC is calculated, however it uses a weaker assumption. To our knowledge [22] is the only paper that deals with spectral efficiency of MC-CDMA, where it considers synchronous transmitters which is difficult to achieve practically.

In this chapter, we find simple expressions for the spectral efficiency of asynchronous multicarrier CDMA systems, which to our knowledge have not been analyzed. We do not assume the MAI to be purely Gaussian; furthermore, the fading experienced by the subcarriers are considered correlated. We consider MRC due to its optimality and generality. The complexity of the numerical calculations of our results depend on the number of subcarriers and do not increase with an increase in the number of interferers.

The carrier frequency offset that we analyzed in Chapter 4 is also considered in this chapter. The frequency offset of the desired transmitter is considered as a deterministic value that is to be estimated and the offset of the interferers is taken as a random quantity that varies with the interferer. We follow the same model and assumptions as in Chapter 3, the transmitted signals for MC-CDMA, MC DS-CDMA and MT-CDMA schemes are the same as given in 2.2, 2.3 and 2.4 respectively. The spectral efficiency of the three multicarrier CDMA schemes are analyzed in detail in the following sections.

5.1 MC-CDMA

We consider the receiver of interest to be surrounded by K similar nodes, uniformly distributed in a large area. The received signal $r(t)$ at the receiver of interest, after removing the cyclic prefix, is given as

$$r(t) = \sum_{k=1}^{K} \frac{1}{\sqrt{N_p}} \sum_{n=0}^{N_p-1} G_{n,k}\, b_k\,(t)\, c_k\,[n]\, \mathrm{e}^{j2\pi f_{n,k} t} \mathrm{e}^{j2\pi \frac{\triangle_k}{T} t} + \eta\,(t)$$

where Δ_k is the carrier frequency offset of the kth transmitter, $b_k\,(t)$ is the information bearing signal, $c_k\,[n]$ is the nth component of the spreading signal, N_p is the total number of subcarriers, $f_{n,k}$ is the frequency of the nth subcarrier, $G_{n,k}$ is the channel transfer function of the nth subcarrier of the kth transmitter and $\eta\,(t)$ is the AWGN component.

The received signal is decoded by a conventional correlation receiver with MRC. Let Z represent the receiver decision variable and let $k = 1$ represent the desired transmitter, then

$$Z = \sum_{m=0}^{N_p-1} \frac{1}{T} \int_0^T G^*_{m,1}\, c_1\,[m]\, \mathrm{e}^{-j2\pi f_{m,1} t}\, r\,(t)\, \mathrm{d}t$$

where $G^*_{m,1}$ is the complex conjugate of the channel transfer function of the mth subcarrier. The decision variable Z can be separated into four distinct components $Z = S + I_1 + I_2 + N$, where S is the desired signal component, I_1 is the MAI component, I_2 is the ICI component and N is the noise component, these are given respectively as

$$S = b_1\,(t)\, \frac{1}{\sqrt{N_p}} \sum_{m=0}^{N_p-1} \frac{1}{T} \int_0^T |G_{m,1}|^2\, \mathrm{e}^{j2\pi \frac{\triangle_1}{T} t} \mathrm{d}t$$

$$I_1 = \sum_{m=0}^{N_p-1} \int_0^T G^*_{m,1} c_1[m] \, \mathrm{e}^{-j2\pi f_{m,1} t} \sum_{k=2}^{K} \frac{1}{\sqrt{N_p}} \sum_{n=0}^{N_p-1} G_{n,k} b_k(t) \, c_k[n] \, \mathrm{e}^{j2\pi f_{n,k} t} \mathrm{e}^{j2\pi \frac{\triangle_k}{T} t} \mathrm{d}t \tag{5.1}$$

$$I_2 = b_1(t) \frac{1}{\sqrt{N_p}} \sum_{m=0}^{N_p-1} \sum_{n=0, n\neq m}^{N_p-1} c_1[m] \, c_1[n] \, \frac{1}{T} \int_0^T G^*_{m,1} G_{n,1} \, \mathrm{e}^{j2\pi (\frac{n-m}{T}) t} \mathrm{e}^{j2\pi \frac{\triangle_1}{T} t} \mathrm{d}t \tag{5.2}$$

$$N = \sum_{m=0}^{N_p-1} G^*_{m,1} \, c_1[m] \, \frac{1}{T} \int_0^T \mathrm{e}^{-j2\pi f_{m,1} t} \eta(t) \, \mathrm{d}t.$$

Note that the ICI component is due to the frequency offset Δ_1 only and it can be easily verified that I goes to zero in (5.2) when $\Delta_1 = 0$, where Δ_1 is the frequency offset of the desired transmitter with the receiver, it is a deterministic quantity that can be estimated. For simplicity we replace Δ_1 with just Δ in the rest of the chapter. As far as the statistics of MAI in (5.1) and ICI in (5.2) are concerned, note that they are large sums of correlated random variables and because of the correlation the central limit theorem can not be applied hence the assumption of I_1 and I_2 being Gaussian random variables can not be justified. However if we condition on $G_{0,1}, \ldots G_{N_p-1,1}, \ldots, G_{0,K}, \ldots G_{N_p-1,K}$ then the central limit theorem is applicable as $c_1[m]$ and $c_k[n]$ are independent random variables. We therefore approximate Z as a conditional Gaussian random variable, conditioned on $G_{0,1}, \ldots G_{N_p-1,K}$. The conditional mean is

$$\mathbb{E}\left[Z | G_{0,1}, \ldots G_{N_p-1,K}\right] = \sqrt{\frac{E_s}{TN_p}} \sum_{m=0}^{N_p-1} |G_{m,1}|^2 \mathrm{sinc}(\pi \triangle)$$

and the conditional variance of Z can be calculated as

$$\begin{aligned}\mathrm{Var}\left[Z|G_{0,1},\dots G_{N_p-1,K}\right] &= \frac{E_s}{TN_p}\sum_{k=2}^{K}\sum_{m=0}^{N_p-1}\sum_{n=0}^{N_p-1}|G_{m,1}|^2|G_{n,k}|^2 \\ &\times\frac{1-\mathrm{sinc}\left(2\pi\left(m-n+\Delta_k\right)\right)}{\left(\pi\left(m-n+\Delta_k\right)\right)^2}+\frac{E_s}{TN_p}\sum_{m=0}^{N_p-1}\sum_{n=0,n\neq m}^{N_p-1}|G_{m,1}|^2|G_{n,1}|^2 \\ &\times\mathrm{sinc}^2\left(\pi\left(m-n+\Delta\right)\right)+\sum_{m=0}^{N_p-1}|G_{m,1}|^2\frac{N_0}{T}.\end{aligned}$$

The instantaneous SINR is therefore a random variable given by the ratio

$$\begin{aligned}\mathrm{SINR} = \left(\sum_{m=0}^{N_p-1}|G_{m,1}|^2\right)^2 &\left[\sum_{k=2}^{K}\sum_{m=0}^{N_p-1}\sum_{n=0}^{N_p-1}|G_{m,1}|^2|G_{n,k}|^2\rho_{m,n,k}\right. \\ &\left.+\sum_{m=0}^{N_p-1}\sum_{n=0,n\neq m}^{N_p-1}|G_{m,1}|^2|G_{n,1}|^2\rho_{m,n}+\sum_{m=0}^{N_p-1}|G_{m,1}|^2\frac{N_0}{E_s\mathrm{sinc}^2\left(\pi\triangle\right)}\right]^{-1} \qquad (5.3)\end{aligned}$$

where $\rho_{m,n,k}=\frac{1-\mathrm{sinc}(2\pi(m-n+\Delta_k))}{(\pi(m-n+\Delta_k))^2\mathrm{sinc}^2(\pi\triangle)}$ and $\rho_{m,n}=\left(\frac{\Delta}{n-m+\Delta}\right)^2$.

The instantaneous signal to interference and noise ratio in (5.3) can now be used to analyze the spectral efficiency.

5.1.1 Spectral Efficiency Analysis

The spectral efficiency of the system is given as

$$\mathrm{C}=\frac{K}{N_p}\mathbb{E}\left[\log_2\left(1+\mathrm{SINR}\right)\right] \qquad (5.4)$$

where the random variable SINR is given in (5.3) which itself consists of $N_p\times K$ random variables $G_{0,1},\dots G_{N_p-1,1},\dots,G_{0,K},\dots G_{N_p-1,K}$.

The direct method to solve (5.4) requires $N_p\times K-$fold integrations making it too complex. Gaussian approximation of the interference in the denominator

in (5.3), though incorrect due to the correlation between the numerator and the denominator would still require finding K pdf's of the summations $\sum_{m=0}^{N_p-1}|G_{m,k}|^2$ where $k \in [1, K]$. Furthermore the summations $\sum_{m=0}^{N_p-1}|G_{m,k}|^2$ can not be considered as chi square distributed– because of the correlation that exists between $G_{m,k}$'s.

We now find an accurate and simpler solution to (5.4). Let

$$\chi_{n,k} = \sum_{m=0}^{N_p-1} \frac{|G_{m,1}|^2}{\sum_{m=0}^{N_p-1}|G_{m,1}|^2}\rho_{m,n,k}$$

$$\chi = \sum_{m=0}^{N_p-1}\sum_{n=0,n\neq m}^{N_p-1} \frac{|G_{m,1}|^2}{\sum_{m=0}^{N_p-1}|G_{m,1}|^2}\frac{|G_{n,1}|^2}{\sum_{m=0}^{N_p-1}|G_{m,1}|^2}\rho_{m,n}. \tag{5.5}$$

Then (5.4) can be rewritten as

$$\mathrm{C} = \frac{K}{N_p}\mathbb{E}\left[\log_2\left(1 + \frac{\sum_{m=0}^{N_p-1}|G_{m,1}|^2}{\sum_{k=2}^{K}\sum_{n=0}^{N_p-1}|G_{n,k}|^2\chi_{n,k} + \chi\sum_{m=0}^{N_p-1}|G_{m,1}|^2 + \frac{N_0}{E_s\mathrm{sinc}^2(\pi\triangle)}}\right)\right]. \tag{5.6}$$

Now, Jensen inequality asserts that

$$\mathrm{C} \geq \frac{K}{N_p}\mathbb{E}\left[\log_2\left(1 + \frac{\sum_{m=0}^{N_p-1}|G_{m,1}|^2}{\sum_{k=2}^{K}\sum_{n=0}^{N_p-1}|G_{n,k}|^2\hat{\chi}_{n,k} + \hat{\chi}\sum_{m=0}^{N_p-1}|G_{m,1}|^2 + \frac{N_0}{E_s\mathrm{sinc}^2(\pi\triangle)}}\right)\right] \tag{5.7}$$

where the differences between (5.7) and (5.6) besides the inequality are $\hat{\chi}_{n,k}$ instead of $\chi_{n,k}$ and $\hat{\chi}$ instead of χ, where $\hat{\chi}_{n,k} = \mathbb{E}\left[\chi_{n,k}|\sum_{m=0}^{N_p-1}|G_{m,1}|^2\right]$ and $\hat{\chi} = \mathbb{E}\left[\chi|\sum_{m=0}^{N_p-1}|G_{m,1}|^2\right]$.

As far as the statistics of $\hat{\chi}_{n,k}$ and $\hat{\chi}$ are concerned, note firstly that when $\sigma = 0$ then $\hat{\chi}_{n,k}$ and $\hat{\chi}$ are independent of the sum $\sum_{m=0}^{N_p-1}|G_m|^2$. Furthermore, it

can also be verified (by the using [61, The. 1.5.6]) that when $\sigma \gg 1$ then the random vector $\left\{ \frac{G_{0,1}}{\sum_{m=0}^{N_p-1}|G_{m,1}|^2}, \frac{G_{1,1}}{\sum_{m=0}^{N_p-1}|G_{m,1}|^2}, \ldots, \frac{G_{N_p-1,1}}{\sum_{m=0}^{N_p-1}|G_{m,1}|^2} \right\}$ becomes independent of the sum $\sum_{m=0}^{N_p-1}|G_{m,1}|^2$, and hence $\mathbb{E}\left[\chi_{n,k}|\sum_{m=0}^{N_p-1}|G_{m,1}|^2\right] = \mathbb{E}[\chi_{n,k}]$ (independently of the sum $\sum_{m=0}^{N_p-1}|G_{m,1}|^2$) and similarly $\mathbb{E}\left[\chi|\sum_{m=0}^{N_p-1}|G_{m,1}|^2\right] = \mathbb{E}[\chi]$. Therefore we conjecture that only marginal errors might by introduced if we replace the conditional averages $\mathbb{E}\left[\chi_{n,k}|\sum_{m=0}^{N_p-1}|G_m|^2\right]$ and $\mathbb{E}\left[\chi|\sum_{m=0}^{N_p-1}|G_m|^2\right]$ by the unconditional averages $\mathbb{E}[\chi_{n,k}]$ and $\mathbb{E}[\chi]$ in (5.7).

The expectation in $\mathbb{E}[\chi_{k,n}] = \sum_{m=0}^{N_p-1}\mathbb{E}\left[\frac{|G_{m,1}|^2}{\sum_{m=0}^{N_p-1}|G_{m,1}|^2}\rho_{k,m,n}\right]$ can be simplified by considering the well known mathematical identity

$$\frac{1}{y^c} = \int_0^\infty \frac{z^{c-1}}{\Gamma(c)}\exp(-yz)\,dz, \quad \forall y, c > 0 \tag{5.8}$$

using $c = 1$ and $y = \sum_{m=0}^{N_p-1}|G_{m,1}|^2$ we get

$$\mathbb{E}\left[\frac{|G_{m,1}|^2}{\sum_{m=0}^{N_p-1}|G_{m,1}|^2}\rho_{k,m,n}\right] = \mathbb{E}\left[|G_{m,1}|^2\rho_{k,m,n}\int_0^\infty \exp\left(-z\sum_{m=0}^{N_p-1}|G_{m,1}|^2\right)\,\mathrm{d}z\right].$$

Let

$$\phi(z_1, z_2, \ldots, z_{N_p}) = \mathbb{E}\left[\exp\left(-\sum_{m=0}^{N_p-1} z_m|G_{m,1}|^2\right)\right]$$

then

$$\mathbb{E}\left[|G_{m,1}|^2\exp\left(-\sum_{m=0}^{N_p-1} z_m|G_{m,1}|^2\right)\right] = -\frac{\partial}{\partial z_m}\phi(z_1, z_2, \ldots, z_{N_p})$$

from [36, eq. (4a)] for the MGF of the Gaussian quadratic forms we know that

$$\phi(x_1, x_2, \ldots, x_{N_p}) = \frac{1}{\left|\mathbf{I}_{N_p} + \mathrm{diag}(x_1, x_2, \ldots, x_{N_p})\,\mathbf{\Lambda}\right|}$$

where $\mathbf{I}_{N_p}$ is the $N_p \times N_p$ identity matrix and Λ is $N_p \times N_p$ correlation matrix

where a typical element is given by $\Lambda_{ij} = \mathbb{E}\left[G_{i,1}G_{j,1}^{*}\right]$. We have to find its partial derivative which is given as [62, eq. (29)]

$$\frac{\partial}{\partial x_m}\phi\left(x_1, x_2, \ldots, x_{N_p}\right) = -\left|\text{diag}\left(1, 1, \ldots, 0_m, \ldots, 1\right)\right. \\ \left.+\text{diag}\left(x_1, x_2, \ldots, 1_m, \ldots, x_{N_p}\right)\mathbf{\Lambda}\right|\left|\mathbf{I}_{N_p} + \text{diag}\left(x_1, x_2, \ldots, x_{N_p}\right)\mathbf{\Lambda}\right|^{-2}. \quad (5.9)$$

This gives us

$$\mathbb{E}\left[\chi_{k,n}\right] = \sum_{m=0}^{N_p-1}\left(\mathbb{E}\left[\rho_{k,m,n}\right]\int_0^{\infty}\left|\text{diag}\left(1, 1, \ldots, 0_m, \ldots, 1\right)\right.\right. \\ \left.\left.+\text{diag}\left(z_1, z_2, \ldots, 1_m, \ldots, z_{N_p}\right)\mathbf{\Lambda}\right|\left|\mathbf{I}_{N_p} + \text{diag}\left(z_1, z_2, \ldots, z_{N_p}\right)\mathbf{\Lambda}\right|^{-2}\mathrm{d}z.$$

The derivation of $\mathbb{E}\left[\chi\right]$ follows similarly, where using $c = 2$ and $y = \sum_{m=0}^{N_p-1}\left|G_{m,1}\right|^2$ in (5.8) we get

$$\mathbb{E}\left[\frac{\left|G_{m,1}\right|^2}{\sum_{m=0}^{N_p-1}\left|G_{m,1}\right|^2}\frac{\left|G_{n,1}\right|^2}{\sum_{m=0}^{N_p-1}\left|G_{m,1}\right|^2}\rho_{m,n}\right] = \rho_{m,n}\mathbb{E}\left[\left|G_{m,1}\right|^2\left|G_{n,1}\right|^2\right. \\ \left.\times\int_0^{\infty}\exp\left(-z\sum_{m=0}^{N_p-1}\left|G_{m,1}\right|^2\right)z\,\mathrm{d}z\right] \quad (5.10)$$

where $\rho_{m,n}$ is a deterministic value and hence comes out of the expectation. Now

$$\mathbb{E}\left[\left|G_{m,1}\right|^2\left|G_{n,1}\right|^2\exp\left(-\sum_{m=0}^{N_p-1}z_m\left|G_{m,1}\right|^2\right)\right] = \frac{\partial}{\partial z_n}\frac{\partial}{\partial z_m}\phi\left(z_1, z_2, \ldots, z_{N_p}\right). \quad (5.11)$$

We already know the first partial derivative of $\phi\left(z_1, z_2, \ldots, z_{N_p}\right)$, the second

partial derivative can similarly be found and is given as

$$\frac{\partial}{\partial x_n}\frac{\partial}{\partial x_m}\phi\left(x_1,x_2,\ldots,x_{N_p}\right) = \frac{2\left|\mathrm{diag}(1,\ldots,0_m,\ldots,1)+\mathrm{diag}\left(x_1,\ldots,1_m,\ldots,x_{N_p}\right)\mathbf{\Lambda}\right|}{\left|\mathbf{I}_{N_p}+\mathrm{diag}\left(x_1,x_2,\ldots,x_{N_p}\right)\mathbf{\Lambda}\right|^3} \times \left|\mathrm{diag}\left(1,\ldots,0_n,\ldots,1\right)+\mathrm{diag}\left(x_1,\ldots,1_n,\ldots,x_{N_p}\right)\mathbf{\Lambda}\right| - \frac{\left|\mathrm{diag}(1,\ldots,0_m,\ldots,0_n,\ldots,1)+\mathrm{diag}\left(x_1,\ldots,1_m,\ldots,1_m,\ldots,x_{N_p}\right)\mathbf{\Lambda}\right|}{\left|\mathbf{I}_{N_p}+\mathrm{diag}\left(x_1,x_2,\ldots,x_{N_p}\right)\mathbf{\Lambda}\right|^2}. \quad (5.12)$$

Using (5.10), (5.11) and (5.12) exact unified expressions for$\mathbb{E}\left[\chi\right]$ can be found.

Our numerical results suggest that only marginal errors might be introduced when the following approximate expressions are used instead for reduced computational complexity

$$\hat{\chi}_{n,k} = \frac{1}{N_p}\sum_{m=0}^{N_p-1}\hat{\rho}_{m,n,k} \quad (5.13)$$

$$\hat{\chi} = \frac{1}{N_p^2}\sum_{m=0}^{N_p-1}\sum_{n=0,n\neq m}^{N_p-1}\rho_{m,n} \quad (5.14)$$

where $\rho_{m,n}$ is a deterministic value to be estimated and $\hat{\rho}_{m,n,k} = \mathbb{E}\left[\rho_{m,n,k}\right] = \mathbb{E}\left[\frac{1-\mathrm{sinc}(2\pi(m-n+\Delta_k))}{(\pi(m-n+\Delta_k))^2\mathrm{sinc}^2(\pi\triangle)}\right]$,- where the expectation is over Δ_k which represents the normalized frequency offset of the k'th interferer's local oscillator with that of the receiver . For the sake of simplicity we take it as a zero mean normal random variable with a small variance.

As far as the evaluation of the average in (5.7) is concerned, we can invoke [35, Lemma 1] to rewrite (5.7) in a more desirable form

$$\mathrm{C} \geq \frac{K}{N_p}\log_2\mathrm{e}\int_0^\infty\frac{1}{z}\left(\mathbb{E}\left[\exp\left(-z\left(\sum_{k=2}^{K}\sum_{n=0}^{N_p-1}\left|G_{n,k}\right|^2\hat{\chi}_{n,k}+\hat{\chi}\sum_{m=0}^{N_p-1}\left|G_{m,1}\right|^2\right)\right)\right] - \mathbb{E}\left[\exp\left(-z\left(\sum_{k=2}^{K}\sum_{n=0}^{N_p-1}\left|G_{n,k}\right|^2\hat{\chi}_{n,k}+(1+\hat{\chi})\sum_{m=0}^{N_p-1}\left|G_{m,1}\right|^2\right)\right)\right]\right)\mathrm{e}^{-\frac{zN_0}{E_s\mathrm{sinc}^2(\pi\triangle)}}\mathrm{d}z$$

where the Gaussian quadratic forms $\sum_{m=0}^{N_p-1} |G_{m,k}|^2$ appear only in the exponent. Therefore, known results for the moment generating function (MGF) of the Gaussian quadratic forms [36, eq. (4a)] can be applied to obtain the following explicit expression for the lower bound on the spectral efficiency of the multicarrier CDMA in the presence of frequency offset

$$\mathrm{C} \geq \frac{K}{N_p} \log_2 \mathrm{e} \int_0^\infty \frac{1}{z} \left(\frac{1}{|\mathbf{I}_{N_p} + z\tilde{\mathbf{\Lambda}}|} \right)^{K-1} \left(\frac{1}{|\mathbf{I}_{N_p} + z\hat{\chi}\mathbf{\Lambda}|} - \frac{1}{|\mathbf{I}_{N_p} + z\,(1+\hat{\chi})\,\mathbf{\Lambda}|} \right) \times \mathrm{e}^{-\frac{zN_0}{E_s \mathrm{sinc}^2(\pi\triangle)}} \mathrm{d}z. \quad (5.15)$$

Here, $|.|$ represents determinant of a matrix, $\mathbf{I}_{N_p}$ is the $N_p \times N_p$ identity matrix, whereas Λ is $N_p \times N_p$ correlation matrix where a typical element is given as $\Lambda_{ij} = \mathbb{E}\left[G_{i,1} G_{j,1}^*\right]$, $\tilde{\mathbf{\Lambda}}$ is also a $N_p \times N_p$ matrix where a typical element is given as $\tilde{\mathbf{\Lambda}}_{i,j} = \mathbb{E}\left[G_{i,k} G_{j,k}^* \sqrt{\hat{\chi}_{i,k}\hat{\chi}_{j,k}}\right]$.

Equation (5.15) is the desired expression for the spectral efficiency with frequency offset. Please note that (5.15) requires a single integration as compared to $N_p \times K$ integrations in the direct method.

5.1.2 Numerical Results

In this section we present some numerical and simulation results which show the tightness of the spectral efficiency bound. In Fig. 5.1 spectral efficiency using (5.15) is plotted against frequency offset (Δ), the simulation result was generated using (5.4) with 10^6 iterations and the approximation result was generated using (5.13) and (5.14) instead of the exact values of $\hat{\chi}_{n,k}$ and $\hat{\chi}$. We used E_s/N_0 of 10dB and the results are shown for 8, 16 and 32 number of subcarriers (N_p) for a fully loaded system i.e. total number of interferers (K) is equal to N_p. A 312.5 kHz frequency separation ($1/T$) between neighboring subcarriers (IEEE 802.11a [37]) and channel delay spread (α) of 0.1μs is used. It can be clearly seen that our

Table 5.1: Comparison of simulation, analysis and approximation results

Δ	0.01	0.02	0.05	0.1	0.2	0.5	1.0
Simulation	1.0137	1.0126	1.0083	0.9897	0.9176	0.4960	0
Analysis	1.0128	1.0120	1.0069	0.9885	0.9169	0.4948	0
Approximation	1.0111	1.0104	1.0053	0.9873	0.9169	0.4994	0

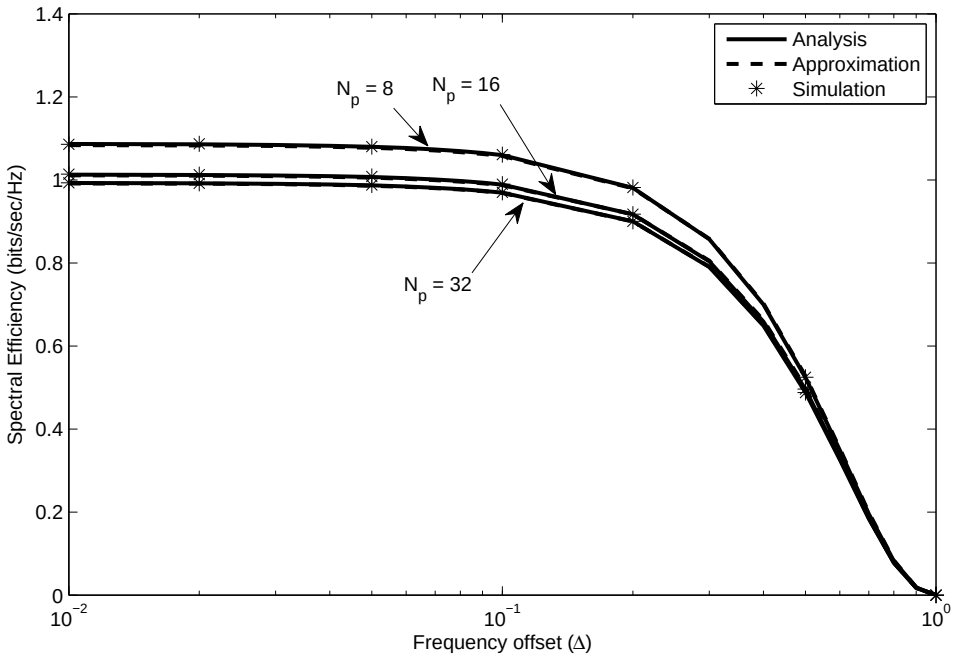

Figure 5.1: Degradation in spectral efficiency due to frequency offset for 8, 16 and 32 subcarriers.

analysis provides a tight lower bound and the approximation follows the analysis and simulation very closely. Numerical values of the analysis, approximation and simulation results are also shown in table 5.1 for N_p of 16, the results clearly show the tightness of the lower bound found by our analysis.

Fig. 5.1 also shows that the degradation in spectral efficiency is small for $\Delta < 0.1$ but sharply increases at higher values meaning small values of frequency offset do not degrade performance.

In Fig. 5.2 spectral efficiency versus E_s/N_0 calculated with our analysis is

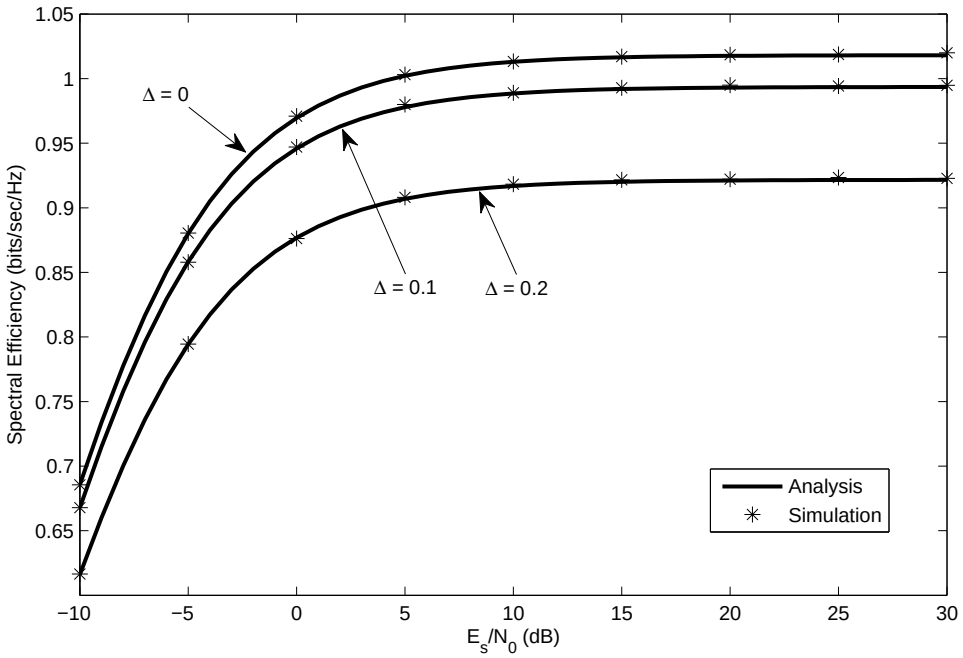

Figure 5.2: Spectral Efficiency versus E_s/N_0 for frequency offsets (Δ) of 0, 0.1 and 0.2.

compared against simulation. The analysis results are very close to the simulation results again showing the tightness of the bound. The spectral efficiency curves are drawn for frequency offset (Δ) values of 0, 0.1 and 0.2, the spectral efficiency increases with E_s/N_0 as expected and the decrease in spectral efficiency with increasing frequency offset is also evident. Note that the spectral efficiency increases sharply in the range of -10dB to 10dB while there is a marginal increase after 10dB.

Fig. 5.3 shows the degradation in spectral efficiency against normalized delay spread (σ) for $\Delta = 0.2$, $E_s/N_0 = 10$dB, $N_p = 16$ and $K = 16$. Larger values of σ result in smaller coherence bandwidth and hence lower correlation between subcarriers, resulting in better spectral efficiency. This is because the correlation between subcarriers decay faster when the normalized delay spread is increased, as given in (3.3). Higher correlation between subcarriers reduces the diversity

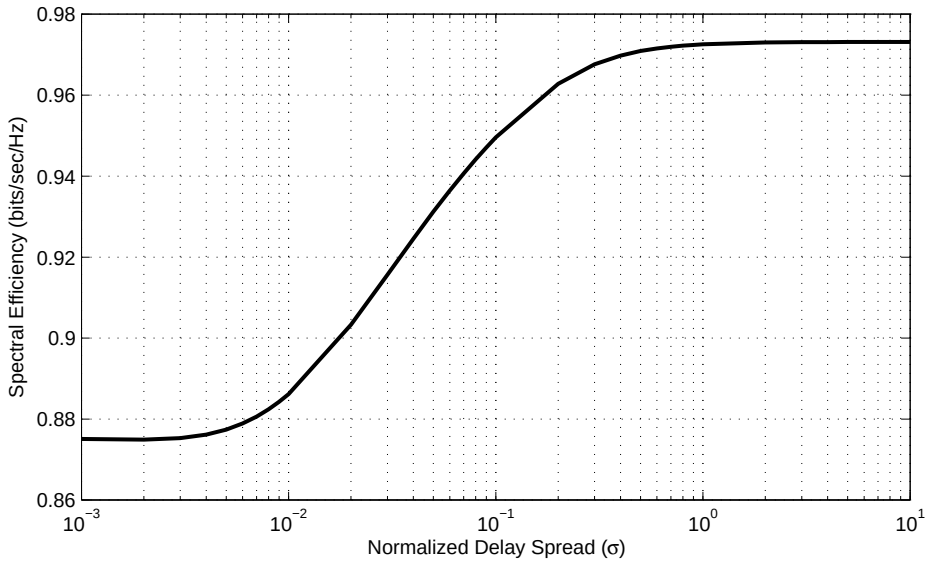

Figure 5.3: Spectral efficiency versus normalized delay spread (σ) for $\Delta = 0.2$.

gain and hence spectral efficiency, the diversity gain and spectral efficiency are maximized when there is no correlation between subcarriers ($\sigma \gg 1$) and vice versa. Fig. 5.4 also compares the spectral efficiency for fully correlated ($\sigma \approx 0$) and uncorrelated subcarrier fading ($\sigma \gg 1$). There is a marked difference between the two curves, which also confirms that uncorrelated subcarrier fading assumption over estimates performance and hence correlated subcarrier fading models should be used for performance analysis.

Fig. 5.5 shows the spectral efficiency versus total number of interferers (K) for 64 number of subcarriers. The maximum value for K is also 64 which represents a fully loaded system. The spectral efficiency monotonically increases as the system goes from being partially loaded to fully loaded.

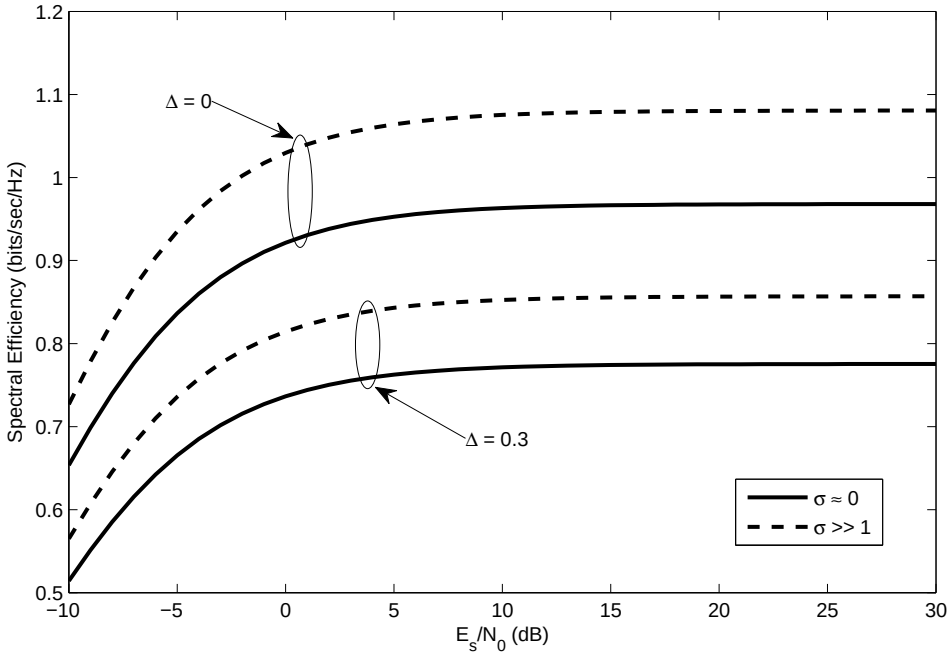

Figure 5.4: Spectral efficiency versus E_s/N_0 for frequency offsets (Δ) of 0 and 0.3.

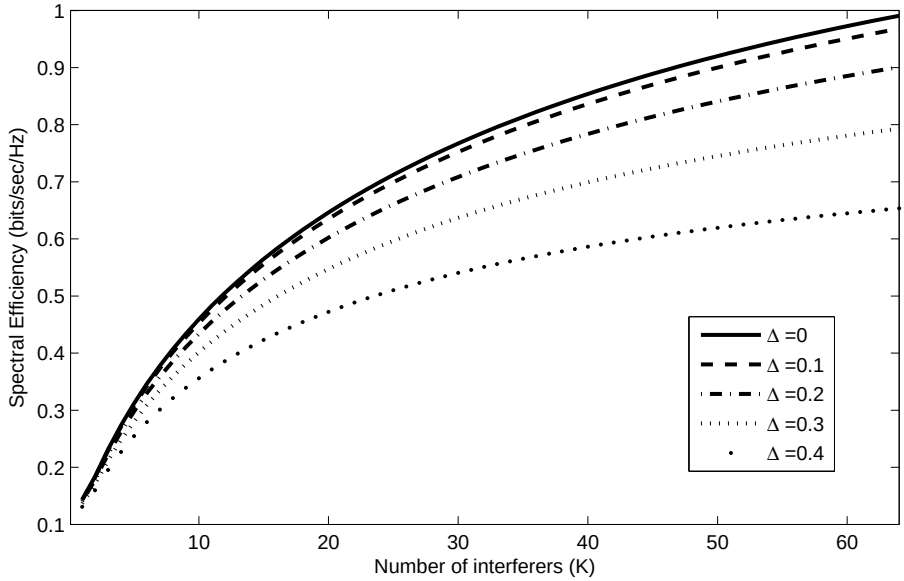

Figure 5.5: Spectral efficiency versus total number of interferers (K) for some frequency offset values.

5.2 Multi-Carrier DS-CDMA

The MC DS-CDMA transmitted signal representation for the K transmitters is same as given in (3.7), the received signal is different as now it also contains the interference component from other transmitters. It is given as

$$r(t) = \sum_{k=1}^{K} \sum_{l=1}^{N_c} G_{l,k}\, b_{l,k}\,(t)\, c_k\,(t)\, \mathrm{e}^{j2\pi\left(f_{l,k}+\Delta f_k\right)t} + \eta\,(t)\,.$$

Let $k = 1$ represent the desired transmitter, the decision variable for the first symbol which is transmitted on the first subcarrier becomes

$$Z_1 = \frac{1}{N_c T} \int_0^{N_c T} G_{1,1}^{*} c_1\,(t)\, \mathrm{e}^{-j2\pi f_{1,1} t} \left(\sum_{k=1}^{K} \sum_{l=1}^{N_c} G_{l,k}\, b_{l,k}\,(t)\, c_k\,(t)\, \mathrm{e}^{j2\pi\left(f_{l,k}+\Delta f_k\right)t} + \eta\,(t) \right). \tag{5.16}$$

The decision variable can be divided into four parts i.e. $Z_1 = S + I_1 + I_2 + N$, which are respectively desired signal, interference from other subcarriers of the desired transmitter, interference from other transmitters (interferers) and noise. The desired signal (S), interference from other subcarriers of the desired transmitter (I_1) and noise (N) are the same as in the section 4.2 and reproduced below

$$S = |G_{1,1}|^2\, b_{1,1}\,(t)\, \frac{1}{N_c T} \int_0^{N_c T} \mathrm{e}^{j2\pi\Delta f t} \mathrm{d}t$$

$$I_1 = \frac{1}{N_c T} G_{1,1}^{*} \sqrt{s} \sum_{l=2}^{N_c} G_l b_l \mathrm{e}^{j\phi} \int_0^{N_c T} \mathrm{e}^{j2\pi(f_l - f_1 + \Delta f)t} \mathrm{d}t$$

$$N = \frac{1}{N_c T} G_{1,1}^{*} c \int_0^{N_c T} \mathrm{e}^{-j2\pi f_1 t} \eta\,(t)\, \mathrm{d}t.$$

The interference from the $K-1$ interferers can be found using (5.16) as

$$I_2 = \frac{1}{N_c T} \int_0^{N_c T} G_{1,1}^* c_1(t)\, \mathrm{e}^{-j2\pi f_{1,1} t} \sum_{k=2}^{K} \sum_{l=1}^{N_c} G_{l,k}\, b_{l,k}(t)\, c_k(t)\, \mathrm{e}^{j2\pi\left(f_{l,k}+\Delta f_k\right)t} \mathrm{d}t. \quad (5.17)$$

Similar to the analyses in Chapter 4 and section 5.1, when we condition on $\left\{\left\{G_{0,1},\ldots,G_{N_p-1,1}\right\},\left\{G_{0,2},\ldots,G_{N_p-1,2}\right\},\ldots,\left\{G_{0,K},\ldots,G_{N_p-1,K}\right\}\right\}$ and Δ_k, the decision variable becomes a zero mean Gaussian random variable. The conditional mean during a signaling interval is not zero and is same as in (4.13) and given below

$$\mathbb{E}\left[Z|G_{0,1},\ldots,G_{N_p-1,K},\Delta_k\right] = |G_{1,1}|^2 \sqrt{\frac{E_s}{N_c T}} \mathrm{sinc}\left(\pi N_p \Delta\right). \quad (5.18)$$

The conditional variance has three components, the contribution from I_1 and N are the same as in section (4.2), the contribution from I_2 can be found from (5.17) as

$$\mathrm{Var}\left[I_2|G_{0,1},\ldots,G_{N_p-1,K},\Delta_k\right] = |G_{1,1}|^2 \sum_{k=2}^{K} \sum_{l=1}^{N_c} |G_{l,k}|^2 \left(\frac{E_s}{N_c T}\right) \left(\frac{1}{\pi\left(l-1+\Delta_k\right)N_p}\right)^2 \left(1-\mathrm{sinc}\left(2\pi\left(l-1+\Delta_k\right)N_p\right)\right). \quad (5.19)$$

The instantaneous SINR can now be constructed as

$$\mathrm{SINR} = \frac{E_s}{N_c T}\left|G_{1,1}\right|^4 \mathrm{sinc}^2\left(\pi N_p \Delta\right)\Bigg[\left|G_{1,1}\right|^2 \frac{E_s}{N_c T}\sum_{l=2}^{N_c}\left|G_{l,1}\right|^2 \mathrm{sinc}^2\left(\pi N_p\left(l-1+\Delta\right)\right)$$
$$+\left|G_{1,1}\right|^2 \sum_{k=2}^{K}\sum_{l=1}^{N_c}\left|G_{l,k}\right|^2 \left(\frac{E_s}{N_c T}\right)\left(\frac{1}{\pi\left(l-1+\Delta_k\right)N_p}\right)^2 \left(1-\mathrm{sinc}\left(2\pi\left(l-1+\Delta_k\right)N_p\right)\right)$$
$$+\frac{1}{N_c T}\left|G_{1,1}\right|^2 N_0\Bigg]^{-1}. \quad (5.20)$$

The spectral efficiency using (5.20) is analyzed in the next section.

5.2.1 Spectral Efficiency Analysis

The spectral efficiency using Shannon's capacity theorem and (5.20) can be found as

$$\mathrm{C} = \frac{K}{N_p}\mathbb{E}\Bigg[\log_2\Bigg(1+\frac{E_s}{N_c T}\left|G_{1,1}\right|^4 \mathrm{sinc}^2\left(\pi N_p \Delta\right)\Bigg[\left|G_{1,1}\right|^2 \frac{E_s}{N_c T}\sum_{l=2}^{N_c}\left|G_{l,1}\right|^2$$
$$\times \mathrm{sinc}^2\left(\pi N_p\left(l-1+\Delta\right)\right) + \left|G_{1,1}\right|^2 \sum_{k=2}^{K}\sum_{l=1}^{N_c}\left|G_{l,k}\right|^2 \left(\frac{E_s}{N_c T}\right)\left(\frac{1}{\pi\left(l-1+\Delta_k\right)N_p}\right)^2$$
$$\times\left(1-\mathrm{sinc}\left(2\pi\left(l-1+\Delta_k\right)N_p\right)\right)+\frac{1}{N_c T}\left|G_{1,1}\right|^2 N_0\Bigg]^{-1}\Bigg)\Bigg]$$

which can be simplified to

$$\mathrm{C} = \frac{K}{N_p}\mathbb{E}\Bigg[\log_2\Bigg(1+\left|G_{1,1}\right|^2\Bigg[\sum_{l=2}^{N_c}\left|G_{l,1}\right|^2\left(\frac{\Delta}{l-1+\Delta}\right)^2+\sum_{k=2}^{K}\sum_{l=1}^{N_c}\left|G_{l,k}\right|^2$$
$$\times\left(\frac{1}{\pi\left(l-1+\Delta_k\right)N_p}\right)^2\left(\frac{1-\mathrm{sinc}\left(2\pi\left(l-1+\Delta_k\right)N_p\right)}{\mathrm{sinc}^2\left(\pi N_p\Delta\right)}\right)+\frac{N_0/E_s}{\mathrm{sinc}^2\left(\pi N_p\Delta\right)}\Bigg]^{-1}\Bigg)\Bigg] \quad (5.21)$$

where the expectation is over all channel realizations and Δ_k.

Contrary to the MC DS-CDMA analyses in the previous chapters we can not find an exact solution to (5.21) because of Δ_k in the denominator. However a lower bound can be found using Jensen inequality and is given as

$$\mathrm{C} \geq \frac{K}{N_p}\mathbb{E}\left[\log_2\left(1+\frac{|G_{1,1}|^2}{\sum_{l=2}^{N_c}|G_{l,1}|^2\left(\frac{\Delta}{l-1+\Delta}\right)^2+\sum_{k=2}^{K}\sum_{l=1}^{N_c}|G_{l,k}|^2\rho_{k,l}+\frac{N_0}{E_s\mathrm{sinc}^2(\pi N_p\Delta)}}\right)\right] \tag{5.22}$$

where $\rho_{k,l}$ is given as

$$\rho_{k,l}=\mathbb{E}\left[\frac{1-\mathrm{sinc}\left(2\pi\left(l-1+\Delta_k\right)N_p\right)}{\left(\pi\left(l-1+\Delta_k\right)N_p\mathrm{sinc}\left(\pi N_p\Delta\right)\right)^2}\right].$$

Note that $\rho_{k,l}$ is similar to $\hat{\rho}_{m,n,k}$ in section 5.1.1 and in fact if we take $n=1$ in $\hat{\rho}_{m,n,k}$ they become the same. To evaluate (5.22) we invoke [35, Lemma 1] to get the expression in a more desirable form as

$$\begin{aligned}\mathrm{C} \geq \frac{K}{N_p}\log_2\mathrm{e}\int_0^\infty\frac{1}{z}\Bigg(&\mathbb{E}\left[\exp\left(-z\left(\sum_{l=2}^{N_c}\frac{|G_{l,1}|^2\Delta^2}{(l-1+\Delta)^2}+\sum_{k=2}^{K}\sum_{l=1}^{N_c}|G_{l,k}|^2\rho_{k,l}\right)\right)\right]\\ &-\mathbb{E}\left[\exp\left(-z\left(\sum_{l=1}^{N_c}\frac{|G_{l,1}|^2\Delta^2}{(l-1+\Delta)^2}+\sum_{k=2}^{K}\sum_{l=1}^{N_c}|G_{l,k}|^2\rho_{k,l}\right)\right)\right]\Bigg)\mathrm{e}^{-\frac{zN_0/E_s}{\mathrm{sinc}^2(\pi N_p\Delta)}}\mathrm{d}z.\end{aligned}$$

Again using MGF of Gaussian quadratic forms [36, eq. (4a)] to get

$$\mathrm{C} \geq \frac{K}{N_p}\log_2\mathrm{e}\int_0^\infty\frac{1}{z}\left(\frac{1}{|\mathbf{I}_{N_p}+z\boldsymbol{\Lambda_1}|}\right)^{K-1}\left(\frac{1}{|\mathbf{I}_{N_c-1}+z\boldsymbol{\Lambda_2}|}-\frac{1}{|\mathbf{I}_{N_c}+z\boldsymbol{\Lambda_3}|}\right)\mathrm{e}^{-\frac{zN_0/E_s}{\mathrm{sinc}^2(\pi N_p\Delta)}}\mathrm{d}z \tag{5.23}$$

where $\boldsymbol{\Lambda_2}$ and $\boldsymbol{\Lambda_3}$ are respectively $(N_c-1)\times(N_c-1)$ and $N_c\times N_c$ matrices with

elements given as

$$\Lambda(i,j) = \mathbb{E}[G_i G_j] \frac{\Delta^2}{(i-1+\Delta)(j-1+\Delta)}$$

for $1 < i \leq N_c$ and $1 < j \leq N_c$ and $\mathbf{\Lambda_1}$ is $N_p \times N_p$ matrix with elements $\Lambda_1(i,j) = \mathbb{E}\left[G_{i,2} G^*_{j,2} \sqrt{\rho_{k,i}\rho_{k,j}}\right]$. Equation (5.23) is the desired expression for the spectral efficiency of MC DS-CDMA in the presence of interferers and carrier frequency offset.

5.2.2 Numerical Results

In Fig. 5.6 the spectral efficiency of MC DS-CDMA is plotted against E_s/N_0 where analysis results were generated using (5.23) and simulation results were generated using (5.21) with 10^5 iterations. The results are generated for $N_p = 8$, $N_c = 8$ and 8 number of transmitters (K). As seen in the figure when $\Delta = 0.1$ i.e. %10 of subcarrier separation; the spectral efficiency at even E_s/N_0 of 30dB is lower than that for $\Delta = 0$ at E_s/N_0 of -10dB. This shows the relative degradation effect of frequency offset with respect to signal to noise ratio.

Fig. 5.7 shows spectral efficiency versus frequency offset for E_s/N_0 of 0dB and 10dB at $N_p = 8$, $N_c = 8$, $K = 8$ and 10^5 iterations were used for simulation. The spectral efficiency drops to zero at 0.125, i.e. $1/N_p$ and the performance is similar for E_s/N_0 of 0dB and 10dB. Note that there is a regular drop in the spectral efficiency even when Δ is smaller than 0.1 and when after 0.1 there is a sudden drop. This shows the vulnerability of a fully loaded MC DS-CDMA system to frequency offset.

The spectral efficiency degradation w.r.t. frequency offset at different values of N_p is shown in Fig. 5.8 for E_s/N_0 of 10dB. In order to have a fair comparison between different N_p values we plot the spectral efficiency with respect to frequency offset normalized to the symbol rate instead of frequency separation.

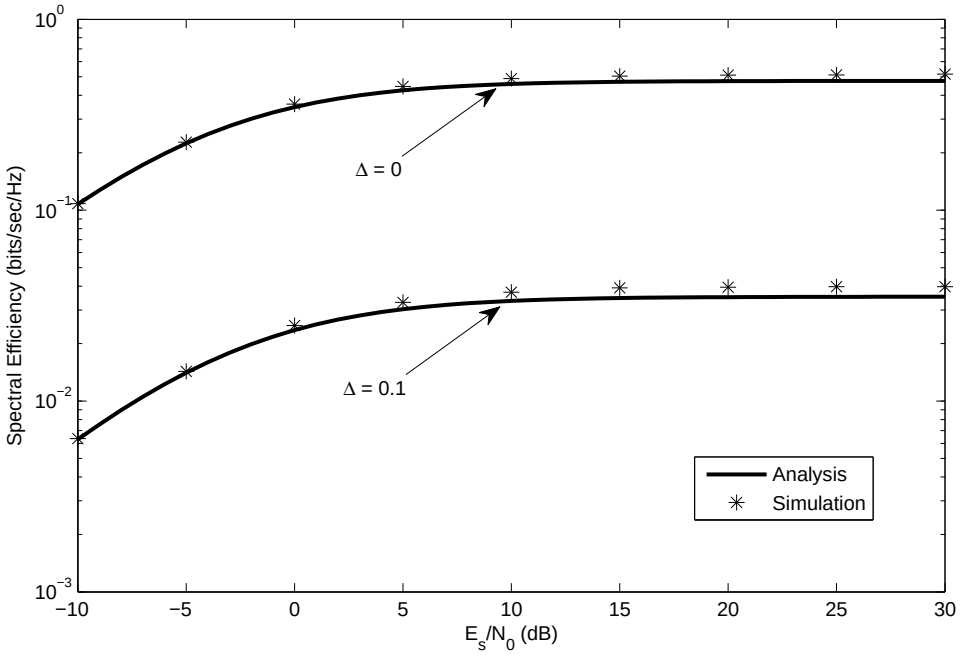

Figure 5.6: Spectral efficiency versus E_s/N_0 for frequency offset of 0 and 0.1.

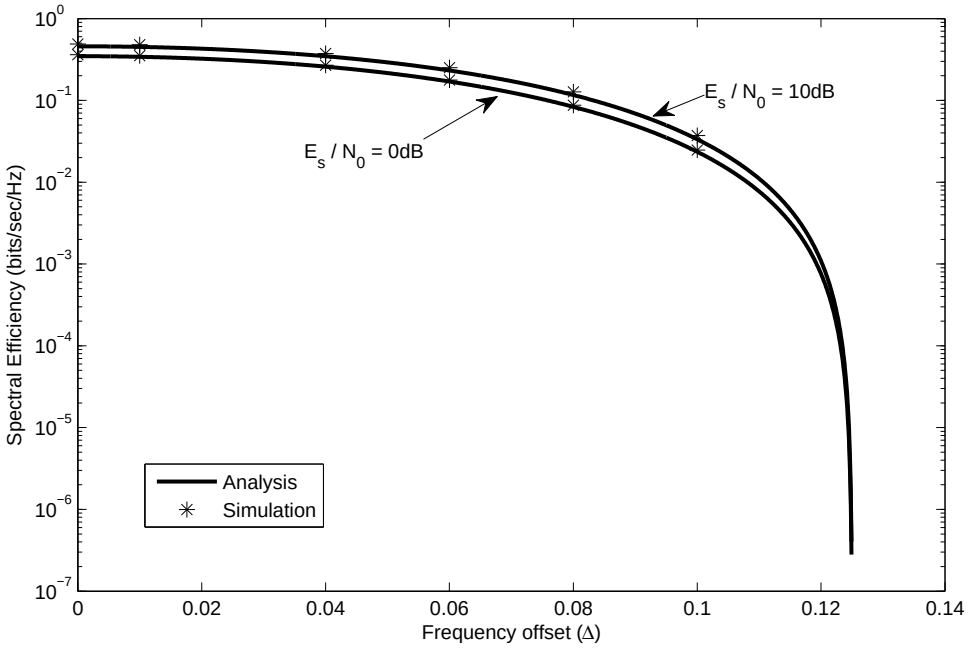

Figure 5.7: Spectral efficiency versus frequency offset for E_s/N_0 of 0dB and 10dB.

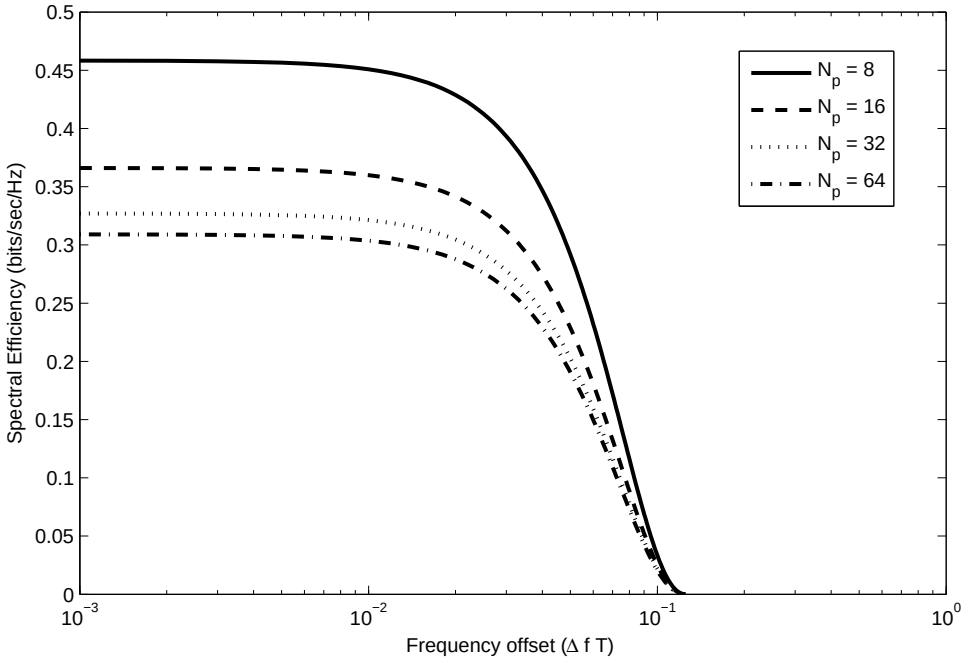

Figure 5.8: Spectral efficiency versus normalized frequency offset ($\Delta f\, T$) at N_p values of 8, 16, 32 and 64.

This is because the frequency separation between adjacent subcarriers changes with N_p. As seen in the figure the spectral efficiency for processing gain (N_p) values of 8, 16, 32 and 64 decay to zero at the same normalized frequency of $1/N_c$, where the number of subcarriers (N_c) was selected as 8. This dependence was also seen in Chapter 4 and is due to the S/P converter which reduces the frequency separation between adjacent subcarriers.

Fig. 5.9 shows the spectral efficiency when the total number of transmitters is increased from 1 to 32 i.e. unloaded system to a fully loaded system for $N_p = 32$, $N_c = 8$ and $E_s/N_0 = 10$dB. The difference in spectral efficiency between $\Delta = 0$ and $\Delta = 0.02$ can be seen to increase greatly from an unloaded system to a fully loaded system. This shows that frequency offset degrades the performance of a fully loaded system more severely than it does that of a partially loaded and/or unloaded system.

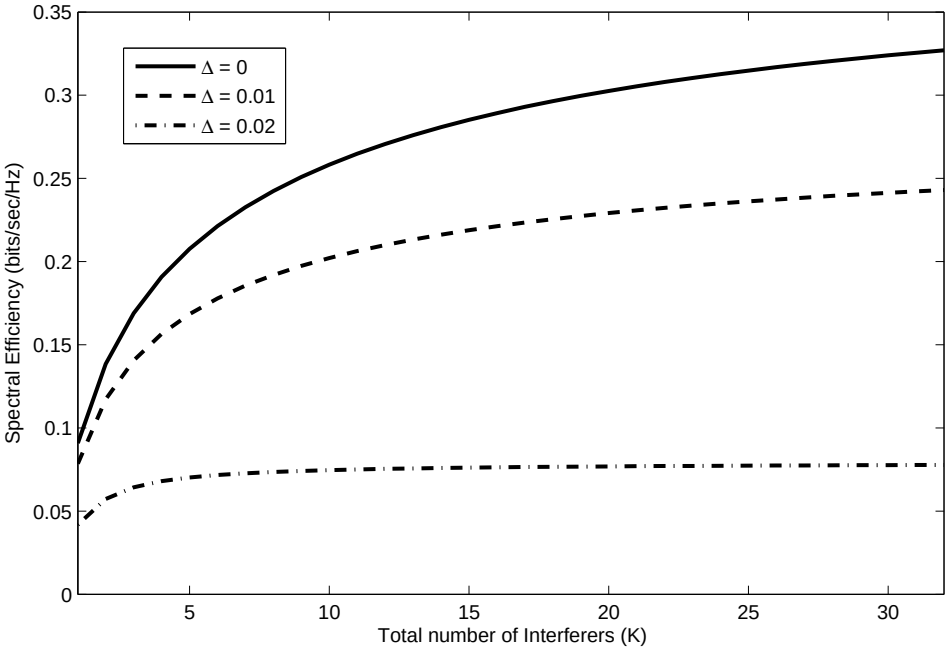

Figure 5.9: Spectral efficiency versus total number of interferers for Δvalues of 0, 0.01 and 0.02.

5.3 Multi-Tone CDMA

The transmitted signal for MT CDMA is given in (3.11) and is the same for the K transmitters. The received MT CDMA signal is given below

$$r(t) = \sum_{k=1}^{K} \sum_{l=1}^{N_c} \sum_{i=0}^{L-1} g_{i,k}\, b_{l,k} c_k \left(t - i\tau\right) \mathrm{e}^{j2\pi(f_l + \Delta f_k)(t - i\tau)} + \eta\left(t\right).$$

Let $k = 1$ be the desired transmitter as before, the decision variable for the first symbol, which is modulated on the first subcarrier, can be written as

$$Z_{1,1} = \sum_{m=0}^{L-1} \frac{1}{N_c T} \int_{0}^{N_c T} g_{m,1}^{*} c(t - m\tau) \mathrm{e}^{-j2\pi f_1 (t - m\tau)} r(t) \mathrm{d}t.$$

The decision variable can be divided into five components i.e. $Z_1 = S + I_1 + I_2 + I_3 + N$, which are respectively desired signal, self interference of the rake receiver, intercarrier interference, interference from other transmitters (interferers) and

noise. The desired signal (S), self interference of the rake receiver (I_1), intercarrier interference (I_2) and noise (N) are the same as in section 4.3. The interference component I_3 can be found as

$$I_3 = \sum_{m=0}^{L-1} \frac{1}{N_c T} \int_0^{N_c T} g_{m,1}^* c(t - m\tau) \mathrm{e}^{-j2\pi f_1 (t-m\tau)} \sum_{k=2}^{K} \sum_{l=1}^{N_c} \sum_{i=0}^{L-1} g_{i,k}\, b_{l,k} c_k \left(t - i\tau\right) \times \mathrm{e}^{j2\pi (f_l + \Delta f_k)(t - i\tau)} \mathrm{d}t.$$

When we condition on all channel conditions and Δ_k the decision variable $Z_{1,1}$ becomes a Gaussian random variable with expected value given in (4.18) and reproduced below

$$\mathbb{E}\left[Z_{1,1} | g_{0,1}, \ldots, g_{L-1,K}\right] = \sqrt{\frac{E_s}{N_c T}} \sum_{l=0}^{L-1} |g_{l,1}|^2 \operatorname{sinc}(\pi \triangle).$$

The conditional variance can similarly be found as

$$\begin{aligned}\mathrm{Var}\left[Z_{1,1} | g_{0,1}, \ldots, g_{L-1,K}\right] = {} & \frac{E_s}{T N_c} \left(\sum_{m=2}^{N_c} \operatorname{sinc}^2 \left(\pi \left(m - 1 + \Delta_1\right)\right) \right) \left(\sum_{n=0}^{L-1} |g_{n,1}|^2 \right)^2 + \frac{1}{N_p} \\ & \times \frac{E_s}{N_c T} \left(\sum_{k=1}^{N_c} \operatorname{sinc}^2 \left(\frac{\pi}{N_p} \left(k - 1 + \triangle_1\right) \right) \right) \left(\sum_{l=0}^{L-1} |g_{l,1}|^2 \sum_{m=0, m\neq l}^{L-1} |g_{m,1}|^2 \right) \\ & + \sum_{m=0}^{L-1} \sum_{k=2}^{K} \sum_{l=1}^{N_c} \sum_{i=0}^{L-1} |g_{m,1}|^2 |g_{i,k}|^2 \frac{E_s}{T N_c} \mathbb{E}\left[\frac{1 - \operatorname{sinc}\left(2\pi \left(l - 1 + \Delta_k\right)\right)}{\left(\pi \left(l - 1 + \Delta_k\right)\right)^2} \right] + \frac{N_0}{N_c T} \left(\sum_{l=0}^{L-1} |g_{l,1}|^2 \right).\end{aligned}$$

The signal to interference and noise ratio can now be found as

$$\mathrm{SINR} = \frac{\frac{E_s}{N_c T} \operatorname{sinc}^2 \left(\pi \triangle\right) \left(\sum_{l=0}^{L-1} |g_{l,1}|^2 \right)^2}{\mathrm{Var}\left[Z | g_{0,1}, \ldots, g_{L-1,K}\right]}. \tag{5.24}$$

Equation (5.24) can be used to find the spectral efficiency.

5.3.1 Spectral Efficiency Analysis

The spectral efficiency of the system depends on the SINR in (5.24) and can be evaluated by using the well known Shannon's capacity expression as

$$\mathrm{C} = \frac{N_c K}{N_c + N_p - 1}\mathbb{E}\left[\log_2\left(1 + \frac{\frac{E_s}{N_c T}\mathrm{sinc}^2\left(\pi\triangle\right)\left(\sum_{l=0}^{L-1}\left|g_l\right|^2\right)^2}{\mathrm{Var}\left[Z|g_{0,1},\ldots,g_{L-1,K}\right]}\right)\right]. \tag{5.25}$$

Let

$$\rho\left(m,l\right) = \mathbb{E}\left[\frac{\left|g_l\right|^2}{\sum_{l=0}^{L-1}\left|g_l\right|^2}\frac{\left|g_m\right|^2}{\sum_{m=0}^{L-1}\left|g_m\right|^2}\right]$$

where $\rho\left(m,l\right)$ is similar to ζ in (4.6) and the differences are the limits of the summations. The analysis of $\rho\left(m,l\right)$ also follows that for ζ in (4.6) and so we do not repeat it here. As far as the analysis of (5.25) is concerned, applying Jensen's inequality to (5.25) gives us

$$\begin{aligned}\mathrm{C} \geq \frac{N_c K}{N_c + N_p - 1}\mathbb{E}\Bigg[\log_2\Bigg(1 + \mathrm{sinc}^2\left(\pi\triangle\right)\sum_{l=0}^{L-1}\left|g_l\right|^2\Bigg[\left(\sum_{l=0}^{L-1}\left|g_l\right|^2\right)\Bigg(\frac{1}{N_p}\\ \times\sum_{k=1}^{N_c}\mathrm{sinc}^2\left(\frac{\pi}{N_p}\left(k-1+\triangle\right)\right)\sum_{l=0}^{L-1}\sum_{m=0,m\neq l}^{L-1}\rho\left(m,l\right) + \sum_{m=2}^{N_c}\mathrm{sinc}^2\left(\pi\left(m-1+\Delta\right)\right)\Bigg)\\ +\sum_{k=2}^{K}\sum_{l=1}^{N_c}\sum_{i=0}^{L-1}\left|g_{i,k}\right|^2\mathbb{E}\left[\frac{1-\mathrm{sinc}\left(2\pi\left(l-1+\Delta_k\right)\right)}{\left(\pi\left(l-1+\Delta_k\right)\right)^2}\right] + \frac{N_0}{E_s}\Bigg]^{-1}\Bigg)\Bigg].\end{aligned}$$

Let

$$\hat{\chi}\left(\triangle\right)=\frac{1}{N_p}\left(\sum_{k=1}^{N_c}\mathrm{sinc}^2\left(\frac{\pi}{N_p}\left(k-1+\triangle\right)\right)\right)\sum_{l=0}^{L-1}\sum_{m=0,m\neq l}^{L-1}\rho\left(m,l\right)+\left(\sum_{m=2}^{N_c}\mathrm{sinc}^2\left(\pi\left(m-1+\Delta\right)\right)\right)$$

and

$$\chi_k=\sum_{l=1}^{N_c}\mathbb{E}\left[\frac{1-\mathrm{sinc}\left(2\pi\left(l-1+\Delta_k\right)\right)}{\left(\pi\left(l-1+\Delta_k\right)\right)^2}\right]$$

where $\hat{\chi}\left(\triangle\right)$ and χ_k are deterministic values. The spectral efficiency can be written in terms of $\hat{\chi}\left(\triangle\right)$ and χ_k as

$$\mathrm{C}\geq\frac{N_cK}{N_c+N_p-1}\mathbb{E}\left[\log_2\left(1+\frac{\mathrm{sinc}^2\left(\pi\triangle\right)\sum_{l=0}^{L-1}\left|g_{l,1}\right|^2}{\sum_{l=0}^{L-1}\left|g_{l,1}\right|^2\hat{\chi}\left(\triangle\right)+\sum_{k=2}^{K}\sum_{i=0}^{L-1}\left|g_{i,k}\right|^2\chi_k+\frac{N_0}{E_s}}\right)\right]$$

which we can rewrite using lemma 1 in [35] as

$$\mathrm{C}\geq\frac{N_cK\ \log_2\mathrm{e}}{N_c+N_p-1}\int_0^\infty\frac{1}{z}\left(\mathbb{E}\left[\exp\left(-z\left(\hat{\chi}\left(\triangle\right)\sum_{l=0}^{L-1}\left|g_{l,1}\right|^2+\sum_{k=2}^{K}\sum_{i=0}^{L-1}\left|g_{i,k}\right|^2\chi_k\right)\right)\right]-\mathbb{E}\left[\exp\left(-z\left(\mathrm{sinc}^2\left(\pi\Delta\right)+\hat{\chi}\left(\triangle\right)\right)\sum_{l=0}^{L-1}\left|g_{l,1}\right|^2+\sum_{k=2}^{K}\sum_{i=0}^{L-1}\left|g_{i,k}\right|^2\chi_k\right)\right]\right)\times\exp\left(-z\frac{N_0}{E_s}\right)\mathrm{d}z.\quad(5.26)$$

Rearranging terms in (5.26) gives us

$$\mathrm{C} \geq \frac{N_c K \log_2 \mathrm{e}}{N_c + N_p - 1} \int_0^\infty \frac{1}{z} \mathbb{E}\left[\exp\left(-z \sum_{k=2}^{K} \sum_{i=0}^{L-1} |g_{i,k}|^2 \chi_k\right)\right] \left(\mathbb{E}\left[\exp\left(-z\hat{\chi}\left(\triangle\right)\right.\right.\right.$$
$$\left.\left.\left. \times \sum_{l=0}^{L-1} |g_{l,1}|^2\right)\right] - \mathbb{E}\left[\exp\left(-z\left(\mathrm{sinc}^2\left(\pi\Delta\right) + \hat{\chi}\left(\triangle\right)\right) \sum_{l=0}^{L-1} |g_{l,1}|^2\right)\right]\right) \mathrm{e}^{-z\frac{N_0}{E_s}} \mathrm{d}z. \tag{5.27}$$

And finally using MGF of the Gaussian quadratic forms [36, eq. (4a)] we can rewrite (5.27) as

$$\mathrm{C} \geq \frac{N_c K \log_2 \mathrm{e}}{N_c + N_p - 1} \int_0^\infty \frac{1}{z} \left(\frac{1}{|\mathbf{I}_L + z\chi_k \mathbf{\Lambda}|}\right)^{K-1} \left(\frac{1}{|\mathbf{I}_L + z\hat{\chi}\left(\triangle\right) \mathbf{\Lambda}|}\right.$$
$$\left. - \frac{1}{|\mathbf{I}_L + z(\mathrm{sinc}^2\left(\pi \mathbf{\Delta}\right) + \hat{\chi}\left(\triangle\right)) \mathbf{\Lambda}|}\right) \exp\left(-z\frac{N_0}{E_s}\right) \mathrm{d}z. \tag{5.28}$$

Equation (5.28) is the desired expression for the spectral efficiency of MT-CDMA in the presence of K number of transmitters each having a random carrier frequency offset of Δ_k.

5.3.2 Numerical Results

In Fig. 5.10 spectral efficiency is plotted against frequency offset (Δ) for E_s/N_0 of 0dB and 20dB. The analysis result was generated using (5.28) and Monte Carlo simulation result was generated using (5.25) with 10^5 iterations. The results are for $N_c = 16$, $N_p = 1024$, $L = 16$ and $K = 20$. The analysis results are very close to the simulation results confirming the tightness of the bound. The spectral efficiency degradation due to frequency offset is evident from the results, note that the degradation is negligible for $\Delta < 0.1$ but sharply increases afterward. This shows that a frequency offset of %10 of frequency separation would not harm

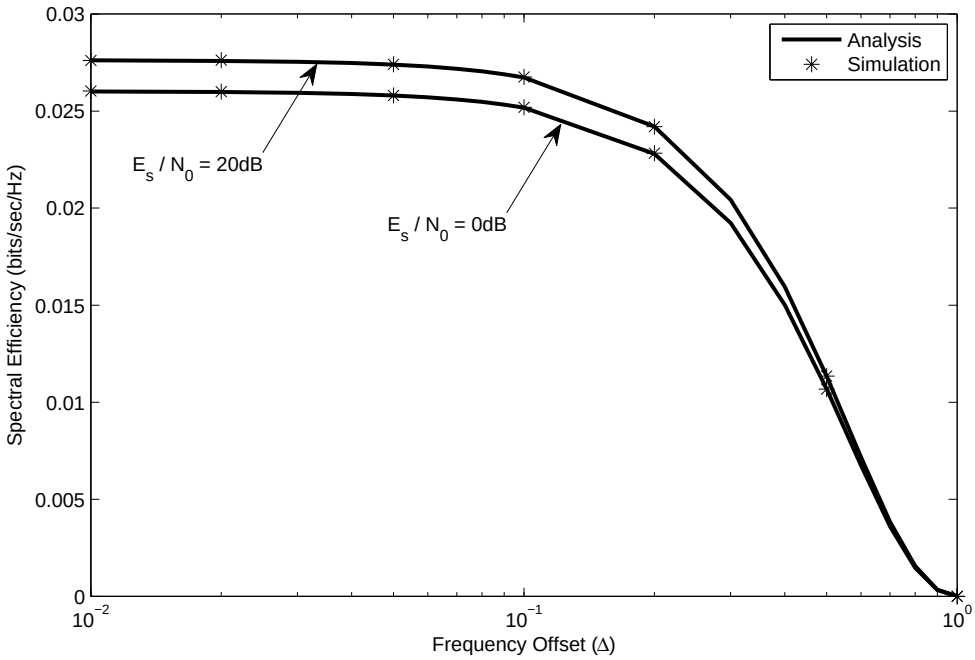

Figure 5.10: Spectral efficiency versus frequency offset for E_s/N_0 of 0dB and 20dB.

the performance but anything greater would severely limit it. For example, as seen in the figure, the performance at E_s/N_0 of 20dB falls to less than that for 0dB when Δ goes from 0.1 to 0.2.

Fig. (5.11) shows the spectral efficiency performance against E_s/N_0 for frequency offsets of 0, 0.2 and 0.4. The results were generated for $N_c = 16$, $N_p = 1024$, $L = 16$, $K = 10$. The results clearly show the benefits of having higher E_s/N_0 and note that there is not much improvement in performance after 10dB. Another important result is that the performance when $\Delta = 0.2$ at 30dB is lesser than the performance when $\Delta = 0$ and E_s/N_0 is 0dB showing the relative importance of frequency offset to signal to noise ratio.

Fig. (5.12) show the spectral efficiency versus total number of interferers (K) for frequency offsets of 0 and 0.2. The results were calculated for $N_c = 16$, $N_p = 1024$, $L = 16$ and $E_s/N_0 = 10$dB. The spectral efficiency decreases when the

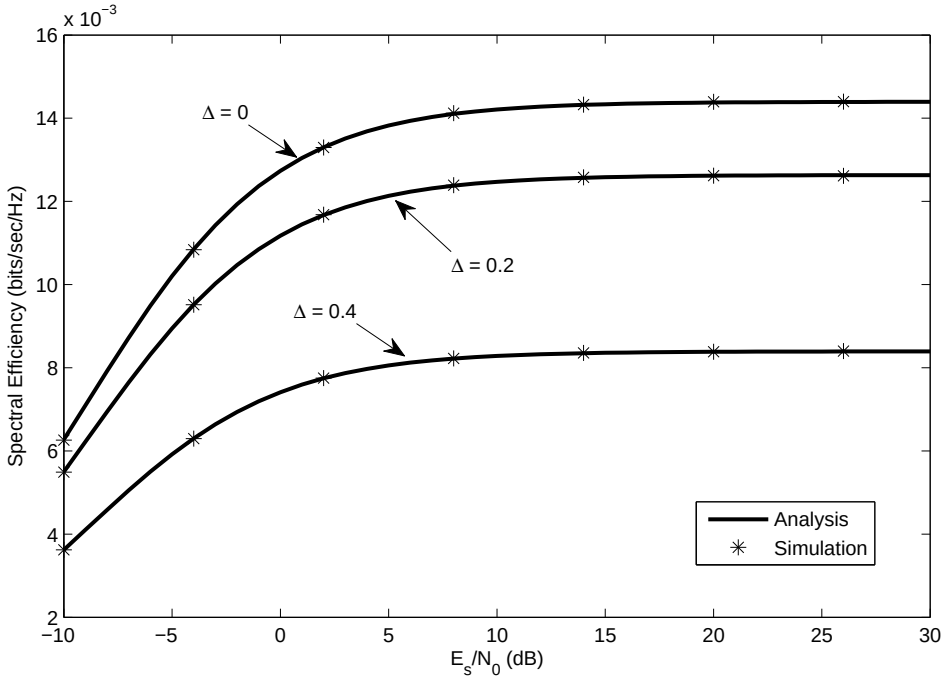

Figure 5.11: Spectral efficiency versus E_s/N_0 for frequency offset of 0, 0.2 and 0.4.

number of transmitters is increased, this is due to the multiple access interference from the interferers. This result is contrary to a similar result for MC-CDMA in Fig. 5.5, where the spectral efficiency increases instead of decreasing. This shows that MT-CDMA can not handle multiple access interference as well as MC-CDMA.

5.4 Chapter Conclusion

In this chapter we presented new expressions for the spectral efficiency of the three types of multicarrier CDMA. In numerical results we have compared simulation results with those found with our expressions and all results are in agreement; proving the validity of our analysis.

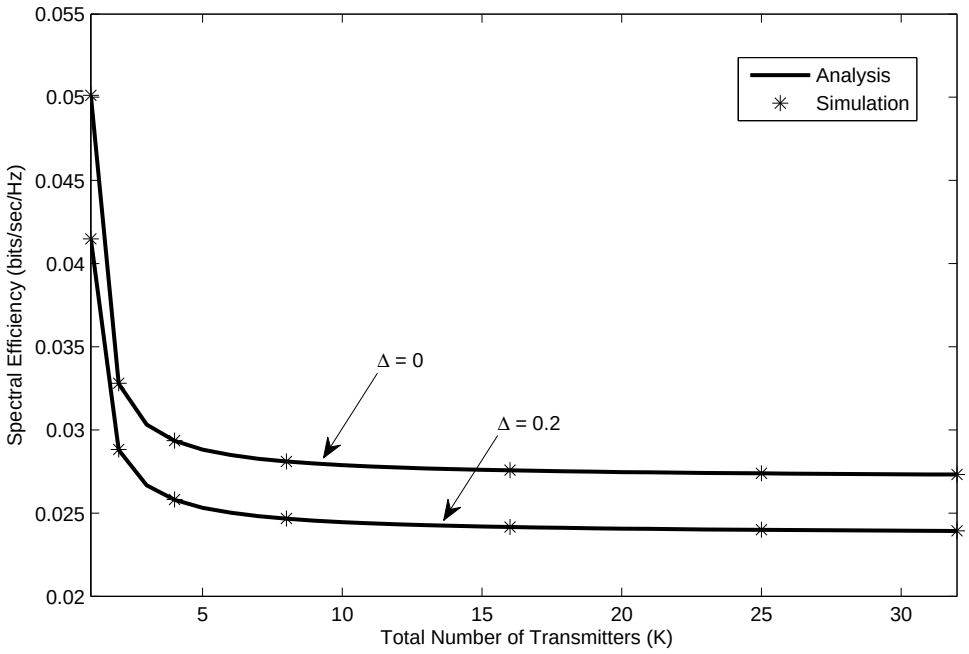

Figure 5.12: Spectral efficiency versus total number of interferers (K) for frequency offsets of 0 and 0.2.

Fig. 5.13 shows the spectral efficiency comparison for the three multicarrier schemes against total number of transmitters for normalized frequency offset $\Delta f\,T$ of 0 and 0.01. In order to have a fair comparison between the three schemes we have used frequency offset normalized to the symbol time rather than frequency separation. This was necessary since the frequency separation is different in the three schemes for the same N_p and N_c. The results are calculated for $N_p = 32$, $N_c = 32$, $L = 16$ and $E_s/N_0 = 10$dB. A 312.5 kHz frequency separation $(1/T)$ between neighboring subcarriers and channel delay spread (α) of 0.1μs was used. The results clearly show that MC-CDMA system performs best at full load while MT-CDMA system performs the best at no loading or partial loading when there is no frequency offset. However, when there is a small frequency offset (in our example 0.01) there is no loss of performance for MC-CDMA while the performance of MT-CDMA system is severely degraded, MT-CDMA is still best at

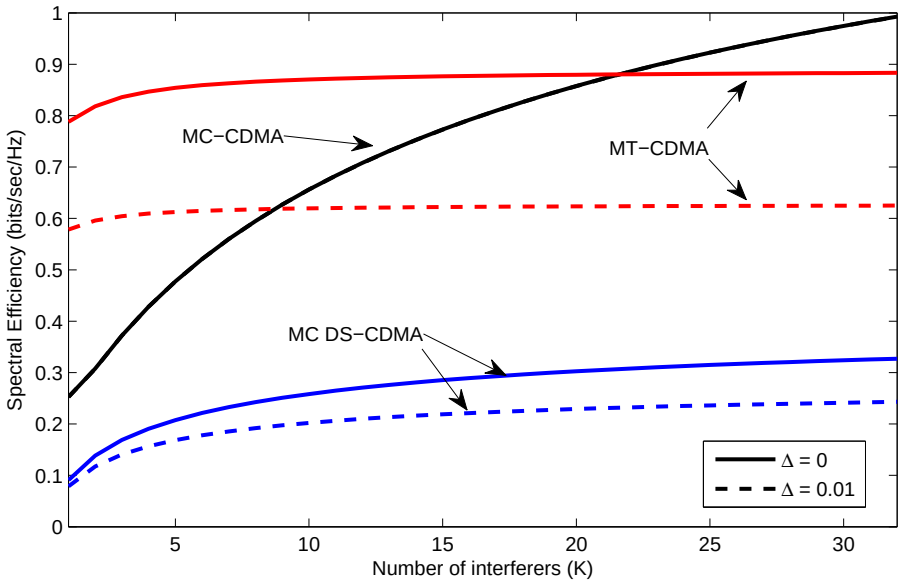

Figure 5.13: Spectral efficiency comparison of three multicarrier schemes against total number of transmitters.

no loading condition but at partial loading MC-CDMA is now the best choice. MC DS-CDMA systems which maybe easier to implement as they resemble DS-CDMA systems but in spectral efficiency their performance is the lowest of the three. The degradation due to frequency offset is not as stark as MT-CDMA but still remains much lower than that for MT-CDMA.

Chapter 6

Performance of Coexistence Protocols in Large CDMA based Ad-hoc Networks

There has been a dramatic increase in the demand for wireless products and services. This has resulted in shortage of wireless spectrum bringing in the need of dynamic spectrum sharing between uncoordinated devices. With more devices using the same wireless channels in a large area, interference becomes an important impairment effecting performance. In such interference limited systems simple coexistence etiquettes can reduce interference and improve spectral efficiency and throughput. A common etiquette is to use small request-to-send (RTS), clear-to-send (CTS) packets before the actual transmission [74, 75]. This protocol tends to create an exclusion zone around the receiver where others do not transmit. This etiquette has been studied and methods to optimize exclusion region radii have also been proposed [76, 77]. It can be further improved by also sensing the received signal to interference and noise ratio (SINR) at the receiver and only returning the CTS when SINR is higher than a threshold. We study

the performance of these coexistence etiquettes in direct-sequence CDMA (DS-CDMA), which is also a form of spread spectrum communication scheme. Spread spectrum communication schemes are widely used in interference limited systems such as ad-hoc networks [76, 78–83] and cognitive radio networks [84, 85] due to their ability to combat interference and improve error rate performance.

Performance of a transmitter receiver pair communicating using DS-CDMA, in a wireless network of similar nodes is degraded by the interference it receives from other nodes in the neighborhood. This interference depends on a number of factors including the spatial distribution of nodes, their transmission power levels, propagation losses etc. Accurate models to describe the self interference have been developed and used to analyze performance [86–88], accurate results for bit error rates (BER) in Rayleigh fading are available [89] however the method does not extend to packet error rate (PER) analysis. In [90] PER that account for bit-to-bit error dependence were obtained while assuming constant received power which is not always a valid assumption because of the geometric distribution of nodes. The aforementioned analyses do not consider the stochastic distribution of interferers around the receiver of interest hence their work can not be easily extended to include the effects of coexistence etiquettes.

Poisson point process can be used to model the stochastic distribution of wireless nodes, it assumes that all nodes are uniformly distributed in a two dimensional area around the receiver of interest and the total number of nodes in a particular area is Poisson distributed. It is not a new technique, it has been used before for capacity analysis [76, 91], to find optimum transmission range [30], to characterize interference of ultrawideband and narrow band transmitters on each other [92] etc. In [93] Poisson point process was used to model the interference in general communication systems but it does not give PER that account for bit-to-bit error dependence and no coexistence etiquettes were examined.

In this chapter we analyze coexistence etiquettes in a large DS-CDMA based ad-hoc network. We focus on PER and throughput of the network that account for bit-to-bit error dependence and use Poisson point process to model the spatial location of transmitters.

The rest of the chapter is organized as follows. System model is explained in Section 6.1, which also has an explanation of the access protocols that represent the coexistence etiquettes. In Section 6.2 we derive expressions for the cumulative density function of SINR for the three access protocols. In Section 6.3 we find expressions for packet success probability and throughput for performance measurement. Numerical results and conclusion are provided in Section 6.4 and Section 6.5 respectively.

6.1 The System Model

We consider a transmitter-receiver pair communicating packets using DS-CDMA in an additive white Gaussian noise Rayleigh fading environment. This pair is surrounded by similar pairs uniformly distributed in a large area. Let $r(t)$ be the received signal of an arbitrary reference packet at the receiver then

$$r(t) = v_0(t) + \sum_{k=1}^{K} v_k(t - \tau_k) + \eta(t) \tag{6.1}$$

where $v_0(t)$ is the signal of interest, K is the total number of interfering signals, $v_k(t - \tau_k)$ is the kth interfering (packet) signal, τ_k is the kth packet's relative time offset and $n(t)$ is the additive white Gaussian noise (AWGN) with two sided power spectral density N_0. We assume that all τ_k's are independent uniformly distributed random variables. The signal $v_k(t)$ $(k = 0, 1, \ldots, K)$ can be written

in its baseband representation as

$$v_k(t) = \sqrt{2s_k} g_k \sum_{i=0}^{L_s-1} b_{k,i} \operatorname{rect}\left(\frac{t}{T} - i\right) a_k(t) \tag{6.2}$$

where s_k is the mean receive power of the kth signal and depends on the transmit power ($s_{t,k}$), the distance of the interferer to the receiver of interest (r_k) and the path loss exponent (β) such that $s_k = s_{t,k} r_k^{-\beta}$. We initially assume the transmit power of all nodes to be equal, which is a plausible assumption when power control is too complex to implement. Later we also consider the case when nodes use a pairwise power control mechanism [76] to reduce interference to other nodes while maintaining a fixed receive power at the intended receiver. The transmit power without power control is given as $s_{t,k} = E_s/T$, where E_s is the energy used to transmit one symbol and T is the symbol duration. When power control is used the transmit power is $s_{t,k} = d_k^{\beta} E_s/T$, where d_k is the distance between the kth transmitter-receiver pair and we assume d_k's to be uniformly distributed in $[0, 1]$.

In order to find the statistics of r_k which is the distance of the kth interferer to the receiver of interest, we model the spatial distribution of the interferers according to a two dimensional Poisson point process with density λ. The interferers are assumed to be uniformly distributed in a circular area of radius b with the receiver of interest at its origin. The total number of interferers (K) would be Poisson distributed with probability $(\lambda\pi b^2)^K \, \mathrm{e}^{-\lambda\pi b^2}/K!$ and expected value $\mathbb{E}[K] = \lambda\pi b^2$. We initially consider a finite b and later take the limit $b \to \infty$. When the interferers are not allowed to be closer than distance R to the reference receiver due to the access protocol the probability density function (pdf) of r_k

becomes

$$f_{r_k}(r) = \begin{cases} \frac{2r}{b^2-R^2}, & R \leq r \leq b \\ 0, & \text{otherwise} \end{cases} \tag{6.3}$$

when there is no restriction on the minimum interferer distance the pdf of r_k can be found by taking $R = 0$ in (6.3).

In (6.2), g_k is the complex channel gain that represents slow-flat Rayleigh fading. It is assumed that all g_k's are independent zero mean complex Gaussian random variables with unit variance. $b_{k,i}$ represents the ith symbol of the kth signal, it takes values in $\{-1, +1\}$ for binary CDMA (B-CDMA) and $\{\pm 1, \pm j\}$ for quadriphase CDMA (Q-CDMA) and all possible values are assumed to be equally likely. L_s is the number of symbols per packet and $a_k(t)$ are the signature sequence signals which can be expressed as $a_k(t) = \sum_{j=-\infty}^{\infty} a_{k,j}\psi\left(t - jT_c\right)$ where $a_{k,j}$ is the spreading code sequence which takes values of ± 1 for B-CDMA and $\{\pm 1, \pm j\}$ for Q-CDMA independently with equal probability. $\psi(t)$ is the chip waveform, which is assumed to be time limited in $[0, T_c]$. The chip transmission time T_c is given as $T_c = T/N_p$ where N_p is the processing gain, i.e. the number of chips per symbol.

The received waveform is decoded by a conventional correlation receiver. Let Z_i denote the receiver decision variable for the ith bit of the reference packet, where $i = 0, 1, \ldots, L-1$. Then

$$Z_i = \mathrm{Re}\left\{\sqrt{s_0} g_0 b_{0,i} + \sum_{k=1}^{K} \delta_k \sqrt{s_k} g_k b_{k,i} W_{k,i} + \frac{N_0}{2T_s}\right\} \tag{6.4}$$

where $W_{k,i}$ is the multiple access interference (MAI) component during the interval $[iT, (i+1)T]$ from kth interfering packet and is given as

$$W_{k,i} = \frac{1}{T}\int_{iT}^{(i+1)T_s} \sum_{j=0}^{L_s-1} b_{k,j}\,\mathrm{rect}\left(\tfrac{t-\tau_k}{T} - j\right) a_k\left(t - \tau_k\right) a_0\left(t\right) \mathrm{d}t. \tag{6.5}$$

In (6.4), δ_k is a binary random variable that represents the effect of access protocol

$$\delta_k = \begin{cases} 1, & \text{if } k\text{th node has the permission to transmit} \\ 0, & \text{otherwise.} \end{cases} \tag{6.6}$$

The three access protocols that we analyze are described below.

- Protocol I: We first consider ALOHA type communication where the transmitter nodes transmit the packets irrespective of channel condition. For this scheme δ_k equals 1 for all k as every node has the permission to transmit packet at its arrival.

- Protocol II: The second protocol functions such that at packet arrival at a node, it transmits a small request-to-send packet to the receiver. The receiver, if available, calculates the received SINR and replies with a clear-to-send packet if the calculated SINR is higher than a threshold (γ_{th}). For this protocol δ_k's are correlated as the permission for one node to transmit would effect the received SINR at the nearby node. This simple protocol can be easily implemented in ad-hoc and cognitive radio networks.

- Protocol III: The third protocol uses RTS/CTS packets before starting transmission. This etiquette has the effect of an exclusion zone around every receiving node. It has been used previously by [76, 77, 94, 95] for capacity calculations in ad-hoc networks and by [93, 96] in cognitive radio. It can be implemented by the standardized protocols like MACA [74] and MACAW [97]. For this protocol too δ_k's are correlated as geometric location of nodes in an area effect each others transmission permission.

As far as the statistics of the decision variable is concerned, it is well known that the MAI components $W_{k,i}$ in (6.4) can be accurately approximated by a

conditional Gaussian random variable [42,86,90] with zero mean and (conditional) variance given by

$$\mathrm{Var}\left(W_{k,i}|\xi_k\right) = \frac{1}{N}\left(\rho^2\left(\xi_k\right) + \hat{\rho}^2\left(\xi_k\right)\right)$$

where ξ_k is the differential chip delay which is assumed to be uniformly distributed in $[0, T_c]$. The functions $\rho(.)$ and $\hat{\rho}(.)$ are the partial correlation functions for the chip waveform. They are defined as $\rho(\tau) = 1-\hat{\rho}(\tau) = 1-(1/T_c)\int_{\tau}^{T_c}\psi(t)\psi(t-\tau)\mathrm{d}t$.

Therefore, the instantaneous signal to interference plus noise ratio (SINR) is a random variable and can be expressed as

$$\mathrm{SINR} = \frac{|g_0|^2 s_0}{\frac{N_0}{T} + \frac{2}{N}\sum_{k=1}^{K} s_k\delta_k G_k\left(\rho^2\left(\xi_k\right) + \hat{\rho}^2\left(\xi_k\right)\right)} \tag{6.7}$$

where $G_k = \mathrm{Re}^2\, g_k$ for B-CDMA and $G_k = |g_k|^2$ for Q-CDMA [90].

In the following sections we find expressions for the cumulative distribution function (CDF) of instantaneous SINR in (6.7) for the three protocols in the cases of binary and quadriphase CDMA. These will then be used for the accurate evaluations of packet success probabilities and throughput.

6.2 Statistics of the SINR

In this section we calculate the CDF of SINR for binary and quadriphase CDMA for the three protocols separately. Without any loss of generality let the transmitter of the reference packet be at a unit distance to the receiver ($r_0 = 1$), using (6.7) the probability of instantaneous SINR $> z$ at the receiver of interest can be written as

$$\Pr(\mathrm{SINR} > z) = \Pr\left(\frac{|g_0|^2}{\frac{N_0}{E_s} + \frac{2}{N}\sum_{k=1}^{K} r_k^{-\beta}\delta_k G_k\left(\rho^2\left(\xi_k\right) + \hat{\rho}^2\left(\xi_k\right)\right)} > z\right). \tag{6.8}$$

Here g_0 is a complex Gaussian, implying $|g_o|^2$ is an exponential random variable, hence

$$\begin{aligned}\Pr\left(\text{SINR} > z\right) &= \mathbb{E}\left[\mathrm{e}^{-z\left(\frac{N_0}{E_s}+\frac{2}{N}\sum_{k=1}^{K} r_k^{-\beta}\delta_k G_k(\rho^2(\xi_k)+\hat{\rho}^2(\xi_k))\right)}\right] \\ &= \mathrm{e}^{-z\frac{N_0}{E_s}}\mathbb{E}\left[\prod_{k=1}^{K}\mathrm{e}^{-z\frac{2}{N}r_k^{-\beta}\delta_k G_k\left[\rho^2(\xi_k)+\hat{\rho}^2(\xi_k)\right]}\right]. \end{aligned} \tag{6.9}$$

where the expectation is with respect to all RVs $\{r_k, \delta_k, G_k, \xi_k, k = 0, 1, \ldots, K\}$, which are mutually independent except δ_k's, which may be correlated depending on the protocol in use. Hence the expectation in (6.9) can not be taken inside the multiplication in general so it can not be further simplified. However for protocol I an exact solution is possible and is given next.

6.2.1 Protocol I

For protocol I, $\delta_1 = \delta_2 = \ldots \delta_K = 1$ and hence the expectation in (6.9) can be taken inside the multiplication when we condition on K, giving

$$\Pr(\text{SINR} > z|K) = \mathrm{e}^{-z\frac{N_0}{E_s}}\prod_{k=1}^{K}\mathbb{E}\left[\mathrm{e}^{-z\frac{2}{N_p}r_k^{-\beta}\delta_k G_k\left[\rho^2(\xi_k)+\hat{\rho}^2(\xi_k)\right]}\right]. \tag{6.10}$$

Since we assumed that all nodes experience similar conditions, we can simplify (6.10) to

$$\Pr(\text{SINR} > z|K) = \mathrm{e}^{-z\frac{N_0}{E_s}}\left(\mathbb{E}\left[\mathrm{e}^{-z\frac{2}{N_p}r_1^{-\beta}\delta_1 G_1\left[\rho^2(\xi_1)+\hat{\rho}^2(\xi_1)\right]}\right]\right)^K \tag{6.11}$$

where r_1, G_1, ξ_1 and δ_1 are the distance, gain, differential chip delay and transmission permission of a typical node.

Removing the condition on K and applying the identity for a Poisson random

variable K, $\mathbb{E}\left[A^K\right] = \mathrm{e}^{-\mathbb{E}[K](1-A)}$, to get

$$\Pr(\text{SINR} > z) = \mathrm{e}^{-z\frac{N_0}{E_s}}\mathrm{e}^{-\lambda\pi V(z)} \tag{6.12}$$

where

$$V(z) = \lim_{b\to\infty} b^2\,\mathbb{E}\left[1 - \mathrm{e}^{-r_1^{-\beta}\delta_1 G_1 \frac{2z}{N_p}\left[\rho^2(\xi_1)+\hat{\rho}^2(\xi_1)\right]}\right]. \tag{6.13}$$

It can be shown by solving the expectation for r_1 that

$$V(z) = \left(\tfrac{z}{N_p}\right)^{\frac{2}{\beta}} aA\Gamma\left(1-\tfrac{2}{\beta}\right) \tag{6.14}$$

where $A = \mathbb{E}\left[G_1^{2/\beta}\right]$, and depending on the type of CDMA it is given as

$$A = \begin{cases} \frac{1}{\sqrt{\pi}}\Gamma\left(\frac{1}{2}+\frac{2}{\beta}\right), & \text{B-CDMA} \\ \Gamma\left(1+\frac{2}{\beta}\right), & \text{Q-CDMA.} \end{cases} \tag{6.15}$$

On the other hand, a depends on the pulse shape as follows

$$a = \int_0^\infty \left(2\rho^2(x) + 2\hat{\rho}^2(x)\right)^{2/\beta} \mathrm{d}x. \tag{6.16}$$

In the case of rectangular pulses, (6.16) reduces to $a = {}_2\mathrm{F}_1\left(\frac{1}{2}, -\frac{2}{\beta}, \frac{3}{2}, -1\right)$. ${}_2\mathrm{F}_1(.)$ is the hypergeometric function [98] where ${}_2\mathrm{F}_1(a,b,c,d) = \sum_{n=0}^{\infty}\frac{ab}{c}\frac{d^n}{n!}$. Hence we have a closed form expression for the CDF of SINR for protocol I.

When pairwise power control is used, following similar analysis and assuming the worst case scenario of $d_0 = 1$, we get (6.10) for $\Pr(\text{SINR} > z)$, with $V(z)$ given as

$$V(z) = \left(\frac{z}{N_p}\right)^{\frac{2}{\beta}} \frac{aA}{3}\Gamma\left(1-\tfrac{2}{\beta}\right)$$

where a and A are given in (6.16) and (6.15), respectively.

6.2.2 Protocol II

In this case of protocol II a transmitting node effects the measured SINR of all nodes in the neighborhood. Consequently, $\{\delta_1, \delta_2, \ldots, \delta_K\}$ are no longer mutually independent. Therefore we can not simply take the expectation inside the multiplication in (6.9). Hence an exact solution to (6.9) can not be found. However, we can find a lower bound for $\Pr(\text{SINR} > z)$ by applying Jensen inequality to (6.9) to obtain

$$\Pr(\text{SINR} > z) \geq \mathrm{e}^{-\frac{N_0}{E_s}z}\mathrm{e}^{-\lambda\pi V(z)} \tag{6.17}$$

where now

$$V(z) = \left(\tfrac{z}{N_p}\delta\right)^{2/\beta} aA\Gamma\left(1-\tfrac{2}{\beta}\right). \tag{6.18}$$

In (6.18) a and A are given in (6.16) and (6.15) respectively and $\delta = \mathbb{E}[\delta_k]$ for $k = 1, \ldots, K$. For this protocol

$$\delta_k = \Pr(\text{SINR}_k > \gamma_{th}) \tag{6.19}$$

where SINR_k is the received SINR at the kth receiver. SINR_k is a random variable, since all nodes experience statistically identical conditions, SINR_k and hence δ_k can be regarded as independent of k. In this case we can calculate $\delta = \Pr(\text{SINR} > \gamma_{th})$ from (6.17) and (6.18) by solving the following non linear equation

$$\delta = \exp\left(-\frac{N_0}{E_s}\gamma_{th}\right)\exp\left(-\lambda\pi\left(\frac{\gamma_{th}}{N_p}\delta\right)^{2/\beta} aA\Gamma\left(1-\tfrac{2}{\beta}\right)\right). \tag{6.20}$$

Equation (6.20) can be solved as

$$\delta = \frac{N_p}{\gamma_{th}} \left(\frac{-\beta}{2\lambda\pi a A \Gamma\left(1-\frac{2}{\beta}\right)} \right)^{\frac{\beta}{2}} \left(-\mathrm{W}\left(\frac{2\lambda\pi a A \Gamma\left(1-\frac{2}{\beta}\right)}{\beta} \left(\frac{\gamma_{th}}{N_p}\right)^{\frac{2}{\beta}} \mathrm{e}^{-\frac{2}{\beta}\frac{N_0}{E_s}\gamma_{th}} \right) \right)^{\frac{\beta}{2}} \tag{6.21}$$

where W(.) is the Lambert W function [99] also known as the Omega function or product log and is defined as the inverse function of $f(w) = w\exp(w)$. Using (6.23) and (6.18) $V(z)$ for B-CDMA, is given as

$$V(z) = \frac{\beta}{2\pi\lambda}\left(\frac{z}{\gamma_{th}}\right)^{\frac{2}{\beta}} \mathrm{W}\left(\frac{2\pi\lambda a A \Gamma\left(1-\frac{2}{\beta}\right)}{\beta} \left(\frac{\gamma_{th}}{N_p}\right)^{\frac{2}{\beta}} \exp\left(-\frac{2}{\beta}\frac{N_0}{E_s}\gamma_{th}\right) \right). \tag{6.22}$$

When power control is used, the Pr(SINR $> z$) is as given in (6.17) and the differences appear in δ and $V(z)$, which become

$$\delta = \frac{N_p}{\gamma_{th}} \left(\frac{-3\beta}{2\lambda\pi a A \Gamma\left(1-\frac{2}{\beta}\right)} \right)^{\frac{\beta}{2}} \left(-\mathrm{W}\left(\frac{2\lambda\pi a A \Gamma\left(1-\frac{2}{\beta}\right)}{3\beta} \left(\frac{\gamma_{th}}{N_p}\right)^{\frac{2}{\beta}} \mathrm{e}^{-\frac{2}{\beta}\frac{N_0}{E_s}\gamma_{th}} \right) \right)^{\frac{\beta}{2}} \tag{6.23}$$

$$V(z) = \frac{\beta}{2\pi\lambda}\left(\frac{z}{\gamma_{th}}\right)^{\frac{2}{\beta}} \mathrm{W}\left(\frac{2\pi\lambda a A \Gamma\left(1-\frac{2}{\beta}\right)}{3\beta} \left(\frac{\gamma_{th}}{N_p}\right)^{\frac{2}{\beta}} \exp\left(-\frac{2}{\beta}\frac{N_0}{E_s}\gamma_{th}\right) \right). \tag{6.24}$$

6.2.3 Protocol III

In the case of protocol III, a receiver node prohibits all neighboring nodes from transmission. Hence $\{\delta_1, \delta_2, \ldots, \delta_K\}$ are again correlated and therefore, similar to protocol II, we can only find a lower bound for Pr (SINR $> z$) by applying Jensen inequality to (6.9) to obtain

$$\Pr\left(\mathrm{SINR} > z\right) \geq \mathrm{e}^{-\frac{N_0}{E_s}z} \mathbb{E}\left[\mathrm{e}^{-2\sum_{k=1}^{K} \frac{z}{N_p} r_k^{-\beta} \mathbb{E}[\delta_k] G_k \left(\rho^2(\xi_k) + \hat{\rho}^2(\xi_k)\right)} \right]. \tag{6.25}$$

The expected value of δ_k can be calculated by considering a Matérn hard-core process [100] in which a stationary Poisson point process (of density λ) is dependently thinned such that a minimum distance is maintained between the retained nodes. This minimum distance is the radius (R) of the exclusion zone. The expected value of δ_k is the Palm retaining probability of a typical point [100, pp. 164]

$$\mathbb{E}\left[\delta_k\right] = \frac{1 - \mathrm{e}^{-\lambda\pi R^2}}{\lambda\pi R^2}. \tag{6.26}$$

Following similar analysis as for protocol I, we get

$$\Pr\left(\mathrm{SINR} > z\right) \geq \mathrm{e}^{-\frac{N_0}{E_s}z}\mathrm{e}^{-\lambda\pi V(z)} \tag{6.27}$$

where now

$$V(z) = aA\Gamma\left(1-\tfrac{2}{\beta}\right)\left(\tfrac{z}{N_p}\tfrac{1-\mathrm{e}^{-\lambda\pi R^2}}{\lambda\pi R^2}\right)^{\frac{2}{\beta}} + R^2\left(-1+\frac{2}{\beta}U\left(z\right)\right) \tag{6.28}$$

where a and A are given in (6.16) and (6.15), respectively and $U\left(z\right)$ is given as

$$U\left(z\right) = \mathbb{E}\left[\mathrm{E}_{1+\frac{2}{\beta}}\left(\tfrac{z}{N_p}\tfrac{1-\mathrm{e}^{-\lambda\pi R^2}}{\lambda\pi R^{2+\beta}}G_1\left(2\rho^2\left(x\right)+2\hat{\rho}^2\left(x\right)\right)\right)\right] \tag{6.29}$$

where $\mathrm{E}_{1+\frac{2}{\beta}}\left(.\right)$ is the generalized exponential integral [98]. The expectation in (6.29) can be solved numerically as the pdf's are known.

When power control is used, a similar analysis gives the lower bound on $\Pr(\mathrm{SINR} > z)$ as given in (6.27) and $V(z)$ as

$$V(z) = \frac{aA}{3}\Gamma\left(1-\tfrac{2}{\beta}\right)\left(\tfrac{z}{N_p}\tfrac{1-\mathrm{e}^{-\lambda\pi R^2}}{\lambda\pi R^2}\right)^{\frac{2}{\beta}} + R^2\left(-1+\frac{2}{3\beta}\hat{U}\left(z\right)\right) \tag{6.30}$$

where

$$\hat{U}(z) = \mathbb{E}\left[\mathrm{E}_{1+\frac{2}{\beta}}(\Lambda) - \mathrm{E}_{1-\frac{1}{\beta}}(\Lambda) + \Lambda^{-\frac{1}{\beta}}\Gamma\left(\frac{1}{\beta}\right)\right]$$

and

$$\Lambda = \frac{z}{N_p}\frac{1-\mathrm{e}^{-\lambda\pi R^2}}{\lambda\pi R^{2+\beta}}G_1\left(2\rho^2(x) + 2\hat{\rho}^2(x)\right).$$

The CDF of SINR for the three access protocols can now be used to find the performance measuring parameters including packet success probability and throughput.

6.3 Performance Measurement

We use packet success probability and throughput for performance measurement of the three coexistence protocols. Assuming that the data are transmitted in packets of (relatively) short lengths. Therefore, it is plausible to assume that the SINR over the packet transmission time does not vary during the duration of the (reference) packet. In this regard, it is worth mentioning that even if packets are not short and the SINR varies during the packet transmission, then according to [90] it is possible to approximate the system by an equivalent system where the equivalent SINR is given by the short-term average of the the interference terms over the duration of the packet. In that case results have shown that there is no difference between slotted and unslotted packet transmissions (in the case of CDMA packets). This is in contrast to non-CDMA systems where it is known that slotted systems outperforms the unslotted packet systems.

6.3.1 Packet Success Probability

The packet success probability is taken as the probability that a packet at its arrival is successfully transmitted and decoded at the receiver. The probability of successful decoding depends on the SINR at the receiver and type of employed

error correcting code. The packet success probability in the absence of any error correcting code is given by

$$P_s = \mathbb{E}\left[\left(1 - \frac{1}{2}\operatorname{erfc}\sqrt{\text{SINR}}\right)^{L_s}\right] \tag{6.31}$$

where erfc is the complementary error function defined as $\operatorname{erfc}(x) = 1 - \operatorname{erf}(x)$ where $\operatorname{erf}(x) = \frac{2}{\sqrt{\pi}}\int_0^x \exp\left(-t^2\right) \mathrm{d}t$.

When the packet includes error correcting code that can correct up to c errors we would have instead of (6.31)

$$P_s = \frac{1}{2^{L_s}}\sum_{n=0}^{c}\binom{L_s}{N_p}\mathbb{E}\left[\left(1 + \operatorname{erfc}\sqrt{\text{SINR}}\right)^{L_s-n}\left(\operatorname{erfc}\sqrt{\text{SINR}}\right)^{n}\right]. \tag{6.32}$$

For protocol I the packet success probability, after applying integration by parts to (6.31) can be calculated directly in terms of $\Pr(\text{SINR} > z)$

$$P_s = \frac{1}{2^{L_s}} + \frac{L_s}{2^{L_s}}\int_0^{\infty} \frac{\mathrm{e}^{-z}}{\sqrt{\pi z}}[1 + \operatorname{erf}\sqrt{z}]^{L_s-1}\Pr(\text{SINR} > z)\mathrm{d}z \tag{6.33}$$

where $\Pr(\text{SINR} > z)$ for protocol I is given in (6.12).

For protocol II, the packet success probability, after applying integration by parts to (6.31) can be written as

$$P_s = \left(1 - \frac{\operatorname{erfc}\left(\sqrt{\gamma_{th}}\right)}{2}\right)^{L_s}\delta + \frac{L_s}{2^{L_s}}\int_{\gamma_{th}}^{\infty} \frac{\mathrm{e}^{-z}}{\sqrt{\pi z}}[1 + \operatorname{erf}\sqrt{z}]^{L_S-1}\Pr(\text{SINR} > z)\mathrm{d}z. \tag{6.34}$$

Note that the integration in (6.34) starts from γ_{th} rather than zero, this is because the node is not allowed to transmit if the SINR is less than γ_{th}. In (6.34) δ=$\Pr\left(\text{SINR} > \gamma_{th}\right)$ which is given in (6.23) and lower bound for $\Pr\left(\text{SINR} > \mathbf{z}\right)$ is given in (6.17). When error control code is used the packet success probability

can similarly be found as

$$P_s = \frac{1}{2^{L_s}} \sum_{n=0}^{c} \binom{L_s}{N_p} \Bigg[\left(1 + \operatorname{erf}\sqrt{\gamma_{th}}\right)^{L_s - n} \left(\operatorname{erfc}\sqrt{\gamma_{th}}\right)^{n} \;\; \delta + \int_{\gamma_{th}}^{\infty} \frac{\mathrm{e}^{-z}}{\sqrt{\pi z}} \left(L_s \operatorname{erfc}\sqrt{z} - 2n\right) \left(1 + \operatorname{erf}\sqrt{z}\right)^{L_s - n - 1} \left(\operatorname{erfc}\sqrt{z}\right)^{n-1} \Pr\left(\mathrm{SINR} > z\right) \mathrm{d}z \Bigg] \quad (6.35)$$

where $\delta = \Pr\left(\mathrm{SINR} > \gamma_{th}\right)$ is given in (6.21) and $\Pr\left(\mathrm{SINR} > z\right)$ can be found using (6.17) and (6.22).

The conditional packet success probability for protocol III, given packet is transmitted, is the same as in (6.33) where lower bound for $\Pr(\mathrm{SINR} > z)$ is given in (6.27). The probability of packet transmission due to protocol III is $\exp(-\lambda\pi R^2)$ hence lower bound for unconditional packet success probability for protocol III is found as

$$P_s \geq \exp\left(-\lambda\pi R^2\right) \left(\frac{1}{2^{L_s}} + \frac{L_s}{2^{L_s}} \int_0^{\infty} \frac{\mathrm{e}^{-z}}{\sqrt{\pi z}} [1 + \operatorname{erf}\sqrt{z}]^{L_s - 1} \Pr(\mathrm{SINR} > z) \mathrm{d}z \right) \quad (6.36)$$

where $\Pr(\mathrm{SINR} > z)$ is given in (6.27) .

6.3.2 Throughput

The throughput of the system is taken as the number of successfully decoded packets per packet transmission time per unit area. The aggregate packet arrival rate is taken as λ_a packets/packet transmission time. Now this arrival rate (λ_a) is directly proportional to the node density (λ), we take the constant of proportionality to be unity making $\lambda_a = \lambda$, this has the effect of shifting the numerical analysis of throughput across node density axis by a small value that can be ignored. The throughput for B-CDMA is given as

$$S = \lambda P_s. \quad (6.37)$$

Throughput for Q-CDMA is given as

$$S = 2\lambda P_s. \tag{6.38}$$

The factor of 2 in (6.38) as compared to (6.37) is because Q-CDMA carries twice data rate than B-CDMA. The throughput is a function of λ i.e. the aggregate packet arrival rate. And P_s is the probability that a packet at its arrival is successfully received and decoded at the receiver.

6.4 Numerical Results

In this section we first assess the accuracy of our analytical results by comparing them with the simulation results. Fig. 6.1 shows the comparison for the three protocols, these results were generated for path loss exponent (β) of 4, packet length (L_s) of 100, number of chips in a spreading code (N_p) equal to 100 and E_b/N_0 of 20dB. The minimum SINR threshold for protocol II and the radius of the exclusion zone for protocol III were dynamically selected for each node density such that maximum throughput was achieved. The simulation results closely follow the analytical results confirming the validity of our analysis. It is also observed from Fig. 6.1 that the packet success probability for protocol II is always the highest and it is followed by protocol III while packet success probability for protocol I is the smallest of the three.

When a packet transmission fails i.e. received packet has more bit errors than what it can recover then it has to be retransmitted. Retransmission increases delay and reduces throughput so a higher packet success probability results in higher throughput and lower delay. The difference in packet success probability at lower node density is also smaller compared with that at higher node density. This is because there is a lesser chance of two nodes transmitting at the same

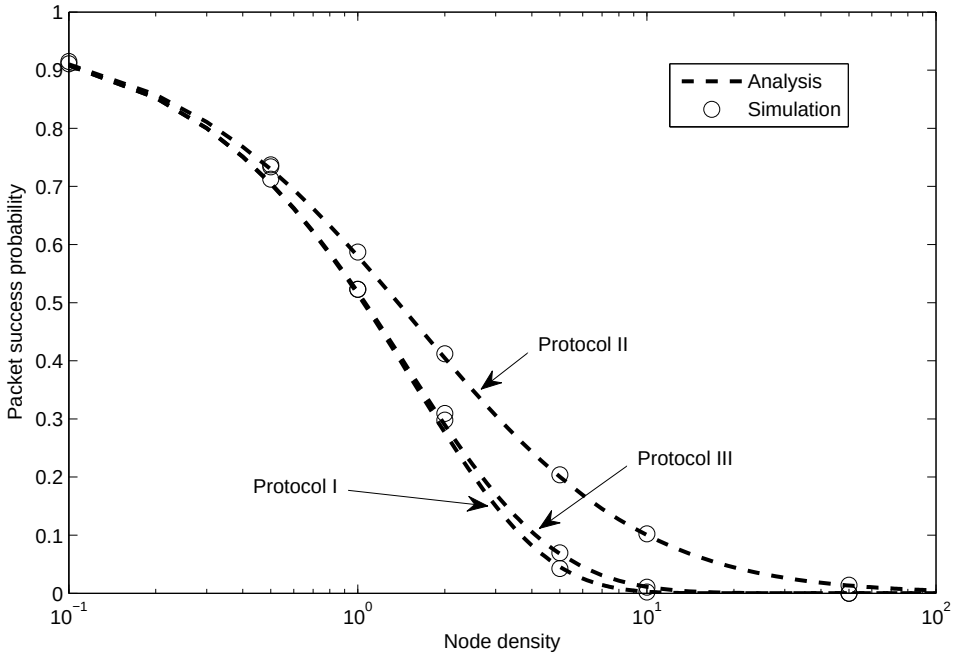

Figure 6.1: Packet success probability versus node density for the three access protocols

time and colliding with each other when there are lesser number of nodes in an area. The packet collision probability increases at higher node density and hence the benefit of one MAC scheme over the other also becomes more visible.

Fig. 6.2 shows the effect of SINR threshold on throughput for protocol II. The throughput increases initially with the increase in threshold showing the advantage of this etiquette. The throughput reduces after an optimum threshold is reached as a further increase in threshold would be meaninglessly blocking nodes from transmitting. The variation in optimum threshold with offered traffic is small meaning a single value can be hard-coded, saving run time calculations with negligible loss of throughput.

Fig. 6.3 shows the effect of the radius of the exclusion zone on throughput for protocol III. The results are similar to those for protocol II, the throughput

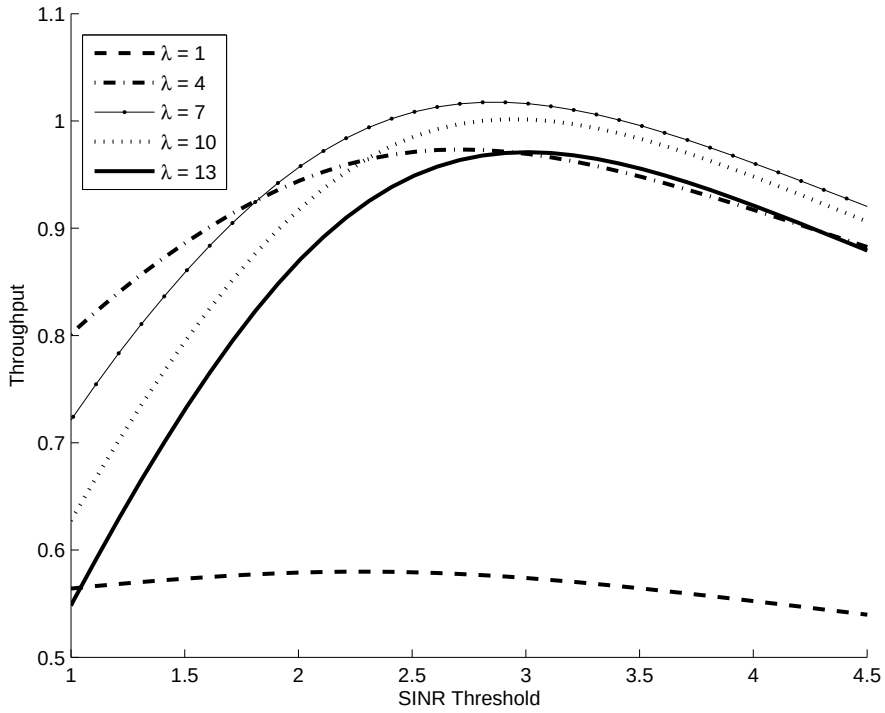

Figure 6.2: Throughput versus SINR threshold for some offered traffic levels for protocol II

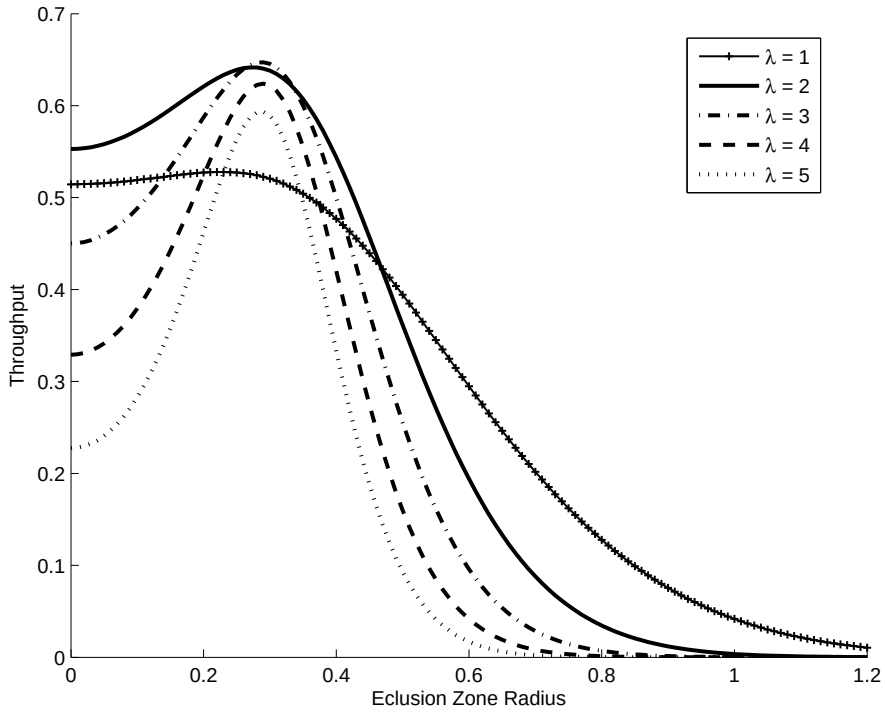

Figure 6.3: Throughput versus exclusion zone radius for some offered traffic levels

initially increases with the increase in the radius since interference is being reduced, after a maximum limit the throughput starts to fall as the exclusion zone is now inhibiting even those nodes that do not cause huge interference. Another interesting fact to note is that the optimum radius i.e. the radius that gives the maximum throughput has a very slight variation as node density changes. This fact can be used to calculate an optimum radius that can be hard-coded in the nodes, saving the need to find it dynamically.

Fig. 6.4 compares the throughput for the three access protocols as found from the analysis. The throughput for protocol II is always highest and is followed by the protocol III. The minimum SINR threshold for protocol II and the radius of the exclusion zone for protocol III were dynamically selected for each node density such that maximum throughput was achieved. This result shows the advantage of using protocol II over the other two protocols. These results do not include

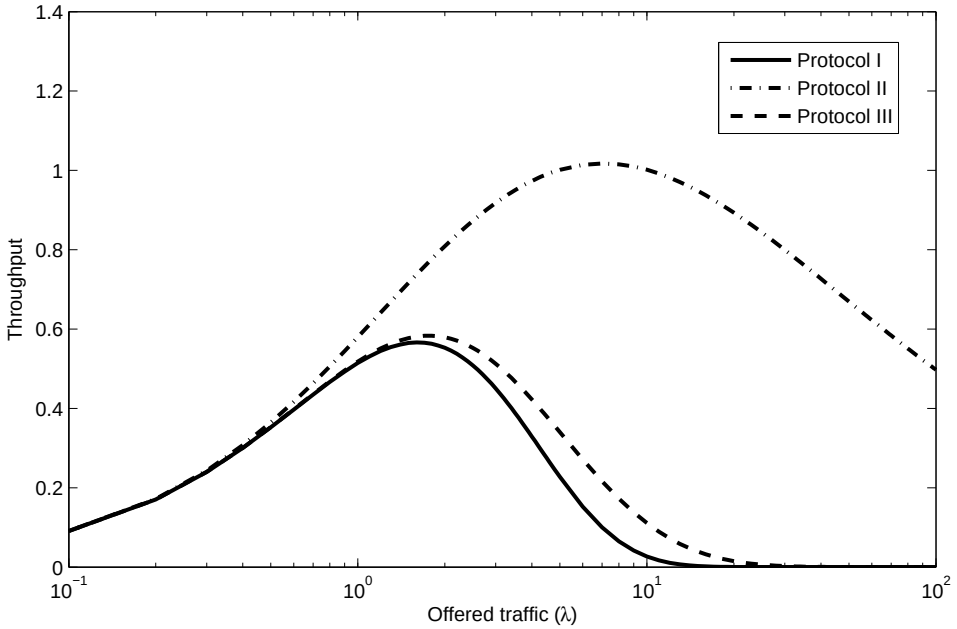

Figure 6.4: Throughput versus offered traffic for the three access protocols for B-CDMA

the loss of throughput due to the initial packet exchange for SINR calculation but that is assumed to be negligible as compared to the difference

Fig. 6.5 shows a comparison of the throughput for B-CDMA and Q-CDMA modulation for protocol I at a path loss of 2.1, 4 and 6. The reason we chose 2.1 rather than 2.0 is because our analysis is only valid for $\beta > 2$. From (6.33) and (6.12) for protocol I it can be seen that

$$P_s^Q(\lambda) = P_s^B\left(\lambda \frac{\sqrt{\pi}\Gamma\left(\frac{2+\beta}{\beta}\right)}{\Gamma\left(\frac{1}{2}+\frac{2}{\beta}\right)}\right) \tag{6.39}$$

where P_s^Q is the packet success probability for Q-CDMA and P_s^B is the packet success probability for B-CDMA. It can be easily shown that (6.39) is also valid

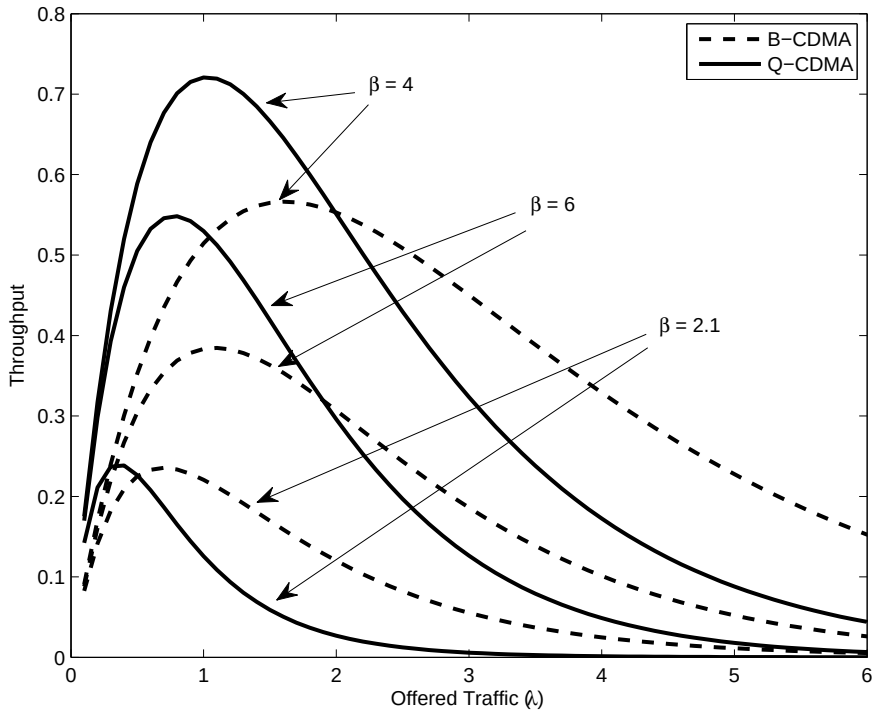

Figure 6.5: Throughput versus offered traffic for B-CDMA and Q-CDMA for three different path loss exponent values

for protocol II and III. Using (6.39), (6.37) and (6.38) we can get

$$S_Q(\lambda) = \lambda \frac{2\Gamma\left(\frac{1}{2}+\frac{2}{\beta}\right)}{\sqrt{\pi}\Gamma\left(\frac{2+\beta}{\beta}\right)} P_s^B\left(\frac{\sqrt{\pi}\Gamma\left(\frac{2+\beta}{\beta}\right)}{\Gamma\left(\frac{1}{2}+\frac{2}{\beta}\right)}\lambda\right) \tag{6.40}$$

using (6.40) we can get a relationship between the throughput achieved using Q-CDMA and that using B-CDMA and is given as

$$S_Q(\lambda) = \frac{2\Gamma\left(\frac{1}{2}+\frac{2}{\beta}\right)}{\sqrt{\pi}\Gamma\left(\frac{2+\beta}{\beta}\right)} S_B\left(\frac{\sqrt{\pi}\Gamma\left(\frac{2+\beta}{\beta}\right)}{\Gamma\left(\frac{1}{2}+\frac{2}{\beta}\right)}\lambda\right).$$

In free space path loss (β) is 2, in our analysis as $\beta \to 2$, $S_Q(\lambda) \to S_B(2\lambda)$ i.e. Q-CDMA achieves the same maximum throughput but at lower node density. Furthermore the throughput for Q-CDMA is not always higher than B-CDMA,

this is because orthogonality is lost due to fading in in-phase and quadrature components of Q-CDMA reducing the receiver SINR. As the path loss increases the difference between the maximum achieved by Q-CDMA and B-CDMA increases and the density points where the maxima are achieved come closer. In the limit when $\beta \to \infty$, $S_Q(\lambda) \to 2S_B(\lambda)$ i.e. the throughput achieved by Q-CDMA is double that of B-CDMA at all density values. An interesting observation is that the maximum throughput when $\beta = 2.1$ is lower than the maximum when $\beta = 4$, furthermore the maximum throughput when $\beta = 6$ is also lower than that when $\beta = 4$. This is because the maximum achievable throughput initially increases with an increase in path loss as the received interference power is getting reduced at a higher rate than that of the desired signal. After a threshold, which in our case was around $\beta = 2.9$, the maximum throughput decreases with an increase in β as the power of the desired signal is now getting reduced at a higher rate than the interference power.

The throughput when error correcting code is used is shown in Fig. 6.6 for protocol II. Error correcting code has two effects, first is a reduction in throughput due to the extra code bits, the second is an increase in throughput due to the improved packet success probability. These can be observed in Fig. 6.6, there is a significant increase in throughput at all packet arrival rates when a single bit error correcting code is used. A further increase is observed when 2 bit error correction is used but the throughput decreases at all arrival rates when 3 bit error correction is used. These results are for a packet length of 100; hence it can be concluded that for this packet length the highest throughput is achieved when 2 bit error correction is used. The effect of reduction in throughput due to the error correcting bits was captured by multiplying the throughput with the ratio of length of packet minus length of error correcting code to the length of packet. The length of error correcting code was taken to be the same as the number of

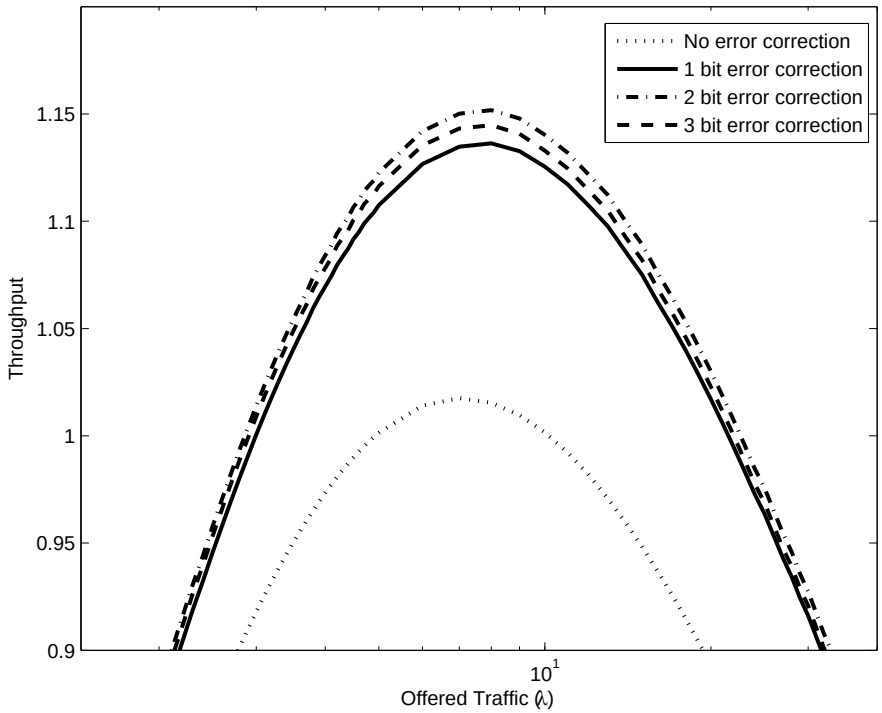

Figure 6.6: Throughput versus offered traffic for some error correcting codes

bits that it can correct.

The effect of packet length on throughput is shown in Fig. 6.7 for some header size lengths. The throughput initially increases with increasing packet length as the overhead due to packet header size reduces. After reaching a peak the throughput starts to decrease this is because the probability of successful transmission of the whole packet reduces with increasing packet length. The packet length that gives the highest throughput changes for different packet header sizes hence the packet size should be selected according to the size of the packet header that is required for transmission.

The increase in throughput for the three protocols when power control is used can be observed in Fig. 6.8. There is more than three fold increase for protocol I, around three fold increase for protocol II and around two fold increase for protocol III. This clearly shows the benefit of using power control in conjunction

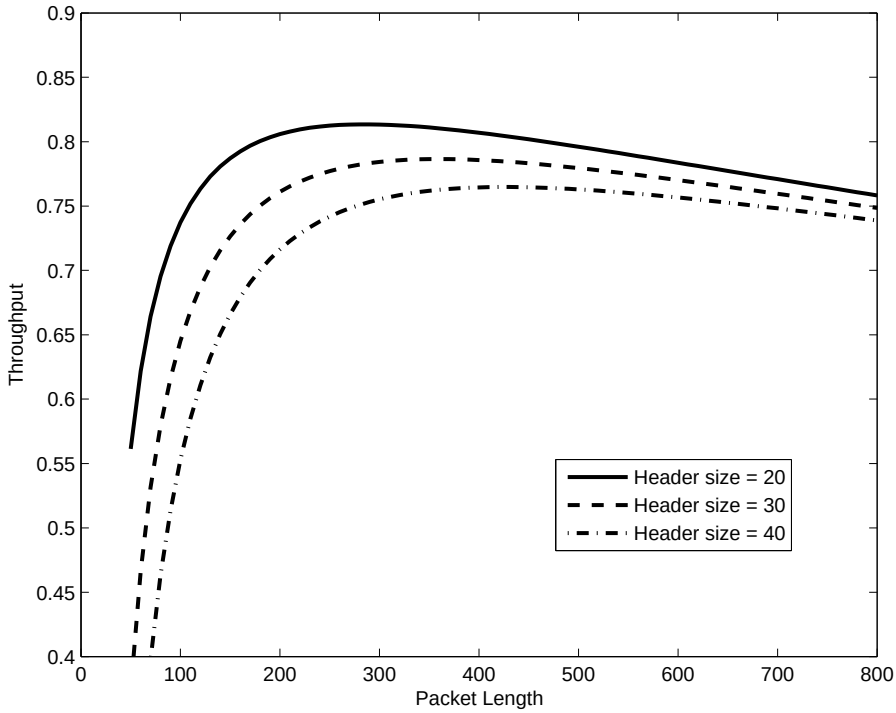

Figure 6.7: Throughput versus packet length for some header size lengths

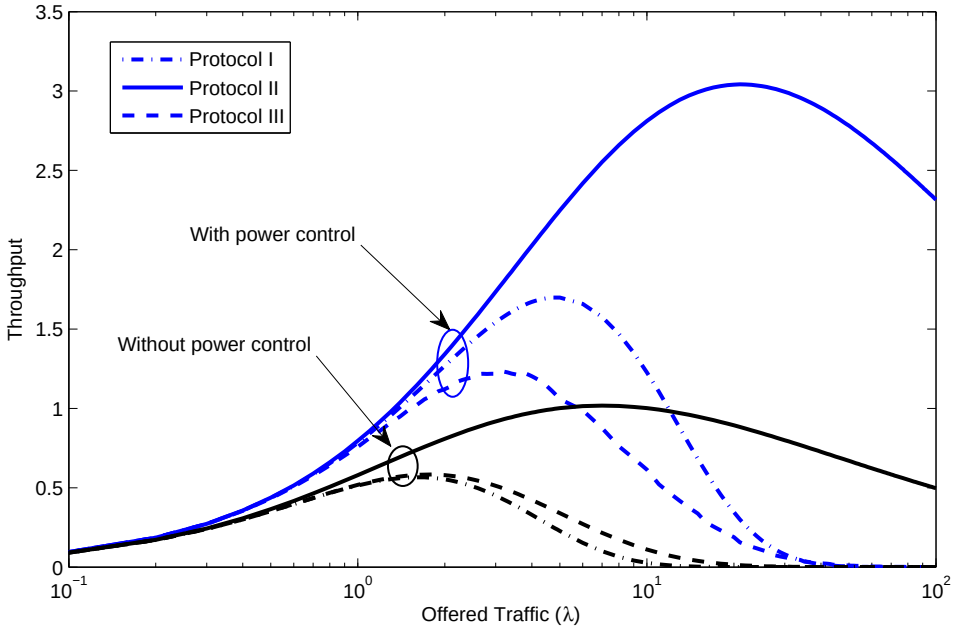

Figure 6.8: Throughput versus offered traffic for the three protocols, with and without power control

with access protocols as part of the coexistence etiquette.

6.5 Chapter Conclusion

We have derived new accurate packet error/success rate expressions for binary and quadriphase CDMA communication over Rayleigh fading environment in the presence of interference and noise. Our method can be easily extended to include the effects of coexistence etiquettes as it does not just consider aggregate interference but instead considers all interferers separately. The closed form expressions for packet success rate also accounts for bit-to-bit error dependence hence design parameters like packet length, effects of packet header sizes, number of error correcting bits can be directly analyzed. The comparison of simulation results and analysis for packet success probability prove the validity of the results for protocol I and the tightness of the bound for protocol II and III. Expressions for

throughput are easily derived from our analysis and can be used as performance measurement parameter. Our results show that implementing RTS/CTS packets and using the receiver SINR to decide whether to transmit or not offers huge improvements in performance. We have also shown that performance can be further improved by also implementing pair-wise power control. Our new accurate results facilitate in designing access protocols using coexistence etiquettes and selection of physical layer parameters in uncoordinated shared wireless channels.

Chapter 7

Lifetime Analysis of Ad-hoc Networks

In [101] network lifetime is defined as the time after which no node is able to fulfill SNR requirement i.e. complete a successful transmission. However [102] and most researchers working at non-cooperative transmission e.g. [103–105] define network lifetime as the time at which the first node within the network drains out of power. We consider the later definition of network lifetime and develop joint node selection and power allocation strategy considering residual energy and channel condition for Rayleigh fading network. We also incorporate re-transmissions due to transmission failure caused by fading in lifetime calculations, which to our knowledge has not been considered by anyone. We compare the results of the new strategy with those of [101] and [102].

In ad-hoc sensor networks power consumption is an important topic as in most cases it determines the lifetime of a network itself. In [106] upper bound on the lifetime of a sensor network for a non-cooperative communication is calculated by considering the power consumption at each relay node. In [103–105] routing node selection for non-cooperative communication to increase lifetime of ad-hoc networks considering power consumption at the nodes which depends on the

channel condition at the node as well as their residual power have been studied.

In [107] and [108] it was shown that the total energy consumption in transmission of data can be reduced by using cooperative communication. In [96,109–111] different power allocation strategies based on respective channel condition were proposed for cooperative communication to achieve different goals including capacity [96], lower probability of outage [109], total energy consumption [110] and probability of error [111]. In [112] relay node selection as well as power allocation method is studies to reduce total power consumption and increase network lifetimes.

In cooperative communication distribution of available power among source and relay nodes depending on their respective channel conditions reduces the total energy consumption and hence increases network lifetime; a further increase in lifetime can be achieved when residual power is also considered [101, 102]. In [101,102] channel condition and residual power is considered in node selection while only channel condition is considered in power allocation in cooperative communication.

7.1 Non-Cooperative Networks

Consider a wireless network with N sensor nodes distributed arbitrarily over a geographical area. Each sensor node senses a particular random phenomenon which can be unique or common throughout the network. Nodes communicate by sending packets of data to a common destination node. The destination node can be a data gathering point, an access point or a base station. We will first discuss a system model for a non cooperative system and then for a cooperative system.

In non-cooperative networks each node transmits to the destination directly. In the beginning all nodes have the same initial energy E_0.

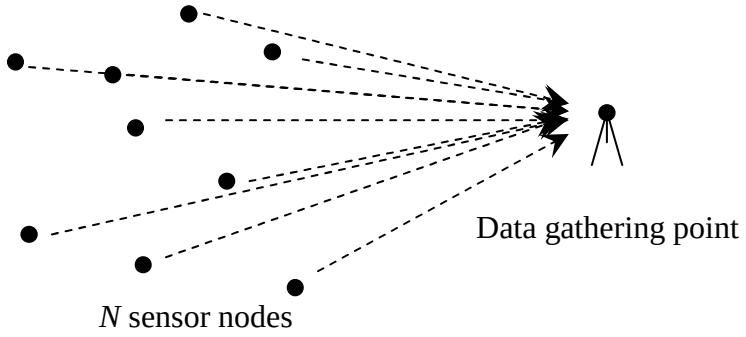

Figure 7.1: A non-cooperative network

Let P_i^T denote the power that node i uses to transmit a packet to the destination. The received power P_i^R at the destination can be expressed as

$$P_i^R = P_i^T |h_{id}|^2 + N_0 \tag{7.1}$$

where h_{id} is the channel coefficient from node i to the destination and N_0 is additive white Gaussian noise (AWGN) i.e. $\mathcal{N}(0, N_0)$. The channel coefficient h_{id} is modeled as complex Gaussian with zero mean and variance σ_i^2, $\mathcal{N}(0, \sigma_i^2)$. The instantaneous signal to noise ratio (γ_i) of this transmission is given by

$$\gamma_i = \frac{P_i^T |h_{id}|^2}{N_0}. \tag{7.2}$$

The transmission is considered successful if the signal to noise ratio is above a threshold γ_{th} i.e.

$$\gamma_i = \frac{P_i^T |h_{id}|^2}{N_0} \geq \gamma_{th}. \tag{7.3}$$

The probability of failed transmission (P_i^{out}) can be calculated as

$$P_i^{out} = \Pr\left(\frac{P_i^T |h_{id}|^2}{N_0} < \gamma_{th}\right). \tag{7.4}$$

Since we consider Rayleigh fading the random variable $|h_{id}|$ is Rayleigh distributed and hence the probability of failed transmission is given as

$$P_i^{out} = 1 - \exp\left(-\gamma_{th}/P_i^T |h_{id}|^2\right)$$

where we have normalized the noise power spectral density to unity i.e. $N_0 = 1$. The lifetime of a node (L_i) is defined as the time when the node loses all energy. It is given as

$$L_i = \frac{E_0}{E_i^T} T_i^{inter} \tag{7.5}$$

where E_i^T is the energy consumed per transmission and T_i^{inter} is the inter transmission time i.e. time between two consecutive transmissions. It is given as $T_i^{inter} = 1/\Pr\{tx_i\}$ where $\Pr\{tx_i\}$ is the probability of transmission i.e. probability at which data is generated at the $i-th$ node. The energy consumed per transmission E_i^T is given as

$$E_i^T = P_i^T T$$

where T is the time taken in a single transmission, lets normalize this time to unity, i.e. $T = 1$. The lifetime of a single node becomes

$$L_i = \frac{E_0}{P_i^T} \frac{1}{\Pr\{tx_i\}}. \tag{7.6}$$

The lifetime of the network is defined as the time when the first node runs

out of energy. It is given as

$$L^{network} = \min\{L_1, L_2, \ldots, L_N\}. \tag{7.7}$$

Equation (7.7) gives the lifetime of a non-cooperative ad-hoc network.

7.2 Cooperative Networks

In a cooperative network nodes cooperate with each other in the transmission to destination. In decode and forward cooperation scheme the cooperating node fully decodes the source signal and re-transmits it. An important constraint in comparing cooperative and non cooperative schemes is the total power consumption, i.e. the power or energy consumed (P_i^T) in transmitting a packet in a non cooperative network should be the same as the total energy spent by the source node (P_i^s) and the relay node (P_i^r) in transmitting the same packet

$$P_i^s + P_i^r = P_i^T. \tag{7.8}$$

The lifetime of a node in a cooperative network can be calculated in a similar way as in (7.6) and is given as

$$L_i = \frac{E_0}{P_i^s \Pr\{tx_i\} + \sum_{k=1,k\neq i}^{N} P_i^r \epsilon_i^k \Pr\{tx_k\})} \tag{7.9}$$

where ϵ_k^i is a Boolean function that is equal to 1 if node k selects node i as relay and 0 otherwise i.e.

$$\epsilon_k^i = \begin{cases} 1, \text{ if node } k\text{selects node } i\text{as relay} \\ 0, \text{ if node } k\text{does not select node } i\text{as relay.} \end{cases} \tag{7.10}$$

The lifetime of the network is given as

$$L^{network} = \min\{L_1, L_2, ..., L_N\}. \tag{7.11}$$

In cooperative communication, given i'th node selects j'th node as relay, the probability of failed transmission is given as

$$\begin{aligned} P_i^{out} &= P_{id}^{out}(1 - P_{ij}^{success} P_{jd}^{success}) && (7.12)\\ &= (1 - \mathrm{e}^{-\gamma_{th}/P_i^s|h_{id}|^2})(1 - \mathrm{e}^{-\gamma_{th}/P_i^s|h_{ij}|^2}\mathrm{e}^{-\gamma_{th}/P_i^r|h_{jd}|^2}). && (7.13)\end{aligned}$$

The objective is to maximize $L^{network}$ while keeping P_i^{out} minimum. The variables are j i.e. the node selected as relay and P_i^s, the portion of P_i^T assigned to the source (the calculation of P_i^r directly follows from the calculation of P_i^s so we only consider P_i^s as a variable). This objective can be simplified by relating P_i^{out} with L^i. This can be achieved by assuming that every failed transmission to the destination will be followed by a re-transmission until a successful transmission. With this assumption and (7.9) the lifetime of a node can be shown as

$$L^i = \frac{E_0}{P_i^s n_i^{tx} \Pr\{tx_i\} + \sum_{k=1,k\neq i}^{N} (P_i^r n_k^{tx} \epsilon_i^k \Pr\{tx_k\})} \tag{7.14}$$

where n_i^{tx} is the number of transmissions before a successful transmission is achieved and is given by

$$n_i^{tx} = \frac{1}{1 - P_i^{out}}.$$

Now the objective is to maximize (7.14), since E_0 is a constant, maximizing (7.14) would require minimizing its denominator. The denominator is minimized

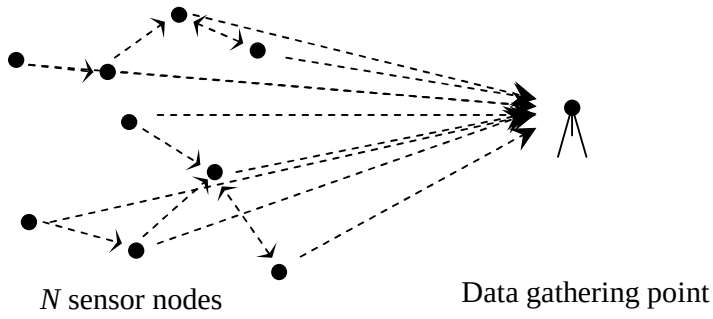

Figure 7.2: Cooperative network

by a careful selection of relay node (which affects $\epsilon_i^k$and n_k^{tx}) and the power distribution (which affects P_i^s, $P_i^r$and n_i^{tx})

7.2.1 Joint Power Allocation and Relay Selection Strategy

We first develop the power allocation strategy and then discuss the relay node selection. Let us consider a 3 node network consisting of node 1 and node 2 which cooperate to transmit to the third node which is the data gathering point. The lifetime of node 1 (L_1) and node 2 (L_2) is respectively given as

$$L_1 = \frac{E_0}{(P_1^s n_1^{tx} \Pr\{tx_1\} + P_1^r n_2^{tx} \Pr\{tx_2\})} \tag{7.15}$$

$$L_2 = \frac{E_0}{(P_2^s n_2^{tx} \Pr\{tx_2\} + P_2^r n_1^{tx} \Pr\{tx_1\})}. \tag{7.16}$$

The lifetime of the network is given as

$$L_{network} = \min\{L_1, L_2\}. \tag{7.17}$$

Finding the values of P_1^s and P_2^s which maximize (7.18) is not easy. A solution

to this problem is to select P_1^s and P_2^s according to the respective channel conditions [110, equation (12)]. This will minimize the probability of outage and hence minimize the number of transmissions required to reach a successful transmission (n_1^{tx} and n_2^{tx}). This scheme, however, does not take into account the residual energy at each node before transmission. Therefore if a node is running out of energy it will still be selected to transmit at high power levels if that reduces the overall probability of outage.

An alternative scheme that takes into account the residual energy is to always select P_1^s and P_2^s according to the residual energy of the nodes

$$\frac{P_1^s}{P_2^r} = \frac{E_1}{E_2} \tag{7.18}$$

where E_1 and E_2 are residual energies at node 1 and 2 respectively. Replacing P_2^r with $P^T - P_1^s$ and rearranging terms gives

$$P_1^s = \frac{P^T}{1 + \frac{E_1}{E_2}}. \tag{7.19}$$

A down side of this scheme is that when the residual energies are equal or close to each other; this scheme will assign the same power to source and relay while considerable energy can be saved by taking into account respective channel conditions. We now develop a scheme that takes into account both channel condition as well as residual energy.

In a 3 node network the probability of outage when node 1 is source and node 2 is relay is given by

$$P_1^{out} = \left(1 - \mathrm{e}^{-\gamma_{th}/P_1^s|h_{1d}|^2}\right)\left(1 - \mathrm{e}^{-\gamma_{th}/P_1^s|h_{12}|^2}\mathrm{e}^{-\gamma_{th}/P_2^r|h_{2d}|^2}\right) \tag{7.20}$$

where P_1^s is the power assigned to node 1 when it is acting as a source and P_2^r

is the power assigned to node 2 when it is acting as relay. We assume that the distance between the two cooperating nodes is always smaller than the distances from the nodes to destination. Therefore, for simplicity, the transmission between the two cooperating nodes is always considered successful with unit probability. The probability of outage would now become

$$P_1^{out} = \left(1 - \mathrm{e}^{-\gamma_{th}/P_1^s|h_{1d}|^2}\right)\left(1 - \mathrm{e}^{-\gamma_{th}/P_2^r|h_{2d}|^2}\right). \tag{7.21}$$

Taking derivative of (7.21) with respect to P_{s1} and equating to zero results in

$$P_1^s = P^T\left[1 + \left(\frac{|h_{1d}|}{|h_{2d}|}\right)\sqrt{\frac{\exp\left(\gamma_{th}/|h_{1d}|^2 P_1^s\right) - 1}{\exp\left(\gamma_{th}/|h_{2d}|^2\left(P^T - P_1^s\right)\right) - 1}}\right]^{-1}. \tag{7.22}$$

Equation (7.22) is similar to what was derived in [110, equation (12)], the difference is due to the assumption mentioned earlier. It can be solved by successive approximation and it is found to be always converging. The resultant value of P_{s1} will be multiplied by the ratio of the residual powers of source and relay given as

$$P_1^{s*} = P_1^s \frac{E_1}{E_2}. \tag{7.23}$$

Equation (7.23) gives our power allocation strategy. Now the relay node is selected by the source node by first calculating $P_1^{s*}$for each neighboring node i.e. the power that the source node will be required to spend if it chooses that particular node. Then the node that requires the least P_1^{s*}will be selected as relay.

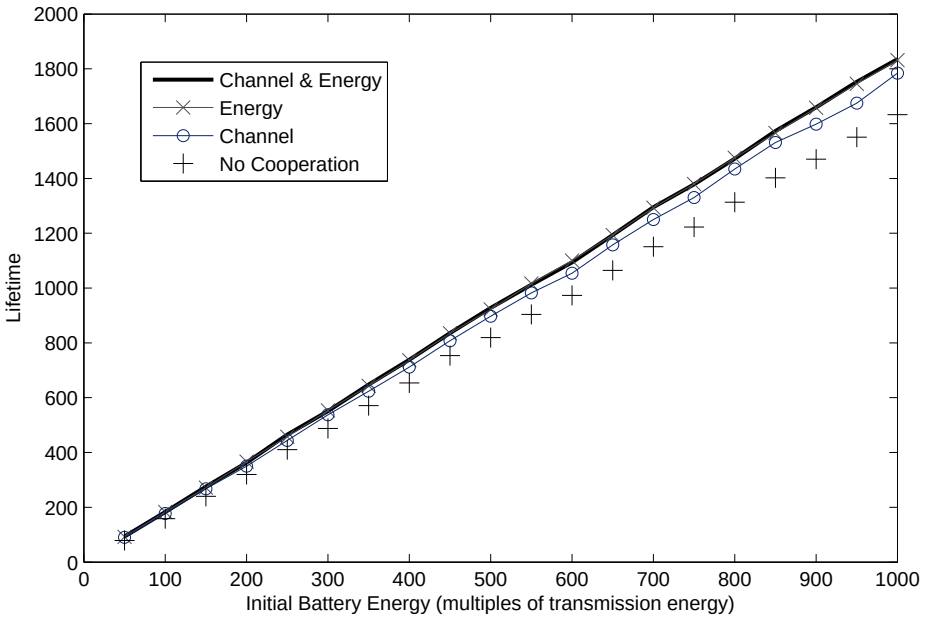

Figure 7.3: Lifetime with nodes transmitting at equal probability

7.3 Numerical Results

We first simulate a 3 node network to compare average lifetime where packet transmission time is taken as the unit of lifetime. Fig. 7.3 shows the lifetime achieved when both node 1 and 2 have the same probability of transmission ($\Pr\{tx_1\} = \Pr\{tx_2\} = 0.5$). Fig. 7.4 shows the lifetime when both nodes have different probability of transmission ($\Pr\{tx_1\} = 0.2$, $\Pr\{tx_2\} = 0.8$). In both figures 'Channel & Energy' refers to power assignment in (7.23), 'Energy' refers to power assignment in (7.19), 'Channel' refers to power assignment in (7.22). As can be seen in the figures (7.3 & 7.4) the lifetime is always higher for cooperative communication than non-cooperative communication. Furthermore the schemes that consider residual energy in power allocation i.e. (7.19) and (7.23), always give higher lifetime than the one that does not consider residual energy i.e. (7.22).

We now compare average lifetime of ad-hoc networks consisting of several nodes; using different node selection and power allocation strategies. Again

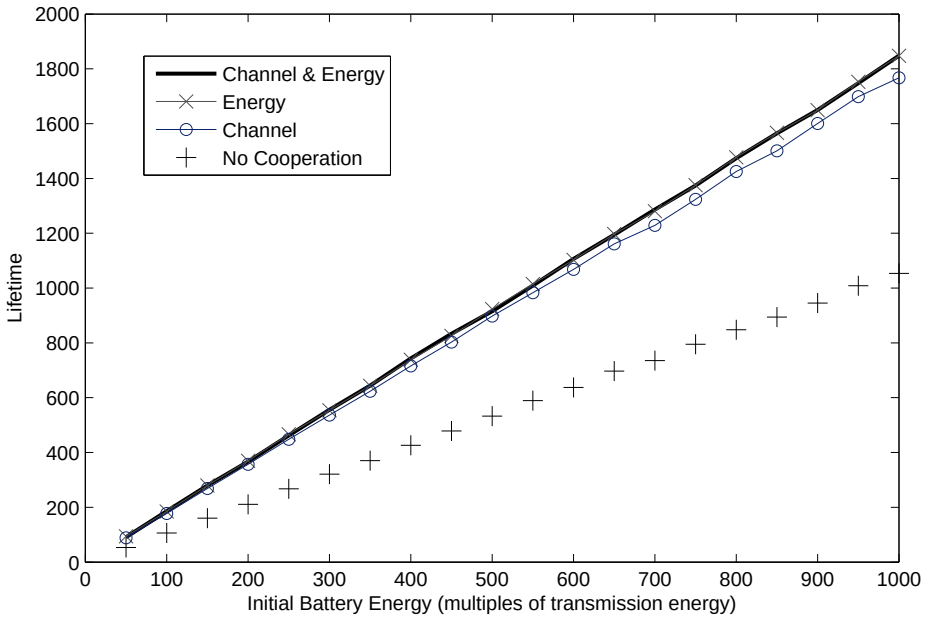

Figure 7.4: Lifetime with nodes transmitting at different probability

packet transmission time is taken as the unit of lifetime. Fig. 7.5, 7.6, 7.7 and 7.8 show the results where 'Hasna' refers to the power allocation strategy mentioned in [110, equation 12] and 'Huang' refers to the third strategy (maximum energy efficiency index) mentioned in [101]. All simulations were run over 250 randomly generated networks. The channel was taken as relay faded with path loss exponent of 4. Fig. 7.5 shows the result for increasing average probability of transmission, the probability of transmission r_s^i always varies from node to node but the average was increased in this simulation. The initial battery energy, the distance of receiver from the center of the nodes and the number of nodes were kept constant. Lifetime decreases with increasing probability of transmission as expected and the first strategy i.e. 'Energy & Distance' always gives the highest result though very closely followed by the second strategy.

Fig. 7.6 shows the simulation result of lifetime while increasing initial battery energy. The average probability of transmission, the distance of receiver from the center of the nodes and the number of nodes were kept constant. Lifetime

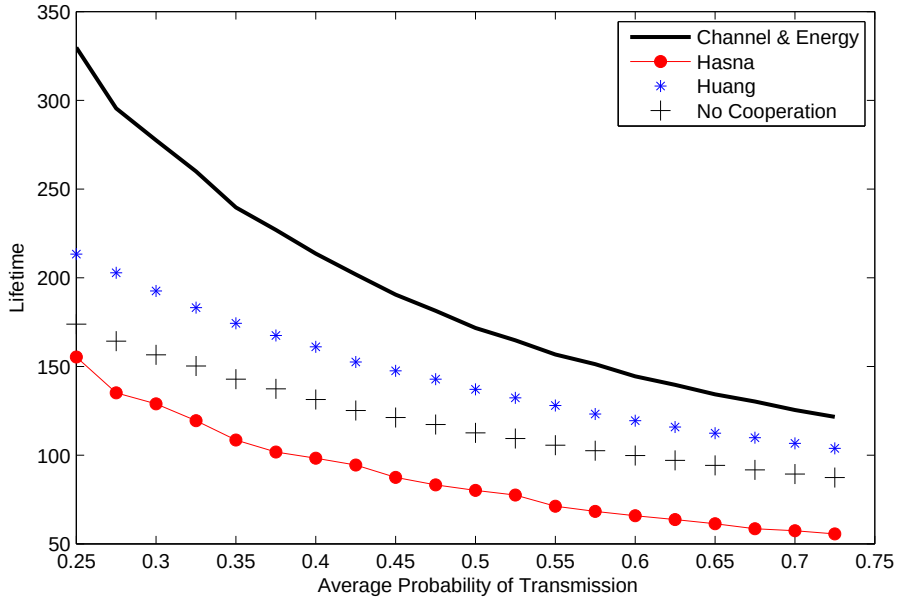

Figure 7.5: Lifetime with increasing average probability of transmission

increases with increasing initial battery energy as expected and the first strategy i.e. 'Energy & Distance' is a clear winner especially at higher values of energy.

Fig. 7.7 shows the simulation result of lifetime while increasing initial the distance of the receiver from the center of the nodes. The average probability of transmission, the initial battery energy and the number of nodes were kept constant. Lifetime decreases with increasing distance as expected. The first strategy i.e. 'Energy & Distance' is a clear winner initially but after a certain distance it dies out along with the third strategy meaning after a certain distance the first strategy can not be used.

Fig. 7.8 shows the simulation result of lifetime while increasing the number of nodes. The average probability of transmission, the distance of receiver from the center of the nodes and the initial battery energy are kept constant. Lifetime

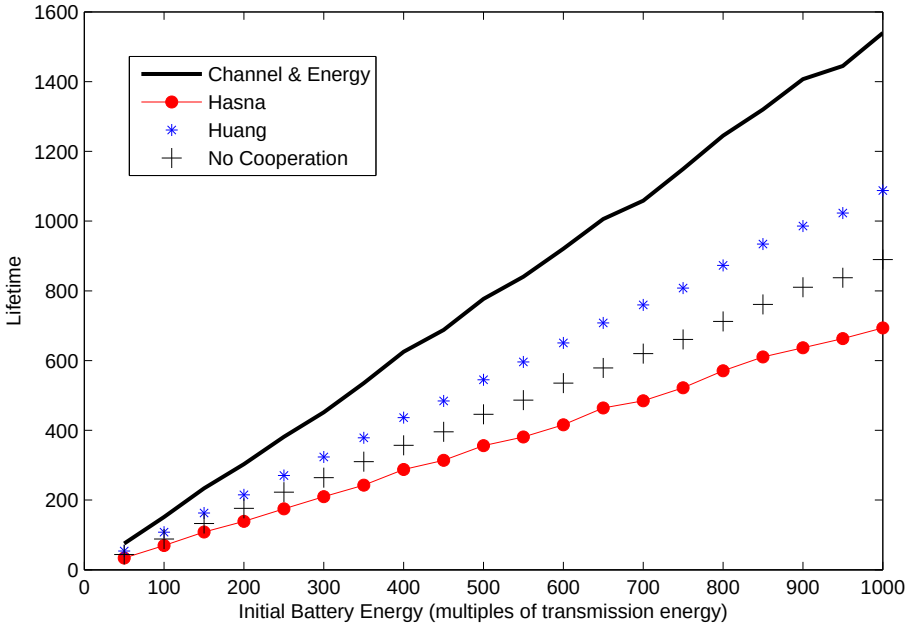

Figure 7.6: Lifetime with increasing initial battery energy

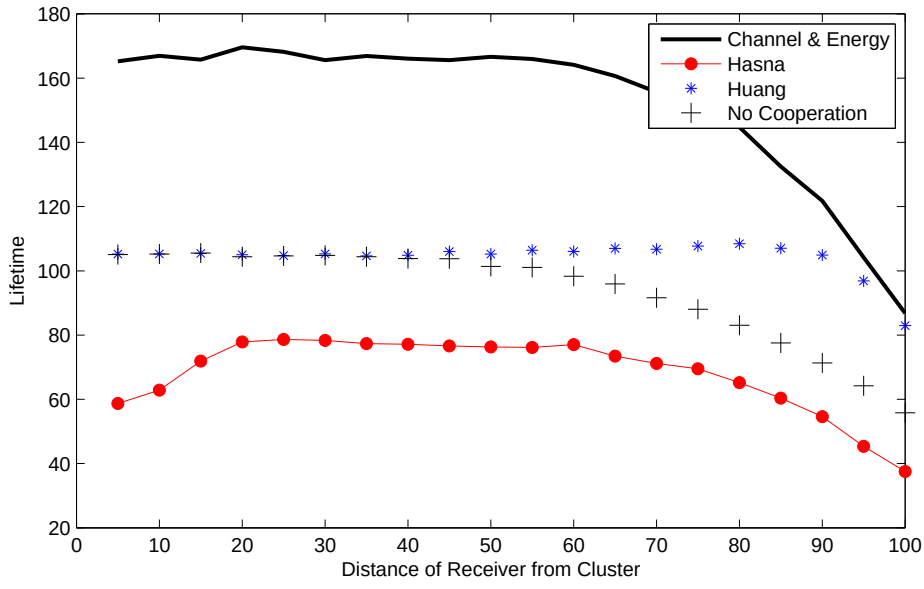

Figure 7.7: Lifetime with increasing distance of receiver from the center of node cluster

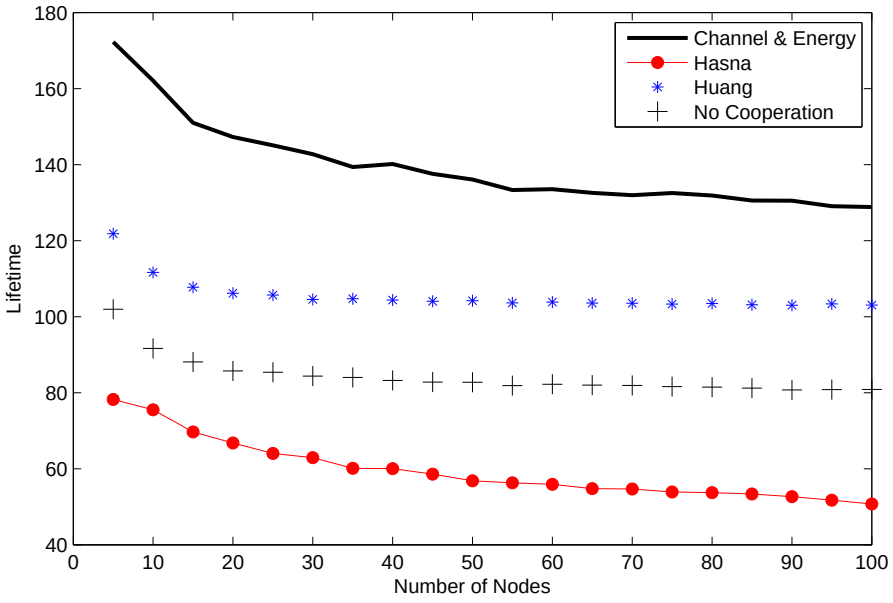

Figure 7.8: Lifetime with increasing number of nodes

decreases with increasing number of nodes, this is contrary to expectation, this is due to the fact that there can always be a node at an odd location and having a high probability of transmission and hence running out of battery power. Since we take the lifetime as the time when the first node runs out of power, increasing the number of nodes increases the chances of having such an odd node. The decrease as seen in the figure is not very profound but in any case the first strategy i.e. 'Energy & Distance' is again giving the highest lifetime.

7.4 Chapter Conclusion

We propose a new power allocation strategy to increase the lifetime of an ad-hoc network that consists of battery powered nodes. Our method is based on cooperative diversity where nodes help each other in transmission. Our simulation results show substantial improvement offered by our strategy over other strategies proposed in the literature, as well as the non-cooperative transmission. This

shows that cooperative communication can increase the lifetime of a battery powered ad-hoc network. Furthermore, careful node selection and power allocation is necessary to reap the full benefits of cooperation.

Chapter 8

Conclusions and Future Work

In this dissertation we study the performance of CDMA and multicarrier CDMA communication systems in ad-hoc networks. We use spectral efficiency and throughput as the performance measuring criterion. The performance of MC-CDMA, MC DS-CDMA and MT-CDMA without any frequency offset or interferer in multipath Rayleigh fading and AWGN environment is analyzed first in Chapter 3. MT-CDMA performs best at most conditions of SNR except at very high SNR where MC-CDMA and MC DS-CDMA perform better. This is due to the rake receiver in MT-CDMA receiver which provides time diversity improving received SNR and better spectrum utilization. MC-CDMA and MC DS-CDMA can not benefit from rake receiver because in MC-CDMA spreading is performed in frequency domain and in the case of MC DS-CDMA only short spreading sequences can be used to avoid intercarrier interference. MC-CDMA provides frequency diversity while MC DS-CDMA provides no diversity and the benefit of diversity can be seen in MC-CDMA, which performs higher than MC DS-CDMA at all conditions of SNR. In Chapter 4 we extend our analysis to include the intercarrier interference due to carrier frequency offset which represents a more practical system. MC-CDMA shows the highest resilience to frequency offset while the performance of MC DS-CDMA and MT-CDMA is severely degraded.

When other asynchronous interferers are also transmitting in the neighborhood, we show in Chapter 5 that at no or negligible frequency offset condition, MT-CDMA performs best at partial loading while the performance of MC-CDMA is highest at full loading. In the presence of small but significant frequency offset performance of MT-CDMA is only best at no loading while at partial loading or full loading MC-CDMA performs the best. The performance of MC DS-CDMA at all loading and frequency offset conditions is minimum since it does not benefit from any time or frequency diversity and is also found to be very susceptible to frequency offset. The results give us a complete picture of the performance of the three multicarrier schemes in the presence of frequency offset and interferers that are unavoidable in practice.

In Chapter 6 we study the benefits of co-existence protocols in a large ad-hoc network of wireless terminals. We study three simple protocols that are easy to implement and do not require a central control. Accurate expressions for packet success rate that accounts for bit-to-bit error dependence are derived and compared with simulation results. The results show that implementing these protocols offer huge improvements in performance. We have also shown that performance can be further improved by also implementing pair-wise power control. Our new accurate results facilitate in designing of access protocols using coexistence etiquettes and selection of physical layer parameters in uncoordinated shared wireless channels.

The lifetime of an ad-hoc network of battery powered nodes is an important research area. We have briefly studied it in Chapter 7 and proposed a new power allocation method that increases the lifetime. However, more improvements can be done in lifetime analysis by also considering packet error rate and throughput. This will also result in better power sharing and cooperative strategies to improve lifetime of an ad-hoc network.

8.1 Future Work

There are a number of directions where the research work can be extended as future work. Throughout this dissertation we have focused on ad hoc networks and used the assumptions that would be valid therein. However, the analyses can be extended in the future to other applications like cellular systems, cognitive radio networks etc. Some specific areas are listed below where future work can be carried out to extend our work.

- The effects of Doppler spread were ignored for simplicity, the analysis is still valid for stationary or slowly moving nodes but not for fast moving nodes. The effects of Doppler spread which is an important impairment in fast moving nodes can be studied as future work.

- OFDM is being widely used in the latest wireless communication applications. It would also be interesting to compare the performance of the three multicarrier schemes with that of an OFDM system in the presence of the same impairments as studied in this dissertation. This comparison would give an insight to where the multicarrier schemes can improve performance of practical OFDM systems in use.

- Channel coding is an important area of research which we did not cover in the research. The performance of different channel codes in the presence of the studied impairments for multicarrier CDMA is also an interesting research direction that can be studied in the future.

- The performance improvements due to simple media access control protocols or coexistence etiquettes, in terms of packet error rate, throughput and capacity can be analyzed for the three multicarrier schemes. In Chapter 6 this analysis has been done for CDMA only and it would be interesting to extend it to the multicarrier schemes.

- Power consumption by the three multicarrier schemes is also an important aspect to be analyzed in an ad-hoc network of battery powered wireless terminals.

- An extension to the work done in Chapter 6 can be done by studying the power consumption of the coexistence etiquettes as high throughput may become meaningless in some instances if it results in high power consumption.

- In a cognitive radio environment the coexistence of secondary users in the absence of primary users and the performance of the three multicarrier schemes in secondary users can also be studied with slight modifications to our analysis.

- Further improvements can be done in the lifetime analysis in Chapter 7 by also considering packet error rate and throughput. This will also result in better power sharing and cooperative strategies to improve lifetime of an ad-hoc network.

References

[1] T. S. Rappaport, *Wireless Communications Principles and Practice.* Prentice-Hall Inc, 2nd ed., 1996.

[2] C. K. Toh, *Ad Hoc Mobile Wireless Networks: Protocols and Systems.* Prentice-Hall Inc, 2001.

[3] N. Yee, J. Linnartz, and G. Fettweis, "Multicarrier CDMA in indoor wireless radio networks," in *Proc. IEEE PIMRC*, pp. 109–113, Sep. 1993.

[4] K. Fazel and L. Papke, "On the performance of convolutionally-coded CDMM/OFDM for mobile communication system," in *Proc. IEEE PIMRC*, pp. 468–472, Sep. 1993.

[5] A. Chouly, A. Brajal, and S. Jourdan, "Orthogonal multicarrier techniques applied to direct sequence spread spectrum CDMA systems," in *Proc. IEEE GLOBECOM*, pp. 1723–1728 vol.3, Nov-2 Dec 1993.

[6] S. Haykin and M. Moher, *Modern Wireless Communications.* Pearson Education, Inc., 2005.

[7] J. G. Proakis, *Digital Communications.* McGraw-Hill, 2000.

[8] R. Scholtz, "The origins of spread-spectrum communications," *IEEE Trans. on Commun.*, vol. 30, pp. 822 – 854, May 1982.

[9] B. J. C. L. Hanzo, M. Munster and T. Keller, *OFDM and MC-CDMA for Broadband Multi-User Communications, WLANs and Broadcasting.* John Wiley and Sons, Ltd, 2004.

[10] G. Cooper and R. Nettleton, "A spread-spectrum technique for high-capacity mobile communications," *IEEE Trans. Veh. Technol.*, vol. 27, pp. 264 – 275, Nov. 1978.

[11] Chang, Robert W., "Synthesis of Band-Limited Orthogonal Signals for Multichannel Data Transmission," *Bell Systems Technical Journal*, vol. 45, pp. 1775–1796, December 1966.

[12] S. Weinstein and P. Ebert, "Data transmission by frequency-division multiplexing using the discrete fourier transform," *Communication Technology, IEEE Transactions on*, vol. 19, no. 5, pp. 628 –634, 1971.

[13] A. F. Molisch, *Wireless Communications*. John Wiley and Sons, Ltd, 2005.

[14] V. DaSilva and E. Sousa, "Performance of orthogonal CDMA codes for quasi-synchronous communication systems," in *Proc. IEEE ICUPC*, vol. 2, pp. 995–999 vol.2, Oct. 1993.

[15] L. Vandendorpe, "Multitone direct sequence CDMA system in an indoor wireless environment," in *Proc. of IEEE First Symp. of Commun. and Veh. Technology*, pp. 4.1.1–4.1.8, Oct. 1993.

[16] S. Hara and R. Prasad, "Overview of multicarrier CDMA," *IEEE Commun. Mag.*, vol. 35, pp. 126–133, Dec 1997.

[17] L. Hanzo and T. Keller, *OFDM and MC-CDMA A Primer*. John Wiley and Sons, Ltd, 2006.

[18] A. Goldsmith, *Wireless Communications*. Cambridge University Press, 2005.

[19] Shannon, C. E., "A mathematical theory of communication," *Bell system technical journal*, vol. 27, 1948.

[20] J. Forney, G.D. and M. Eyuboglu, "Combined equalization and coding using precoding," *IEEE Commun. Mag.*, vol. 29, pp. 25 –34, Dec. 1991.

[21] A. Garcia-Armada, "SNR gap approximation for M-PSK-based bit loading," *IEEE Trans. Wireless Commun.*, vol. 5, pp. 57 – 60, Jan. 2006.

[22] A. Tulino, L. Li, and S. Verdu, "Spectral efficiency of multicarrier CDMA," *IEEE Trans. Inf. Theory*, vol. 51, pp. 479–505, Feb. 2005.

[23] Z. Haas, M. Gerla, D. Johnson, C. Perkins, M. Pursley, M. Steenstrup, C.-K. Toh, and J. Hayes, "Guest editorial wireless ad hoc networks," *IEEE J. Sel. Areas Commun.*, vol. 17, no. 8, pp. 1329–1332, Aug. 1999.

[24] A. Mawira, "Estimate of mean C/I and capacity of interference limited mobile ad-hoc networks," *Proc. Int. Zurich Seminar on Broadband Commun. Access, Transmission, Networking*, pp. 51–1–51–6, 2002.

[25] E. Sousa and J. Silvester, "Optimum transmission ranges in a direct-sequence spread-spectrum multihop packet radio network," *IEEE J. Sel. Areas Commun.*, vol. 8, no. 5, pp. 762–771, Jun. 1990.

[26] X. Liu and M. Haenggi, "Throughput analysis of fading sensor networks with regular and random topologies," *EURASIP J. Wirel. Commun. Netw.*, vol. 5, no. 4, pp. 554–564, 2005.

[27] R. Hekmat and P. V. Mieghem, "Study of connectivity in wireless ad-hoc networks with an improved radio model," *Proc. WiOpt04*, pp. 142–151, Mar. 2004.

[28] R. Hekmat and P. V. Mieghem, "Interference power statistics in ad-hoc and sensor networks," *Wireless Networks*, Jan. 2007.

[29] M. Haenggi, "On the local throughput of large interference-limited wireless networks," *Proc. CISS*, Mar. 2005.

[30] E. Sousa, "Performance of a spread spectrum packet radio network link in a poisson field of interferers," *IEEE Trans. Inf. Theory*, vol. 38, no. 6, pp. 1743–1754, Nov 1992.

[31] I. F. Akyildiz, W. Su, Y. Sankarasubramaniam, and E. Cayirci, "Wireless sensor networks: a survey," *Comput. Networks: The Int. J. Comput. and Telecommun. Networking*, vol. 38, no. 4, pp. 393–422, Mar. 2002.

[32] D. P. Eickstedt and M. R. Benjamin, "Cooperative target tracking in a distributed autonomous sensor network," *OCEANS 2006*, pp. 1–6, Sep. 2006.

[33] S. W. Kim, "Cooperative relaying architecture for wireless video sensor networks," *Proc. Int. Conference Wireless Networks, Commun. and Mobile Computing*, vol. 2, pp. 993–998, Jun. 2005.

[34] W. C. Jakes, Ed., *Microwave Mobile Communications*. IEEE Press, 1974.

[35] K. Hamdi, "A useful lemma for capacity analysis of fading interference channels," *IEEE Trans. Commun.*, vol. 58, pp. 411 –416, Feb. 2010.

[36] G. L. Turin, "The characteristic function of Hermitian quadratic forms in complex normal variables," *Biometrika*, vol. 47, pp. 199–201, June 1960.

[37] "Wireless LAN medium access control (MAC) and physical layer (PHY) specifications," *IEEE Std 802.11*, pp. 1 –721, 1999.

[38] K. Hamdi, "Capacity of MRC on correlated rician fading channels," *IEEE Trans. Commun*, vol. 56, pp. 708 –711, May 2008.

[39] H. Boche and E. Jorswieck, "On the ergodic capacity as a function of the correlation properties in systems with multiple transmit antennas without CSI at the transmitter," *IEEE Trans. Commun.*, vol. 52, no. 10, pp. 1654 – 1657, 2004.

[40] K. Hamdi, "Theoretical analysis of the orthogonality factor in WCDMA downlinks," *IEEE Trans. Wireless Commun.*, vol. 8, pp. 5394 –5399, Nov. 2009.

[41] W. Jang, L. Nguyen, and M. Lee, "MAI and ICI of asynchronous uplink MC-CDMA with frequency offset," *IEEE Trans. Veh. Technol.*, vol. 57, pp. 2164 –2179, July 2008.

[42] M. Lehnert, J.; Pursley, "Error probabilities for binary direct-sequence spread-spectrum communications with random signature sequences," *IEEE Trans. Commun.*, vol. 35, pp. 87–98, Jan 1987.

[43] E. Geraniotis and B. Ghaffari, "Performance of binary and quaternary direct-sequence spread-spectrum multiple-access systems with random signature sequences," *IEEE Trans. Commun.*, vol. 39, pp. 713–724, May 1991.

[44] L. Tomba and W. Krzymien, "Effect of carrier phase noise and frequency offset on the performance of multicarrier CDMA systems," in *Proc. IEEE ICC*, vol. 3, pp. 1513 –1517 vol.3, Jun. 1996.

[45] W. M. Jang, L. Nguyen, and P. Bidarkar, "MAI and ICI of synchronous downlink MC-CDMA with frequency offset," *IEEE Trans. Wireless Commun.*, vol. 5, pp. 693–703, Mar. 2006.

[46] Y. Kim, S. Choi, C. You, and D. Hong, "BER computation of an MC-CDMA system with carrier frequency offset," in *Proc. IEEE ICASSP*, vol. 5, pp. 2555 –2558 vol.5, 1999.

[47] J. Jang and K. B. Lee, "Effects of frequency offset on MC/CDMA system performance," *IEEE Commun. Lett.*, vol. 3, pp. 196 –198, Jul. 1999.

[48] L. Tomba and W. Krzymien, "Sensitivity of the MC-CDMA access scheme to carrier phase noise and frequency offset," *IEEE Trans. Veh. Technol.*, vol. 48, pp. 1657 –1665, Sep. 1999.

[49] H. Steendam and M. Moeneclaey, "The effect of synchronisation errors on MC-CDMA performance," in *Proc. IEEE ICC*, vol. 3, pp. 1510 –1514 vol.3, 1999.

[50] H. Steendam and M. Moeneclaey, "The effect of carrier frequency offsets on downlink and uplink MC-DS-CDMA," *IEEE J. Sel. Areas Commun.*, vol. 19, pp. 2528 –2536, Dec. 2001.

[51] L. Thiagarajan, S. Attallah, K. Abed-Meraim, Y.-C. Liang, and H. Fu, "Non-data-aided joint carrier frequency offset and channel estimator for uplink MC-CDMA systems," *IEEE Trans. Signal Process.*, vol. 56, pp. 4398 –4408, Sept. 2008.

[52] L. Liu and X. Dai, "Carrier frequency offset estimation using hidden pilots for MC-DS-CDMA systems," in *Proc. IEEE. ICCS*, pp. 49 –53, Nov. 2008.

[53] Y. Ma and R. Tafazolli, "Estimation of carrier frequency offset for multicarrier CDMA uplink," *IEEE Trans. Signal Process.*, vol. 55, pp. 2617–2627, June 2007.

[54] Y. Hu and A. Boukerche, "A novel joint detection of frequency offset and MAI for MC-CDMA systems," *IEEE Wireless Commun. Mag.*, vol. 14, pp. 44 –47, June 2007.

[55] F.-T. Chien and C.-C. Kuo, "Blind recursive tracking of carrier frequency offset (cfo) vector in MC-CDMA systems," *IEEE Trans. Wireless Commun.*, vol. 6, pp. 1246–1255, Apr. 2007.

[56] L. Tadjpour, S.-H. Tsai, and C.-C. J. Kuo, "Simplified multiaccess interference reduction for MC-CDMA with carrier frequency offsets (CFO)," *IEEE Trans. Veh. Technol.*, vol. PP, no. 99, pp. 1 –1, 2010.

[57] C.-K. Jao and S.-W. Wei, "Spreading code selection methods for MC-CDMA under carrier frequency offset," in *Proc. IEEE APCC*, pp. 139–143, Oct. 2009.

[58] Q. Shi, Y. Guan, Y. Gong, and C. Law, "Receiver design for multicarrier CDMA using frequency-domain oversampling," *IEEE Trans. Wireless Commun.*, vol. 8, pp. 2236 –2241, May 2009.

[59] L. Sanguinetti, L. Taponecco, and M. Morelli, "Interference-free code design for MC-CDMA uplink transmissions," *IEEE Trans. Wireless Commun.*, vol. 8, pp. 5461 –5465, Nov. 2009.

[60] T. Kim, Y. Kim, J. Park, K. Ko, S. Choi, C. Kang, and D. Hong, "Performance of an MC-CDMA system with frequency offsets in correlated fading," in *Proc. IEEE ICC*, vol. 2, pp. 1095–1099, June 2000.

[61] R. J. Muirhead, *Aspects of multivariate statistical theory.* Wiley, 1982.

[62] K. A. Hamdi, "Moments and autocorrelations of the signal to interference ratio in wireless communications," *Proc. IEEE ICC*, pp. 1345–1348, May 2008.

[63] X. Gui and T. S. Ng, "Performance of asynchronous orthogonal multicarrier CDMA system in frequency selective fading channel," *IEEE Trans. Commun.*, vol. 47, pp. 1084–1091, July 1999.

[64] J. Park, J. Kim, S. Choi, N. Cho, and D. Hong, "Performance of MC-CDMA systems in non-independent Rayleigh fading," in *Proc. IEEE ICC*, vol. 1, pp. 506–510, June 1999.

[65] Z. Li and M. Latva-aho, "Error probability of interleaved MC-CDMA systems with MRC receiver and correlated Nakagami-m fading channels," *IEEE Trans. Commun.*, vol. 53, pp. 919–923, June 2005.

[66] N. Yee, J. P. Linnartz, and G. Fettweis, "Multi-Carrier CDMA in indoor wireless radio networks," *IEICE Trans. Commun.*, vol. E77-B, pp. 900–904, July 1994.

[67] S. Kondo and B. Milstein, "Performance of multicarrier DS CDMA systems," *IEEE Trans. Commun.*, vol. 44, pp. 238–246, Feb. 1996.

[68] L.-L. Yang and L. Hanzo, "Performance of generalized multicarrier DS-CDMA over Nakagami-m fading channels," *IEEE Trans. Commun.*, vol. 50, pp. 956–966, June 2002.

[69] Q. Shi and M. Latva-aho, "An exact error floor for downlink MC-CDMA in correlated Rayleigh fading channels," *IEEE Commun. Lett.*, vol. 6, pp. 196–198, May 2002.

[70] Z. Hou and V. Dubey, "Exact analysis for downlink MC-CDMA in Rayleigh fading channels," *IEEE Commun. Lett.*, vol. 8, pp. 90–92, Feb. 2004.

[71] Y. Feng and J. Qin, "BER of MC-CDMA systems with EGC in correlated Nakagami-m fading," *IEEE Commun. Lett.*, vol. 10, pp. 689–691, Oct. 2006.

[72] Q. Shi and M. Latva-aho, "Exact bit error rate calculations for synchronous MC-CDMA over a Rayleigh fading channel," *IEEE Commun. Lett.*, vol. 6, pp. 276–278, July 2002.

[73] S. Sorooshyari and D. Daut, "Performance of multicarrier CDMA in the presence of correlated fading," *IEEE Trans. Veh. Technol.*, vol. 58, pp. 3837–3843, Sept. 2009.

[74] P. Karn, "MACA: a new channel access method for packet radio," *Proc. IEEE Comput. Networking Conference*, pp. 134 –140, Sep. 1990.

[75] J. Garcia-Luna-Aceves and C. Fullmer, "Performance of floor acquisition multiple access in ad-hoc networks," in *Proc. IEEE ISCC*, pp. 63 –68, June 1998.

[76] A. Hasan and J. Andrews, "The guard zone in wireless ad hoc networks," *IEEE Trans. Wireless Commun.*, vol. 6, pp. 897–906, March 2007.

[77] R. Menon, R. M. Buehrer, and J. H. Reed, "Impact of exclusion region and spreading in spectrum-sharing ad hoc networks," in *Proc. ACM TAPAS*, (New York, NY, USA), p. 7, ACM, 2006.

[78] M. Pursley, "The role of spread spectrum in packet radio networks," *Proc. of the IEEE*, vol. 75, pp. 116 – 134, Jan. 1987.

[79] S. Weber, X. Yang, J. Andrews, and G. de Veciana, "Transmission capacity of wireless ad hoc networks with outage constraints," *IEEE Trans. Inf. Theory*, vol. 51, pp. 4091 –4102, Dec. 2005.

[80] Q. Qu, L. Milstein, and D. Vaman, "Cognitive radio based multi-user resource allocation in mobile ad hoc networks using multi-carrier CDMA modulation," *IEEE J. Sel. Areas Commun.*, vol. 26, pp. 70 –82, Jan. 2008.

[81] S. Sengupta, M. Chatterjee, and K. Kwiat, "A game theoretic framework for power control in wireless sensor networks," *IEEE Trans. Comput.*, vol. 59, pp. 231 –242, Feb. 2010.

[82] D. Pompili, T. Melodia, and I. Akyildiz, "A CDMA-based medium access control for underwater acoustic sensor networks," *IEEE Trans. Wireless Commun.*, vol. 8, pp. 1899 –1909, Apr. 2009.

[83] S. De, C. Qiao, D. Pados, M. Chatterjee, and S. Philip, "An integrated cross-layer study of wireless CDMA sensor networks," *IEEE J. Sel. Areas Commun.*, vol. 22, pp. 1271 – 1285, Sep. 2004.

[84] V. Chakravarthy, X. Li, Z. Wu, M. Temple, F. Garber, R. Kannan, and A. Vasilakos, "Novel overlay/underlay cognitive radio waveforms using SD-SMSE framework to enhance spectrum efficiency- part I: theoretical framework and analysis in AWGN channel," *IEEE Trans. Commun.*, vol. 57, pp. 3794 –3804, Dec. 2009.

[85] A. Attar, M. Nakhai, and A. Aghvami, "Cognitive radio transmission based on direct sequence MC-CDMA," *IEEE Trans. Wireless Commun.*, vol. 7, pp. 1157 –1162, Apr. 2008.

[86] J. Morrow, R.K. and J. Lehnert, "Bit-to-bit error dependence in slotted DS/SSMA packet systems with random signature sequences," *IEEE Trans. Commun.*, vol. 37, pp. 1052–1061, Oct 1989.

[87] J. Morrow, R.K. and J. Lehnert, "Packet throughput in slotted ALOHA DS/SSMA radio systems with random signature sequences," *IEEE Trans. Commun.*, vol. 40, pp. 1223–1230, Jul 1992.

[88] E. Sousa, "Interference modeling in a direct-sequence spread-spectrum packet radio network," *IEEE Trans. Commun.*, vol. 38, pp. 1475–1482, Sep 1990.

[89] J. Cheng and N. Beaulieu, "Accurate DS-CDMA bit-error probability calculation in rayleigh fading," *IEEE Trans. Wireless Commun.*, vol. 1, pp. 3–15, Jan 2002.

[90] K. Hamdi, "Accurate DS-CDMA packet-error rate analysis in rayleigh fading," *IEEE Trans. Commun.*, vol. 55, pp. 551–562, March 2007.

[91] E. Sousa, "Performance of a spread spectrum packet radio network link in a poisson field of interferers," *IEEE Trans. Inf. Theory*, vol. 38, pp. 1743–1754, Nov 1992.

[92] P. Pinto, A. Giorgetti, M. Win, and M. Chiani, "A stochastic geometry approach to coexistence in heterogeneous wireless networks," *IEEE J. Sel. Areas Commun.*, vol. 27, pp. 1268 –1282, september 2009.

[93] M. Win, P. Pinto, and L. Shepp, "A mathematical theory of network interference and its applications," *Proc. of the IEEE*, vol. 97, pp. 205 –230, Feb. 2009.

[94] P. Gupta and P. Kumar, "The capacity of wireless networks," *IEEE Trans. Inf. Theory*, vol. 46, pp. 388–404, Mar 2000.

[95] A. Hasan and J. Andrews, "The critical radius in cdma ad hoc networks," vol. 6, pp. 3568–3572 Vol.6, Nov.-3 Dec. 2004.

[96] Y.-W. Hong, W.-J. Huang, F.-H. Chiu, and C.-C. Kuo, "Cooperative communications in resource-constrained wireless networks," *IEEE Signal Processing Mag.*, vol. 24, pp. 47–57, May 2007.

[97] V. Bharghavan, A. Demers, S. Shenker, and L. Zhang, "MACAW: a media access protocol for wireless LAN's," in *Proc. ACM SIGCOMM*, (New York, NY, USA), pp. 212–225, ACM, 1994.

[98] M. Abramowitz and I. A. Stegun, *Handbook of Mathematical Functions with Formulas, Graphs, and Mathematical Tables.* Dover Publications, 9 ed., 1965.

[99] D. A. Barry, P. J. Culligan-Hensley, and S. J. Barry, "Real values of the W-function," *ACM Trans. Math. Softw.*, vol. 21, no. 2, pp. 161–171, 1995.

[100] D. Stoyan, W. S. Kendall, and J. Mecke, *Stochastic Geometry and its Applications*. John Wiley and Sons, Ltd, second ed., 1995.

[101] W.-J. Huang, Y.-W. Hong, and C.-C. Kuo, "Lifetime maximization for amplify-and-forward cooperative networks," *IEEE Trans. Wireless Commun.*, vol. 7, pp. 1800–1805, May 2008.

[102] Y. Chen, G. Yu, P. Qiu, and Z. Zhang, "Power-aware cooperative relay selection strategies in wireless ad hoc networks," *Proc. IEEE PIMRC*, pp. 1–5, Sep. 2006.

[103] Y. Chen and Q. Zhao, "An integrated approach to energy-aware medium access for wireless sensor networks," *IEEE Trans. Signal Process.*, vol. 55, pp. 3429–3444, July 2007.

[104] Y. Chen and Q. Zhao, "Maximizing the lifetime of sensor network using local information on channel state and residual energy," *39th Conference Inf. Sci. and Syst.*, Mar. 2005.

[105] I. Kang and R. Poovendran, "On the lifetime extension of energy-efficient multihop broadcast networks," *Proc. IEEE IJCNN*, vol. 1, pp. 365–370, 2002.

[106] M. Bhardwaj, T. Garnett, and A. Chandrakasan, "Upper bounds on the lifetime of sensor networks," *Proc. IEEE ICC*, vol. 3, pp. 785–790 vol.3, 2001.

[107] S. Cui, A. Goldsmith, and A. Bahai, "Energy-efficiency of MIMO and cooperative MIMO techniques in sensor networks," *IEEE J. Sel. Areas Commun.*, vol. 22, no. 6, pp. 1089–1098, Aug. 2004.

[108] Z. Chen and C. Yang, "Energy efficiency of cooperative diversity at PHY layer in wireless sensor networks," *proc. IEEE ICOSP*, vol. 4, pp. –, 2006.

[109] J. Luo, R. Blum, L. Cimini, L. Greenstein, and A. Haimovich, "Decode-and-forward cooperative diversity with power allocation in wireless networks," *Proc. IEEE GLOBECOM*, vol. 5, pp. 5 pp.–, Nov.-2 Dec. 2005.

[110] M. Hasna and M.-S. Alouini, "Optimal power allocation for relayed transmissions over rayleigh-fading channels," *IEEE Trans. Wireless Commun.*, vol. 3, no. 6, pp. 1999–2004, Nov. 2004.

[111] W. Su, A. Sadek, and K. Liu, "SER performance analysis and optimum power allocation for decode-and-forward cooperation protocol in wireless networks," *Proc. IEEE WCNC*, vol. 2, pp. 984–989 Vol. 2, Mar. 2005.

[112] T. Himsoon, W. P. Siriwongpairat, Z. Han, and K. J. R. Liu, "Lifetime maximization via cooperative nodes and relay deployment in wireless networks," *IEEE J. Sel. Areas Commun.*, vol. 25, no. 2, pp. 306–317, 2007.